MICELLAR CARRIER SYSTEMS FOR ANTICANCER DRUGS USING NATURAL POLYMERS

A Thesis Submitted to
the Graduate School of
İzmir Institute of Technology
in Partial Fulfillment of the Requirements for the Degree of

DOCTOR OF PHILOSOPHY

in Chemistry

by
Merve ÇEVİK EREN

December 2024
İZMİR

We approve the thesis of **Merve ÇEVİK EREN**

Examining Committee Members:

Prof. Dr. Hürriyet POLAT
Department of Chemistry, İzmir Institute of Technology

Prof. Dr. Gülşah ŞANLI MOHAMED
Department of Chemistry, İzmir Institute of Technology

Assoc. Prof. Dr. Sevgi KILIÇ ÖZDEMİR
Department of Chemical Engineering, İzmir Institute of Technology

Prof. Dr. Erol KAYA
Department of Mining Engineering, Dokuz Eylül University

Assoc. Prof. Dr. Gül AKAR ŞEN
Department of Mining Engineering, Dokuz Eylül University

13 December 2024

Prof. Dr. Hürriyet POLAT
Supervisor, Department of Chemistry
İzmir Institute of Technology

Prof. Dr. Gülşah Şanlı MOHAMED
Head of Department of Chemistry

Prof. Dr. Mehtap EANES
Dean of the Graduate School

ACKNOWLEDGEMENTS

First and foremost, I would like to express my deepest gratitude to my advisors, Prof. Dr. Hürriyet POLAT and Prof. Dr. Mehmet POLAT, for their guidance, motivation, caring, patience, and confidence. Their way of communication provoked me to improve my scientific communication skills. Their contribution to my PhD and personal life is enormous. I have learned much about science from them and how to face life's problems. Their guidance helped me research and write this thesis with an excellent atmosphere. I could not have imagined having better mentors.

I wish to thank the thesis committee members, Prof.Dr. Gülşah ŞANLI MOHAMED, Prof.Dr. Kadir YURDAKOÇ, and Assoc. Prof. Dr. Sevgi ÖZDEMİR for their valuable contributions. I have significantly benefited from their helpful and constructive suggestions throughout the study. I also thank Assoc. Prof. Dr. Nesrin HORZUM POLAT and Assoc. Prof. Dr. Gül AKAR ŞEN, for accepting to be on my defense jury.

I want to thank all IZTECH Integrated Research Center members for all the analyses.

I am thankful to my friends and labmates Hazal PAKER, Esra Sıla GÜNDÜZ, Tuğçe TUNÇ GULİYEV, and Ateş Batıkan ÖZDAMAR for their support and contributions throughout the whole process.

Last but not least, I would like to send my deepest gratitude to my husband, AHMET EREN, and my daughter Zeynep EREN, for the spiritual support they have given me throughout my life; you are the best. I am thrilled and lucky to continue my life journey with them.

I would also like to express my deepest gratitude to my parents and sister for their support

ABSTRACT

MICELLAR CARRIER SYSTEMS FOR ANTICANCER DRUGS USING NATURAL POLYMERS

Transporting anticancer drugs precisely to tumor sites is still challenging, often resulting in low efficacy and notable side effects. Research on encapsulating medications in liposomes, nanoparticles, or micelles to improve chemotherapy is ongoing to solve this issue. Such carriers must fulfill two essential requirements: preserve their structural and physicochemical integrity while appropriately encasing the medication and releasing it to the tumor site when required. Chitosan has emerged as a leading candidate for drug carriers due to its unique properties, including polymerization potential, biocompatibility, pH sensitivity, and charge characteristics. Numerous synthesis methods for chitosan-based nanocarriers have been explored, with a literature search since 2000 yielding 527 relevant articles, highlighting the extensive and complex body of research in this area.

This thesis first examines the stability of synthetic polymer P-123 micelles (both bare and Docetaxel-loaded) in deionized water (DW) and simulated body fluid (SBF) containing bovine serum albumin (BSA). Stability tests under dilution, aging, and varying concentrations of drugs and proteins showed that these micelles lost integrity when diluted beyond a specific limit or when protein concentration exceeded a critical threshold, indicating limited stability in natural blood plasma, contrary to earlier findings on P-123 micelles.

This study developed chitosan-based natural polymeric micelles to enhance the stability of hydrophobic anticancer drugs. While natural micelles exhibited greater stability in physiological fluids than synthetic ones, both types became unstable upon interaction with proteins. To improve stability, fucoidan coating was applied, providing protein resistance and introducing a negative charge that hindered cellular uptake. Drug-loaded micelles achieved approximately 60% cancer cell death, a lower rate than free docetaxel, likely due to the delayed drug release after cellular internalization.

ÖZET

DOĞAL POLİMERLER KULLANILARAK ANTİ-KANSER İLAÇLARI İÇİN MİSEL TAŞIYICI SİSTEMLER

Kanser ilaçlarını tam olarak tümör bölgelerine taşımak hala zorlayıcı bir süreç olup, çoğu zaman düşük etkinlik ve belirgin yan etkilere yol açmaktadır. Bu sorunu çözmek amacıyla, ilaçları lipozomlar, nanopartiküller veya miseller içinde kapsülleyerek kemoterapiyi geliştirme çalışmaları devam etmektedir. Bu tür taşıyıcıların iki önemli gereksinimi karşılaması gerekmektedir: yapısal ve fizikokimyasal bütünlüklerini korumalı, ilacı uygun şekilde kapsayıp gerektiğinde tümör bölgesine salınımını sağlamalıdırlar. Kitosan, polimerizasyon potansiyeli, biyouyumluluğu, pH duyarlılığı ve yük özellikleri gibi benzersiz özellikleri nedeniyle ilaç taşıyıcıları için önde gelen bir aday olarak ortaya çıkmıştır. 2000 yılından itibaren yapılan literatür taraması, "yenilikçi + nano + kitosan" anahtar kelimeleriyle 527 ilgili makale bulunmuş olup, bu alandaki geniş ve karmaşık araştırma birikimini vurgulamaktadır.

Bu çalışmada, sentetik P-123 misellerinin (boş ve docetaxel yüklü) deiyonize su ve simüle vücut sıvısındaki stabilitesini inceleyerek, belirli bir seyreltme veya protein konsantrasyonunun ötesinde bütünlüklerini kaybettiklerini göstermektedir. Bu durum, P-123 misellerinin kan plazmasındaki stabilitesinin sınırlı olduğunu ortaya koymuştur. Çalışma, stabiliteyi artırmak amacıyla kitosan bazlı doğal polimerik miseller geliştirmiş ve doğal misellerin vücut sıvılarında daha stabil kaldığını ancak protein etkileşimleri nedeniyle kararsız hale geldiklerini belirlemiştir. Bu nedenle, protein direnci sağlamak amacıyla kitosan miselleri sülfat grupları içeren fukoidan ile kaplanmıştır. Kanser hücreleri üzerindeki etkiler incelendiğinde, fiziksel ve kimyasal bağlanma yoluyla ilaç kapsüllenen misellerin yaklaşık %60 hücre ölümü sağladığı, ancak serbest docetaxel'e göre daha düşük etkinlik gösterdiği belirlenmiştir. Fukoidan kaplı misellerin ise negatif yük nedeniyle hücre alımında zorlanarak kanser hücrelerini öldürme etkisinin daha da azaldığı gözlemlenmiştir.

TABLE OF CONTENTS

LIST OF FIGURES

Figure **Page**

Figure **Page**

Figure **Page**

Figure **Page**

LIST OF TABLES

Table **Page**

CHAPTER 1

INTRODUCTION

1.1. STATEMENT OF THE PROBLEM

A variety of illnesses that result from malignant cells growing out of control and having the ability to invade or spread to other bodily parts are collectively referred to as cancer. Estimates for 2018 show that cancer, the second most significant cause of mortality worldwide, claimed 9.6 million lives. This means that cancer accounts for roughly one in six deaths worldwide. About 70% of cancer-related deaths take place in low- and middle-income nations. Cancer has a substantial and growing financial impact. In 2010, the WHO (2018) estimated that the yearly economic burden of cancer was roughly US$ 1.16 trillion (Alzehr et al., 2022).

Anti-cancer drugs used in the treatment of cancer are aimed at targeting cancer cells by preventing their growth and proliferation. There are many methods used in the treatment of cancer. These can be sorted as immunotherapy, hormone therapy, radiotherapy, and chemotherapy. However, there are several difficulties during the transportation and distribution of these medicines, i.e., during treatment duration. Anti-cancer drugs can also damage healthy cells while targeting cancer cells. This can lead to serious side effects and systemic toxicity. Chemotherapy drugs can cause side effects such as a weakened immune system, hair loss, nausea, and vomiting. Besides, it is not always possible for drugs to reach the tumor area directly. Physiological barriers such as the blood-brain barrier can make it difficult for medicines to reach the target area (Tiwari et al., 2012). Furthermore, factors such as tumor microcycles and tumor heterogeneity can reduce the drug's effectiveness.

To overcome these challenges, researchers have developed various strategies for targeted drug distribution. These methods aim to concentrate therapeutic agents directly into the tumor area, maximizing the drug's effect on cancer cells and reducing damage to normal tissues (Alley et al., 2010). Techniques such as nanoparticle-based distribution systems, liposomal encapsulation, and antibody-drug conjugates are at the forefront of

this innovative field. Each of these approaches uses unique mechanisms to increase the accuracy and efficiency of drug distribution. Despite these advances, there are still challenges in the distribution of anti-cancer drugs. The transportation of anti-cancer drugs and the challenges encountered directly affect the effectiveness of cancer treatment and patients' quality of life (Pringle et al., 2024). Therefore, continuous research and innovative solutions are being developed to improve transport systems and overcome existing problems.

1.2. ANTICANCER DRUG CARRIERS

Anticancer drug carriers are systems developed to increase the effectiveness of cancer treatment, reduce side effects, and provide targeted drug release. Since traditional chemotherapy drugs attack both cancerous and healthy cells, they can result in serious side effects (Schirrmacher, 2019). Therefore, drug delivery systems are very important in providing more controlled and targeted drug release, especially in cancer treatment. Drug carriers include polymers, lipids, and inorganic nanomaterials. Among these, biopolymers are of great interest due to their biocompatibility and biodegradable properties.

Chitosan is one of the most researched biopolymers (Jiménez-Gómez and Cecilia, 2020). Chitosan is a natural polysaccharide derived from chitin found in shellfish shells. It stands out with its antibacterial, biodegradable, and biocompatible properties. Since chitosan has positively charged amino groups, it can establish electrostatic interactions with the negatively charged cell membrane (Ardean et al., 2021). This feature allows chitosan to be used in drug delivery systems targeted especially to cancer cells. Chitosan also has a structure that can change its solubility depending on environmental conditions, so it can regulate drug release in a controlled manner (Wang et al., 2020).

Chitosan micelles are systems in which hydrophobically modified chitosan molecules spontaneously form micellar structures in water. These micelles are an effective tool for transporting hydrophobic drugs. While hydrophobic drugs dissolve in the micelle's core, the chitosan's hydrophilic parts remain on the outer surface facing the water (Zlotnikov et al., 2023). This allows drugs to be transported stably in a water

environment. Chitosan-based systems can deliver drugs to specific regions more effectively.

According to the literature, chitosan micelles, as anticancer drug carriers, enable the drug to be targeted to cancer cells and regulate drug release in a controlled manner. For example, hydrophobic cancer drugs such as docetaxel can be transported more effectively using chitosan micelles. These systems increase the effectiveness of the treatment by ensuring that the drug reaches the tumor site directly instead of healthy cells and minimizing side effects (Razak et al., 2021).

Another advantage of chitosan micelles is that they are pH sensitive. Cancerous tissues usually have a lower pH level. Chitosan micelles break down at this low pH level, releasing the drug only in cancer cells (Zlotnikov et al., 2023). This targeted release mechanism reduces unwanted side effects in cancer treatment while increasing the effectiveness of the treatment.

Chitosan micelles can also be made more functional with different chemical modifications. Adding polymers such as polyethylene glycol (PEG) to the chitosan structure, the circulation time of the micelles can be extended and made more stable (Hu et al., 2008). In addition, ligands can be added to chitosan micelles to ensure more specific binding to cancer cells. This is another critical factor that increases the effectiveness of treatment (Shakil et al., 2021).

As a result, chitosan micelles are a promising structure among anticancer drug delivery systems and are the subject of intensive research. Due to their biocompatibility, biodegradability, and drug-carrying capacity, they have a significant place as a new-generation drug carrier in cancer treatment.

1.3. SCOPE OF THE STUDY

This study aims to develop a natural polymer-based stable micelle as a drug-delivery system for anticancer hydrophobic drugs. Due to its superior properties, Chitosan will be used as the main model of natural polymer. The study will include the following parts A, B, C, and D (Summarized in Figure 1.1).

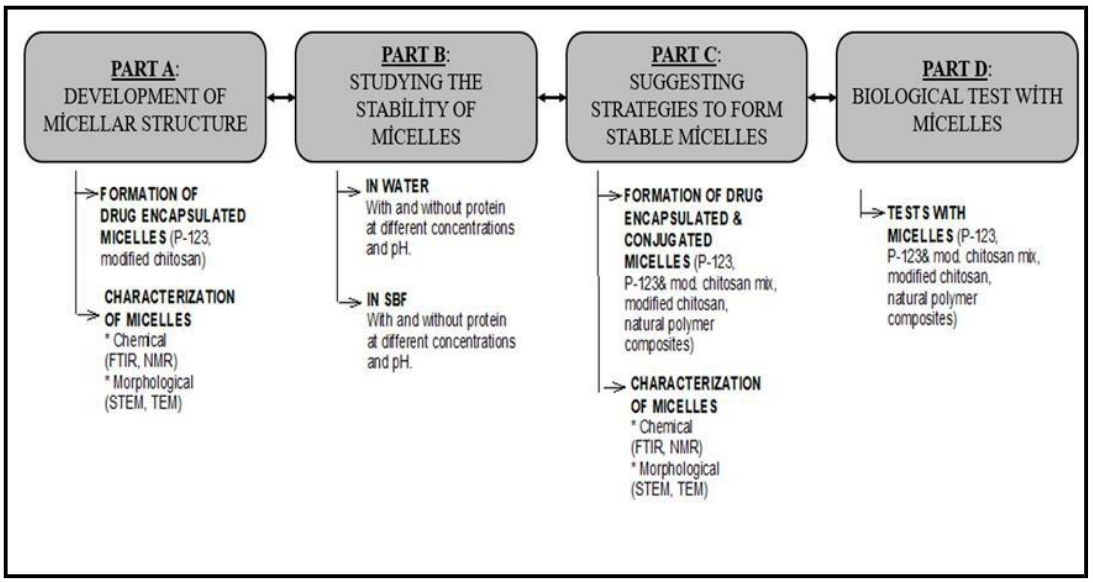

Figure 1.1. Flow sheet of the study.

A. Development of Micellar structures

1. The development of docetaxel-loaded micellar structures will be done using the thin film hydration method with

- a block copolymer, P-123,
- modified (hydrophobic) chitosan

2. FTIR, NMR, STEM, and TEM images will characterize structure chemical and morphological.

B. Studying the stability of micellar structures

The stability of micelles produced will be studied in water and simulated body fluid in the absence and presence of protein which is used bovine serum albumin at different concentrations. These studies will include the dilution-induced disintegration of micelles using size distribution measurements by Dynamic Light Scattering. By evaluating these parameters, the study aims to provide a comprehensive understanding of how micelles behave in environments mimicking the human body, particularly when

exposed to proteins like BSA, which are known to interact with nanoparticles and potentially affect their stability and drug release profiles.

C. Suggesting strategies to form stable micelles

1. Developing docetaxel loaded & conjugated chitosan-based micellar structures will be developed using the thin film hydration method.

- FTIR, NMR, STEM, and TEM images will characterize structures chemically and morphologically.

D. Biological tests with micellar structures

In this study phase, the effects of the synthesized micelle systems on human Caco-2 colorectal adenocarcinoma epithelial cells will be investigated. In addition, the effects of the drugs that make up the micelle systems, such as chitosan and fucoidan, on cancer cells will be examined.

CHAPTER 2

BACKGROUND

2.1. DRUG DELIVERY

Novel drug delivery systems with better targeting ability and stability are needed for cancer prevention, the suppression of adverse side effects, and pain management associated with cancer chemotherapy. The encapsulation of drugs in nanoparticles, micelles, liposomes, dendrimers, nanocapsules, and others, improves the therapeutic index and reduces the adverse side effects (Li et al., 2019). Drug targeting is the selective directing of the pharmacologically active substance to the site of action or absorption, and the prepared preparation is a special structure that carries the active substance. Selective delivery of the drug to specific sites in the body has many benefits. It enables the drug to reach the affected area or areas targeted. The behavior of the drug can be controlled because of the selectivity of the drug in the specified target region and the use of the low-dose active substance (Ravi et al., 2013).

Passive targeting: Passive targeting utilizes the uncommon aspect of the Tumor Microenvironment (TME) of the tumor mass known as the EPR or Enhanced Permeability and Retention effect (Attia et al., 2019).

Active targeting: In this approach, the drug-carrying carrier system is designed to reach a specific site through surface modifications, rather than relying on natural uptake by the RES. Surface modification techniques may involve coating the surface with a bioadhesive, nonionic surfactant, specific cell or tissue antibodies (e.g., monoclonal antibodies), or albumin protein (Agnihotri et al., 2024).

Inverse Targeting: In this type of targeting attempts are made to avoid passive uptake of the colloidal carrier by RES and hence the process is referred to as inverse targeting (Mariam et al., 2019).

Dual Targeting: A therapeutic effect of a drug is enhanced when the carrier molecules have their therapeutic activity, which enhances the therapeutic effect of the drug. For example, a carrier molecule with its antiviral activity can be loaded with

antiviral medications, resulting in a synergistic effect of the drug conjugate (Wu et al.,2023).

2.2. COMMON METHODS OF DRUG DELIVERY

Medicines used to treat cancer are critical to the availability of patients, the success of treatment, and the quality of life of patients. The administration methods of these medicines vary depending on the type of cancer, the specific medication used, and the treatment plan specific to the patient. Each method ensures that the drug effectively reaches the target area, while the other aims to minimize side effects. Typical delivery methods include (Figure 2.1) oral (through mouth), intravenous (IV), intramuscular (IM), subcutaneous (SC), and topical (Anand et al., 2022).

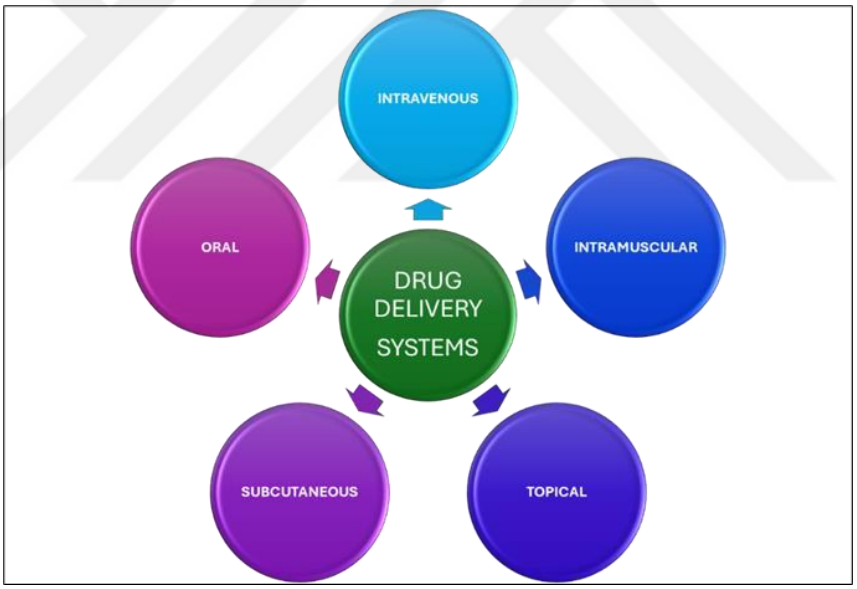

Figure 2. 1. Novel drug delivery systems.

Oral delivery is carried out by taking pills, capsules, or liquid medicines. This method is often preferred due to its ease and practicability at home. However, there may be difficulties in the absorption of the drug, such as variability and gastrointestinal side effects. Intravenous (IV) delivery means medicines are administered directly through a vein. This method offers the advantages of rapid distribution and controlled dosage, with intramuscular (IM) and subcutaneous (SC) injections, by injecting the medicines into the

muscle (IM), or subcutaneous (SC) (Lou et al., 2023). These methods allow for slow and persistent release, but they may experience problems such as pain and limited volume in the injection area. Topical delivery is achieved by applying drugs on the skin and is usually used in skin cancers or tumors near the skin surface. This method directly affects the target area, while reducing systemic side effects (Slavkova et al., 2023).

In cancer treatment, it is essential to understand the various drug delivery methods, optimize treatment outcomes, and improve patients' quality of life. Each method has its advantages and challenges, playing a crucial role in the fight against cancer. Several drug transport systems have been developed to minimize the difficulties and side effects of these transport methods.

2.3. ANTICANCER DRUGS

Chemotherapy drugs function by disrupting the ability of cancer cells to grow, divide, and multiply. By targeting these processes, cancer cells cannot survive and eventually die (Rebucci et al., 2013). Some chemotherapy drugs are designed to act at specific cell cycle phases, while others have broader effects. Chemotherapy can work in several ways: by directly killing cancer cells, inhibiting their ability to form new blood vessels (angiogenesis), or damaging the genetic material (DNA) of the cells, thereby preventing further tumor development. These drugs are often classified based on their mechanisms of action or chemical composition, with each class having a unique way of targeting cancer cells to halt their growth or cause cell death (Ramos et al., 2021).

This approach to chemotherapy is essential because different drugs may work best for different types of cancer, and combining multiple types of chemotherapy agents can be more effective by attacking cancer cells through multiple pathways. However, these drugs can also affect healthy cells, particularly those that divide quickly, such as hair, skin, and digestive tract cells, leading to various side effects. (Brianna et al., 2023) By categorizing chemotherapy drugs into these specific groups, oncologists can tailor treatment plans to target the characteristics of a patient’s cancer, maximizing effectiveness while managing side effects. These chemotherapy drugs can be categorized as follows;

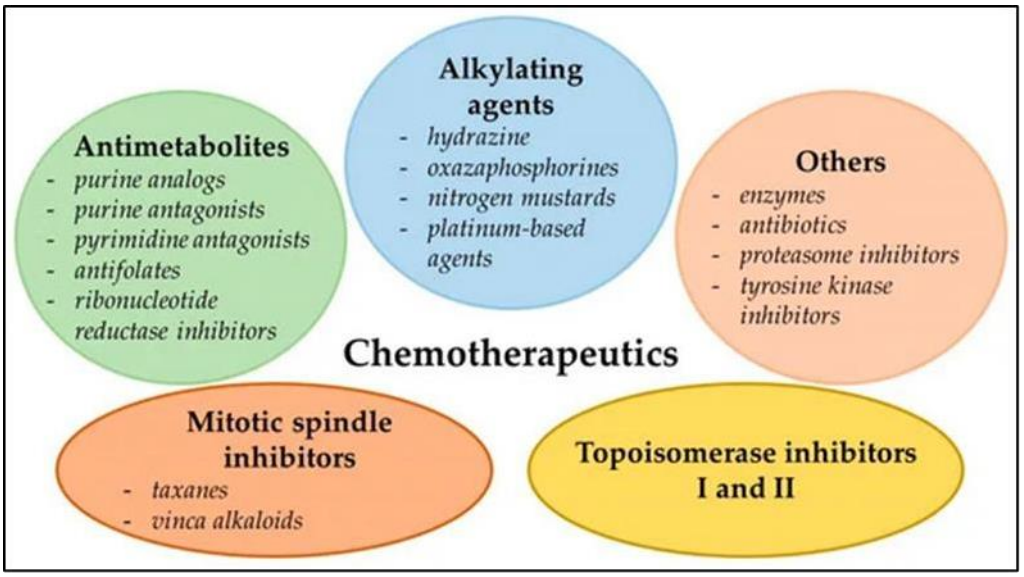

Figure 2.2. The scheme of chemotherapy drugs.

Alkylating agents: Alkylating agents function by impairing cellular reproduction through the induction of DNA damage. These chemotherapeutic drugs are effective across all cell cycle phases, making them versatile in treating various cancers. Specifically, they are utilized in the management of lung, breast, and ovarian cancers, as well as hematological malignancies such as leukemia, lymphoma, and Hodgkin's disease. Additionally, they play a significant role in the treatment of multiple myeloma and various sarcomas (Andrés et al., 2024).

Antibiotics/Antineoplastics: Agents known as antibiotics have a microbial origin, meaning they are derived from microorganisms. Various antibiotic antineoplastic agents impact DNA replication through different cytotoxic actions. These agents are utilized as chemotherapy agents to address numerous cancer types (Gao et al., 2020).

Antimetabolites are crucial in cancer treatment as they interfere with DNA and RNA synthesis by mimicking the natural building blocks of these nucleic acids. This interference inhibits cellular reproduction, effectively preventing cancer cells from proliferating. Antimetabolites are widely utilized for various cancers, including leukemias, breast, ovarian, and colorectal cancers (Kang et al., 2021).

Examples of antimetabolites include 5-fluorouracil (5-FU), 6-mercaptopurine (6-MP), and cytarabine (Ara-C). These drugs target cancer cells and impact normal cells, particularly those that rapidly divide, which can lead to side effects such as nausea, fatigue, and reduced blood cell counts (Al-Dhaheri et al., 2023).

Hormones/Antineoplastics: Anticancer medications that target hormones are prescribed to inhibit the growth of hormone-responsive cancers. Hormones are molecules that communicate with cell receptors, either activating or inhibiting cellular functions. Hormonally responsive cancer can be managed by decreasing the hormone levels necessary for tumor growth and survival, achieved through hormone synthesis inhibitors or hormone receptor antagonists (Min et al., 2022).

Platinum Compounds are a class of chemotherapeutic agents that create highly reactive platinum complexes, which interact with DNA by binding to and crosslinking its strands. This crosslinking occurs within the double-stranded structure of DNA, which resides in the cell's nucleus and regulates various cellular functions. By forming these chemical cross-links, platinum-based drugs effectively inhibit DNA replication and transcription, preventing cancer cell proliferation and ultimately triggering apoptosis in malignant cells. These agents are particularly effective against various types of cancer, including ovarian and testicular cancers, and are often utilized in combination with other chemotherapeutic agents to enhance therapeutic efficacy and overcome resistance (Zhang et al., 2022).

Topoisomerase inhibitors: Plant alkaloids, also known as these drugs, disrupt topoisomerases, enzymes responsible for separating DNA strands for replication. These enzymes, which are proteins that initiate chemical reactions in living cells, are targeted by topoisomerase inhibitors. These inhibitors treat specific leukemias and various cancers, such as lung, ovarian, gastrointestinal, colorectal, and pancreatic cancers (Huang et al., 2022).

Vinca Alkaloids are a type of anticancer medication that hinders the growth of cancer cells by halting cell division, also known as mitosis. These alkaloids, called antimitotic antimicrotubule agents or mitotic inhibitors, were initially extracted from the common periwinkle plant. They have since been synthesized and encompass vinblastine, vincristine, vindesine, and vinorelbine (Dhyani et al., 2022).

2.4. DRUG CARRIER SYSTEMS FOR ANTICANCER DRUGS

Enveloping anticancer agents, whether hydrophobic or hydrophilic, is one of the most sought-after preparation methods. These anticancer drug carriers must offer

nontoxicity, good biodegradation, or bioavailability characteristics. In addition, the carrier must also fulfill the following requirements:

• The correct chemical properties to be able to dissolve and envelop the drug in its structure

• Sufficient stability in the circulation system to protect the drug during transport

• Proper attributes to deliver the drug once it reaches the target cells

Fig. 2 .3 schematically summarizes the problems associated with a career that does not satisfy the above requirements.

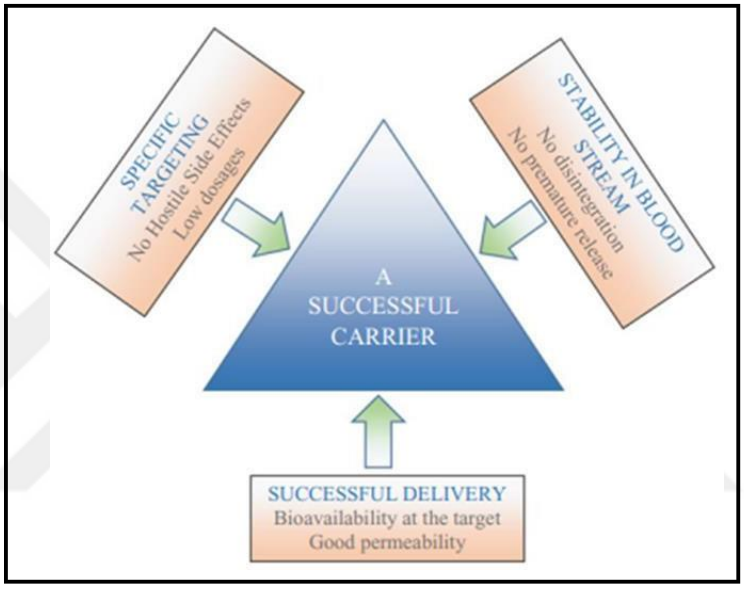

Figure 2.3. A schematic of the general requirements is expected from a successful drug carrier.

So, the main aim of a delivery vehicle is to control the drug concentration in the bloodstream for a considerable time within the limit of minimum inhibitory concentration and therapeutic limit. Although chemotherapy is successful to some extent, it has many adverse effects when it enters the body, such as low therapeutic effects, high dose requirements, poor bioavailability, development of multi-drug resistance, and non-specific targeting (Park et al., 2008).

Therefore, the literature has researched achieving successful drug delivery with minimal adverse side effects to the desired sites of therapeutic action for anticancer drugs. Many materials with different structural properties have been developed as popular delivery vehicles for chemotherapeutic agents. These materials aim to increase treatment

effectiveness by enabling drugs to be directed to specific cells or tissues to provide targeted therapy.

Polymers: Polymeric nanoparticles are one of the simplest forms of soft materials for nano-medicine applications due to their facile synthesis and easy structural modification to allow desired properties to be built into the nanoparticle, such as surface modifications to improve drug loading efficacy, biodistribution, pharmacokinetic control, and therapeutic efficacy (Parveen et al., 2008). Polymeric nanoparticles can be made from synthetic polymers, e.g., poly(lactic acid) (PLA), poly(ε-caprolactone) (PCL), poly(lactic-co-glycolic acid), N-(2-hydroxypropyl)-methacrylamide copolymer (HPMA) and poly(styrene-maleic anhydride) copolymer, or from natural polymers, such as gelatin, dextran, guar gum, chitosan, and collagen (Senapati et al., 2018), (Cragg et al.,1993), (Kumar et al., 2000), (Newman et al., 2003).

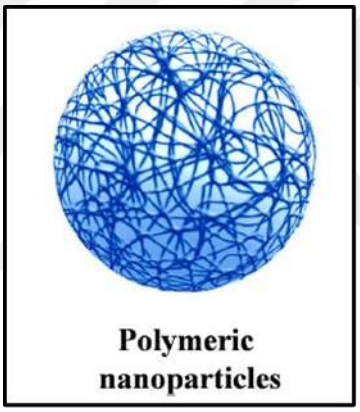

Figure 2.4. Structure of polymeric nanoparticles (Source: Singh et al., 2019).

Lipids: Liposomes are artificially constructed vesicles with a spherical morphology composed of cholesterol and non-toxic natural phospholipids. Their unique size, amphiphilic properties, and biocompatibility position liposomes as promising candidates for drug delivery systems (Akbarzadeh et al., 2013). Their favorable characteristics, including biocompatibility, biodegradability, and low toxicity, allow them to effectively encapsulate hydrophilic and lipophilic pharmaceuticals (Johnston et al., 2007). Furthermore, liposomes facilitate targeted drug delivery to tumor tissues, enhancing the specificity and efficacy of therapeutic interventions (Hofheinz et al., 2005).

Inorganic Carriers: inorganic nanoparticles generally possess versatile properties suitable for cellular delivery, including wide availability, rich functionality, good biocompatibility, the potential capability of targeted delivery (e.g., selectively

destroying cancer cells but sparing normal tissues), and controlled release of carried drugs (Xu et al., 2006). Quantum dots, carbon nanotubes, layered double hydroxides, mesoporous silica, and magnetic nanoparticles are commonly used in cancer treatment in various ways.

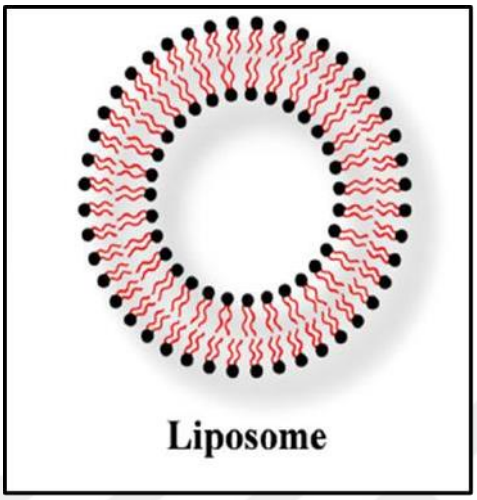

Figure 2.5. Structure of liposomes (Source: Singh et al., 2019).

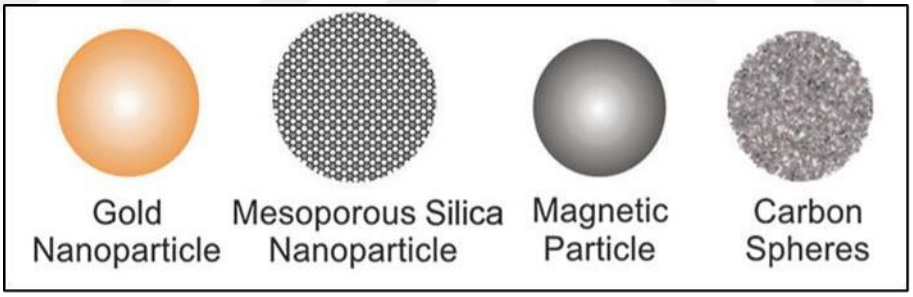

Figure 2.6. Structure of inorganic nanocarriers.

Polymeric Hydrogels: Hydrogels have been identified as effective options for controlled release, bioadhesive, and/or targeted drug delivery due to their ability to contain biomacromolecules such as proteins and DNA and hydrophilic or hydrophobic drugs. Drug delivery systems based on hydrogels can be applied in various ways, including oral, rectal, ocular, epidermal, and subcutaneous applications (Peppas et al., 2000). Additionally, hydrogels can serve as tools for 3D cell culture and as vehicles for drug delivery. Hydrogels stand out as ideal carriers for the controlled release and targeted delivery of anticancer drugs, thanks to their high-water content.

Protein-Based Nanocarriers: Protein-based nanocarriers are essential for drug transport because they have low cytotoxicity, abundant renewable sources, high drug-binding capacity, and significant uptake into the targeted cells. Moreover, the unique protein structure offers the possibility of site-specific drug conjugation and targeting using various ligands modifying the surface of protein nanocarriers (Elzoghby et al., 2012).

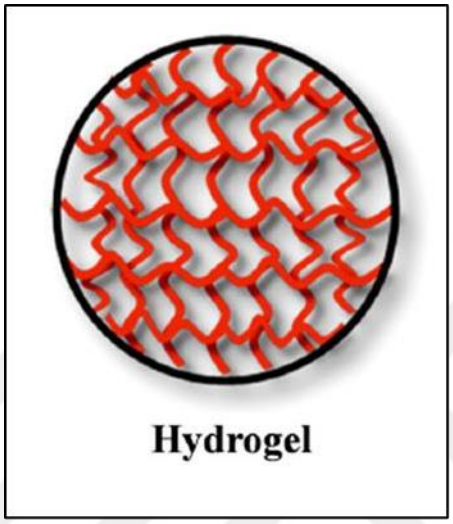

Figure 2.7. Structure of hydrogels (Source: Singh et al., 2019).

Micelles: Polymeric micelles serve as innovative drug delivery systems, exhibiting the capacity to target tumor sites through passive and active targeting mechanisms. Composed of amphiphilic block copolymers, these micelles are particularly adept at encapsulating poorly water-soluble and hydrophobic anticancer agents. Their physicochemical properties facilitate effective tumor targeting via the passive mechanism known as the enhanced permeability and retention (EPR) effect, which exploits the unique vascular characteristics of tumor tissues.

In addition to passive targeting, polymeric micelles can be tailored for active targeting through ligand coupling or incorporating pH-sensitive moieties. These modifications enhance their specificity for the biological characteristics of the diseased site, enabling a more directed approach to delivering therapeutics. Consequently, polymeric micelles emerge as ideal candidates for drug carriers aimed at selectively targeting cancerous cells, thus improving therapeutic efficacy while minimizing side effects (Ayre et al., 2013).

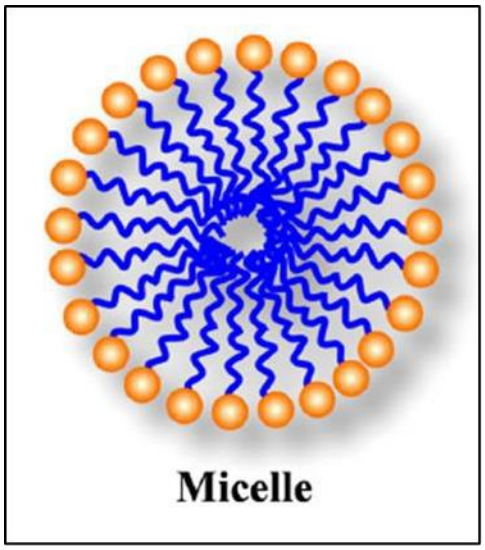

Figure 2.8. Structure of micelles (Source: Singh et al., 2019).

2.5. MICELLAR STRUCTURES AS DRUG DELIVERY VEHICLES

The tendency of the polar water molecules to exclude nonpolar molecules leads to attraction and spontaneous association (self-assembly) of the hydrophobic sections of a copolymer in an aqueous environment. A balance between this attraction and the affinity of the polar hydrophilic sections of a copolymer towards water leads to the creation of self-assembled micellar structures of well-defined size and morphology. The equilibrium position on the concentration scale is termed the Critical Micelle Concentration (CMC). The CMC is the minimum concentration required for the molecules to self-assembly, typically around the micromolar concentration range.

Such equilibrium means that micellization is a reversible process. The surfactant molecules are monomers at concentrations lower than the CMC and tend to accumulate at the air-water (or oil-water) interface. As the surfactant concentration increases, both the bulk and the interface are saturated, and at a specific concentration, the increased activity leads to self-aggregation (or self-assembly). However, the transition is not sharp for the polymeric micelles and is highlighted by the gradual formation of dimers, trimers, etc. (Polat and Chander., 1999). Hence, around the CMC, the micelles are loose and may contain some water in their core. They become more compact, durable, and smaller when the surfactant concentration increases. Further increases in surfactant concentration may lead to changes in micellar morphology, such as a transition from spherical to cylindrical

configuration. Micelle formation characteristics, hence, the CMC of a surfactant, are influenced strongly by the molecular structure, temperature, pH, presence of electrolytes, or other co-surfactants (Figure 2.9.), (Owen et al., 2012).

The morphology of a micelle can differ depending on the chemical structure, chain length, and concentration of the copolymer, which permits tuning the size and shape of the micelle for a specific application. For example, rod-shaped micelles have better mechanical stability; round-shaped micelles provide good colloidal stability; lamella-shaped micelles allow better control of shape and size distribution; worm-shaped micelles have a high tendency to bind and coalesce (Mondon et al.,2008) and cylindrically shaped micelles of simple surfactants are widely employed to prepare soft-templates in manufacturing micro-porous structures (Siretli, 2012).

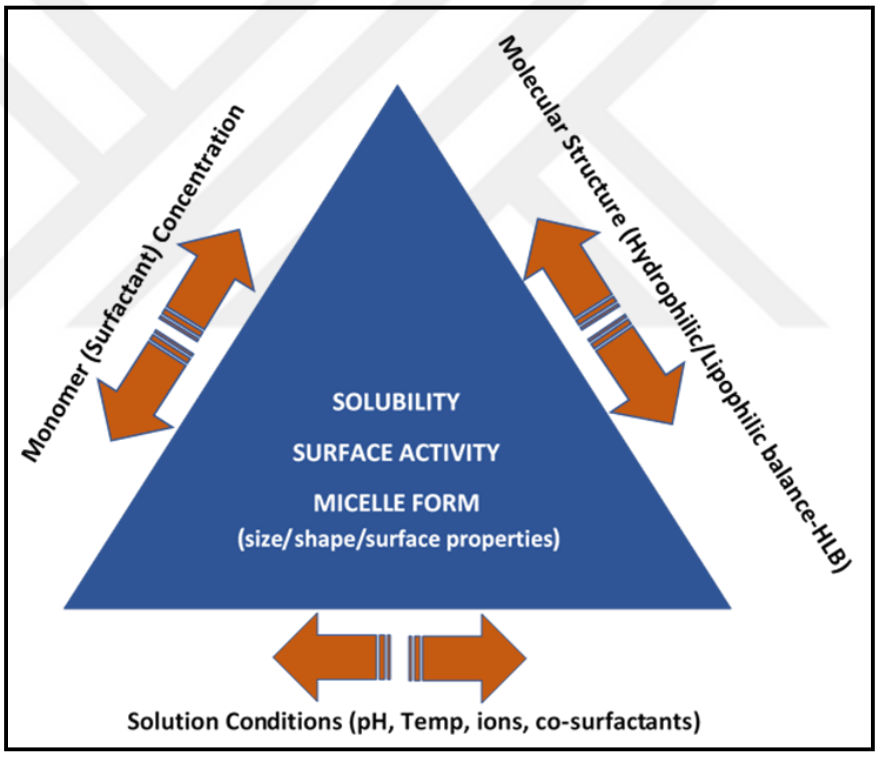

Figure 2.9. Factors that determine micelle formation and micelle properties.

2.6. ALTERNATIVE DRUG CARRIERS

Natural polymers have garnered significant attention due to their advantageous properties and potential applications in drug delivery systems. These biopolymers exhibit

a broad spectrum of functionalities in processes such as drug transportation, controlled release, and targeted therapy. Their unique characteristics—biocompatibility, biodegradability, low toxicity, and sensitivity to environmental conditions—make them particularly suitable for pharmaceutical applications (Adepu et al., 2021). Derived from natural sources, these polymers present several advantages over their synthetic counterparts, primarily their compatibility with biological systems, facilitating seamless integration within the body.

At the forefront of these advantages is biocompatibility. Natural polymers work in harmony with body tissues, minimize adverse reactions of the immune system, and do not cause inflammation (Harun-Or-Rashid et al., 2023). This feature is critical in situations that require long-term treatment. Another advantage is that natural polymers have biodegradable properties. These polymers, which can be biodegradable in the body, can be discharged naturally at the end of the treatment period without harmful accumulation or requiring additional surgical intervention (Kurowiak et al., 2023). This feature also provides an important advantage in terms of environmental and biological safety.

The other advantages are as follows. Natural polymers are generally non-toxic and can be used safely due to their compatible structures with biological systems (Satchanska et al., 2024). In addition, most natural polymers are sensitive to environmental factors (pH, temperature, enzymes), which create a suitable environment for controlled drug release. For example, pH-sensitive polymers protect the drug from gastric acid, allowing it to become active in the intestine (Rizwan et al., 2017). Natural polymers may contain biologically active groups, which enhance cellular interactions, allowing the drug to reach the target region effectively. Natural polymers can be customized by adding different functional groups through chemical modifications. These modifications not only alter the polymer's physical and chemical properties, such as its solubility, stability, and biodegradability, but also enable the drug-carrying systems to exhibit desired characteristics like controlled release, biocompatibility, and targeting ability. As a result, natural polymers have gained significant attention as versatile carriers in drug delivery systems. Their adaptability makes them suitable for a wide range of biomedical applications, including tissue engineering, wound healing, biosensors, and regenerative medicine, where they can contribute to the development of innovative therapeutic strategies and improve patient outcomes.

2.6.1. Chitosan

Chitosan, found in nature as the only cationic polysaccharide, is formed because of the deacetylation of chitin found in the exoskeleton of crustaceans (e.g., shrimp, crab, and lobster). In recent years, chitosan has received increasing attention due to its unique properties and its use in many fields. Its biodegradability, non-toxicity, and good biocompatibility enable chitosan to be used in medical applications as an antimicrobial and wound-healing biomaterial (Baharlouei et al., 2022).

The presence of amino groups in chitosan allows for protonation, giving the polymer a positive charge and contributing to its water solubility and mucoadhesive properties. This positive charge enhances its interaction with negatively charged surfaces, such as mucosal and basal membranes, leading to increased permeability (M. Ways et al., 2018). As positively charged chitosan molecules attach to negatively charged cell walls, they can induce cell death by binding to DNA and inhibiting its replication (Hossain et al., 2022). Furthermore, chitosan's cationic nature endows it with antimicrobial, antibacterial, and antitumor activities. Its glucosamine component also provides anti-inflammatory benefits, effectively managing conditions like arthritis (Desai et al., 2022).

Chitosan is a natural polymer with functional groups such as two hydroxyls and one amino group in its backbone. According to the structure, chitosan is a potential pH-responsive polymer because its amines are protonated and positively charged at low pH, making it a water-soluble cationic polyelectrolyte (Shikuku et al., 2024). In addition, thanks to the functional groups in the structure, a significant number of modifications are allowed, producing polymers with new properties and behaviors.

Chitosan derivatives have been produced to improve chitosan's properties, such as solubility or biodegradability, or introduce new functions or properties. Thanks to the modifications, chitosan can be used as bio-sourced materials, biomaterials, drug/enzyme delivery vehicles, tissue engineering scaffolds, adhesives, texturing agents, support for enzyme immobilization, bioactive agents, etc., used in many fields (Rezaei et al., 2021). Chitosan modification can be done in three ways: physical modification, chemical modification, and molecular imprinting. Physical modifications, such as blending with other polymers or the incorporation of nanoparticles, can enhance the mechanical properties and biocompatibility of chitosan. Chemical modifications, including the

attachment of functional groups or cross-linking, allow for the customization of chitosan for specific applications, such as targeted drug delivery or controlled release systems.

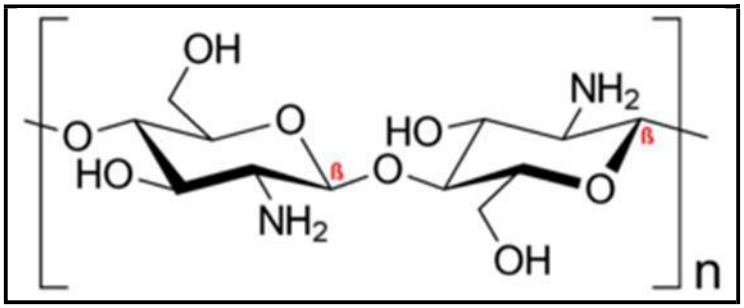

Figure 2.10. Molecular structure of chitosan (Source: Atanase et al., 2021).

2.6.2. Fucoidan

Fucoidan is a sulphurized polysaccharide found in marine marshes, especially in brown marsh species, and it has attracted the scientific community's attention in recent years. This natural component was first discovered in 1913 and has been extensively studied for its various biological properties and therapeutic potential. Fucoidan consists of sulfate groups and other sugar components such as galactose, mannose, and xylose, along with a sugar unit primarily called fucose. This complexity in its structure gives the fucoidan rich biological activity and makes it a popular component in the health, cosmetics, and food industries.

One of the most remarkable features of Fucoidan is its powerful anticoagulant effect. This property offers significant potential in preventing blood clotting, especially in the treatment of cardiovascular diseases. Research has shown that fucoidan can inhibit blood clotting processes and thus reduce the risk of circulatory diseases such as thrombosis (Wang et al., 2019). In addition to this biological effect, fucoidan's blood lipid-regulating effects also stand out as an additional benefit to supporting heart health (Wang et al., 2022).

Antitumor activity is another important biological feature of fucoidan. Various laboratory and animal studies have shown that fucoidan can inhibit the growth of some cancer cells, induce programmed cell death called apoptosis, and prevent tumor angiogenesis (the process of tumors forming blood vessels). These effects have led to the

potential use of fucoidan as a supportive agent in cancer treatment (Cao et al., 2021). Furthermore, the ability of fucoidan to target only cancer cells without damaging healthy cells makes it a very valuable natural compound.

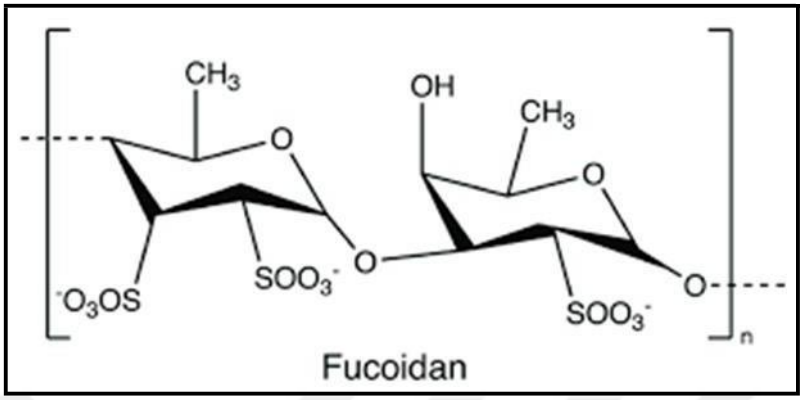

Figure 2.11. Molecular structure of fucoidan (Source: Lin et al., 2022).

The positive effects on the immune system are another feature that highlights the fucoidan. Its ability to modulate the immune system means that fucoidan can increase the body's resistance to infections and balance immune response. This provides a potential benefit in treating autoimmune diseases, infections, and general weakness of the immune system (McFadden et al., 2023). Fucoidan can also play a protective role against infections caused by certain viruses due to its antiviral effects (Oliyaei et al., 2022).

Finally, fucoidans' anti-inflammatory and antioxidant properties are among the important biological functions that support overall health and well-being. Its ability to reduce inflammation can be useful, especially in managing chronic inflammatory diseases. Its antioxidant effects can slow the aging process and reduce the risk of various degenerative diseases by protecting cells from oxidative stress caused by free radicals (Sanjeewa et al., 2021). With all these properties, fucoidan has gained a unique place among natural therapeutic agents, becoming an important component of scientific research and industrial applications. Furthermore, fucoidan's potential to enhance immune function and promote wound healing further adds to its therapeutic value. Its ability to interact with cellular receptors and modulate signaling pathways makes fucoidan a promising candidate for use in drug delivery systems and as an adjuvant in cancer therapy.

2.6.3. Alginate

Alginate is a natural polysaccharide found primarily in sea snails, especially brown snails (Phaeophyceae). It plays a structural role in cell walls, increasing the water retention capacity of plants and providing mechanical stability (Abka-Khajouei et al., 2022). This polysaccharide comprises a linear sequence of mannuronic acid (M) and guluronic acid (G) units. The properties of alginate vary depending on the ratio and distribution of the M and G blocks it contains, allowing it to be used in various applications.

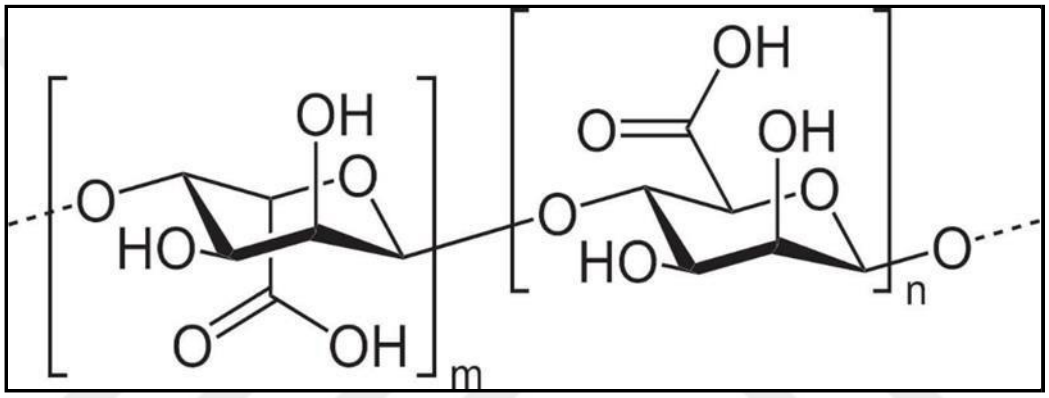

Figure 2.12. Molecular structure of alginate (Source: Mahmoodi et al., 2011).

One of the most essential features of alginate is its ability to gel quickly when in contact with water. This gel formation capacity is precious, especially in biomedical applications. Alginate gels are ideal for wound coverings, tissue engineering, drug transport systems, and cell culture because of their biocompatibility and biodegradability (Lee et al., 2012). Alginate-based wound coverings keep the wound moist by accelerating the healing process and reducing the risk of infection (Aderibigbe et al., 2018). In addition, alginate gels can be designed as systems that can provide controlled drug release, which offers significant advantages in patients' treatment processes.

In the medical field, alginate's biocompatibility and non-toxic structure make it possible to be used in applications such as implants, prosthetics, and cell transplants. Alginate-based substances can be dissolved in the body over time and discharged naturally, providing a safe solution for long-term biomedical applications (Lee et al., 2012). In addition, alginate hydrogels are widely used in cell culture studies and tissue

engineering applications, providing an environment similar to the natural environment of cells (Andersen et al., 2015). Alginate can form a three-dimensional skeleton that supports the proliferation and differentiation of cells, enabling the development of new tissues in vitro (Zhu et al., 2022).

As a result, alginate is a versatile biopolymer with a wide range of applications. Its properties vary according to the ratio of mannuronic acid and guluronic acids, allowing it to be used for various purposes in different industries. From wound coverings in the biomedical field, drug transport systems, and coating agents in the food industry, alginate's natural, biocompatible, and versatile properties have made it an indispensable material for research and industrial applications. In the future, it is envisaged that alginate could further expand its potential uses and offer innovative solutions.

2.7. MODIFICATION METHODS FOR CHITOSAN

Due to the nature of chitosan, its applicability has some limitations. For example, factors such as solubility, pH resistance, and mechanical properties can be shown. Some chemical modifications are needed to bring such properties to the desired state. Chemical modifications additionally increase the chitosan structure's thermal stability, oxidation resistance, and antibacterial properties (Wang et al., 2020). Chitosan contains one amino, primary, and secondary hydroxyl group. These groups are active for modification, and the hydroxyl groups are located at carbons C-3 and C-6 of the cyclic structure. The hydroxyl group at the C-6 position makes the structure more suitable for modification due to the difference in the steric hindrance of the C-3 and C-6 carbons to which the hydroxyl groups are attached (Argüelles-Monal et al., 2018). Chemical modifications are named according to the functional group to which they are connected (Figure 2.13).

Shiff base modification is an amine functional group modification. It can be used for two purposes. The first of these is to modify the amino group in the structure of chitosan and make it suitable for the purpose to be used, and the second is to use it as a preservative. It protects the amino group of structures such as fatty aldehydes or aromatic aldehydes/ketones, which are attached to the amino group, and ensures that the modification occurs through the hydroxyl groups. At the end of the reaction, structures such as fatty aldehydes and aromatic aldehydes/ketones attached to the amino group can

be removed from the chitosan structure by using an acid. Changes in the antibacterial, anticancer, and antioxidant properties of chitosan were observed with the modifications made with the Schiff base reaction (Zhang et al.,2010).

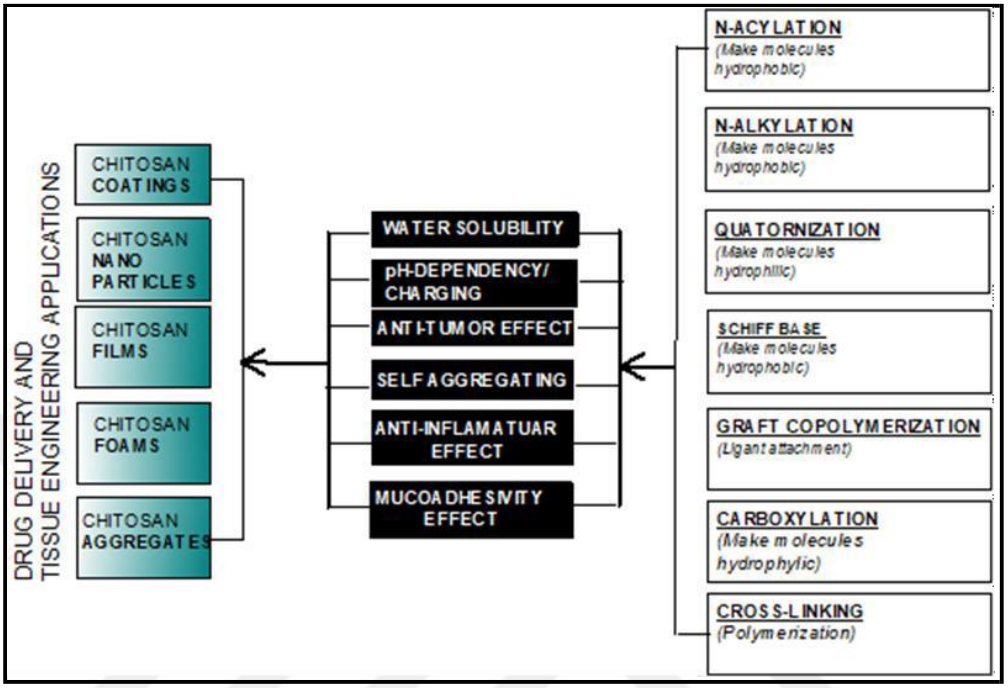

Figure 2.13. Modification methods with the properties of chitosan.

Carboxylation, a unique method, is a modification method applied to the structure of chitosan to form a solubility film and to make the material moist. This modification method is carried out using acid. The acid can bind to each functional group in the structure of chitosan. O-carboxymethylated chitosan in the presence of monochloroacetic acid and sodium hydroxide, N-carboxymethylation, and N-O-carboxymethylation reactions occur when the temperature is applied. Halogenated hydrocarbons of hydroxyl and amino groups in the structure of chitosan reactions can be carried out in an alkaline medium using sulfate or sulfate and are called o-alkylation and n-alkylation modification, respectively (Wang et al., 2020). There is a type of modification in which the amine and hydroxyl groups in the chitosan structure are modified by using organic compounds such as anhydrides and halides, called acylation. Since the amino group of chitosan is more active than the hydroxyl group, the modification takes place over the amine group.

Quaternization reaction, on the other hand, is the amine group modification. It is carried out using a quaternary ammonium salt derivative. There are two types of derivatives used for modification: direct and grafting. In addition, there is another method

called sulfonation, in which the bone structure of chitosan can be modified by using sulfonate groups. It can bind to amine and hydroxyl functional groups (Fabiano et al.,2020).

Grafted copolymerization modification occurs over the amino group attached to the C-2 carbon of chitosan and is formed by the covalent binding of specific monomers to the chitosan structure. In the cross-linking modification, which is another modification method, the monomers of two different or the same chitosan molecules are bonded to each other through amino groups. In this way, it is possible to obtain drug-carrier molecules resistant to high temperatures (Purohit et al., 2023).

Sodium-phosphorylated chitosan is suitable for clinical applications, including pharmaceutical drug delivery. It is a water-soluble phosphate derivative of chitosan. This type of chitosan structure also contributed to having hydrophobic character along its backbone. It has an excellent ability to encapsulate the model hydrophobic drug. The proportion of R sites that are phosphate or hydrogen moieties depends upon the degree of substitution (DS) of phosphate (Chongprakobkit et al.,2013).

Sulfonate groups could be attached directly to free amino groups producing sulfamate products(-NH-SO_3-). The sulfonation reaction may occur on hydroxyl groups, resulting in sulfated products (-O-SO_3-). Sulfated chitosan has a similar structure to heparin in the blood so has anticoagulant properties, but this type of modification increases water solubility and the higher hydrophilicity resulting from the sulfation. There is no exact information about the hydrophobic properties of sulfonated chitosan (Yang et al., 2015). However, one article states that sulfonation increases the chitosan structure's hydrophilic properties (Xu et al., 2017). Even if the amino groups are known to be more nucleophilic compared to hydroxyl groups, the chemical substitution could occur at three key positions in the glucosamine and acetyl glucosamine residues: C-2, C-3, and C-6 positions carrying amino, secondary, and primary hydroxyl groups, respectively. This gives rise to N-modified, O-modified, or N, N-O-substituted chitosan by one-step or multiple-step reactions. Among the strategies, N-alkyl-O-sulfated chitosan shows amphiphilic character and displays the ability to form micelles of size around 100-400 nm.

2.8. CHEMICAL BONDING OF CHITOSAN AND DRUG

Chemical bonding of chitosan and docetaxel is an innovative method to increase cancer treatment's effectiveness. Chitosan is a biopolymer known for its biocompatibility and biodegradability, and docetaxel is a potent chemotherapeutic agent. Conjugation of these two compounds aims to increase the efficacy of the treatment by improving the solubility, stability, and targeted delivery of docetaxel (Lee et al., 2009).

Chitosan is obtained by deacetylation of the polymer chitin. Chitin is extracted from the shells of crustaceans such as crabs and shrimps and chemically processed. Chitosan's biocompatibility and biodegradability make it an ideal candidate for drug delivery systems. Chitosan's amino groups provide reactive sites for chemical bonding. Docetaxel is chemically activated. This process is accomplished by adding reactive groups to the docetaxel molecule. Reactive groups facilitate bonding with chitosan and form a stable conjugate. This bonding is usually accomplished through ester or amide bonds. Ester bonds are formed between carboxyl and hydroxyl groups, while amide bonds are formed between amino and carboxyl groups (Liu et al., 2013).

Chitosan-docetaxel conjugates are processed to form nanoparticles. These nanoparticles provide controlled release and targeted delivery of docetaxel. When used as a drug delivery system, nanoparticles increase the bioavailability of the drug and reduce side effects. The biodegradability of chitosan allows the nanoparticles to break down safely in the body (Wang et al., 2018).

Chitosan-conjugated docetaxel has several advantages. First, chitosan increases the solubility and stability of docetaxel, making it more effective in the body. Second, conjugation allows for more precise targeting of cancer cells, which reduces damage to healthy tissue and minimizes side effects. Third, chitosan nanoparticles provide a controlled release of docetaxel, providing a sustained therapeutic effect (Liu et al., 2013). This chemical bonding process increases the bioavailability of docetaxel and reduces its side effects. The biocompatibility and biodegradability of chitosan make this combination a promising option for cancer treatment. In preclinical studies, chitosan-conjugated docetaxel has increased anticancer efficacy and improved treatment outcomes (Mirzaie et al., 2016).

In conclusion, the chemical bonding of chitosan and docetaxel is an innovative approach to cancer treatment that can potentially improve a patient's quality of life and

treatment outcomes. Further exploring how this technology is applied to specific cancer treatments presents an exciting avenue for future research.

CHAPTER 3

MATERIALS AND METHODS

3.1 Materials

In this study, analytical-grade chemicals were used only. Low molecular weight chitosan powder obtained from Sigma Chemical Company was used to prepare partially N-acylated chitosan. Acetic acid was used to prepare a 1% (v/v) aqueous acetic acid solution. Benzoic anhydrides were used to modify chitosan.

Docetaxel, a potent lipophilic anticancer drug, was the model drug. It is freely soluble in DMSO (C_2H_6OS), dimethyl sulfoxide, DMF $(CH_3)_2NCH$), dimethylformamide, and Ethanol (CH_3OH) but utterly insoluble in water. Albumin from bovine serum (BSA) was used as the model protein to mimic human serum albumin (HSA). All chemicals were purchased from Sigma Aldrich.

Simulated body fluid (SBF) is an electrolyte solution with an ionic strength like human blood plasma. It was buffered at pH 7.4 with 50 mM tris-hydroxy methyl aminomethane (Tris or THAM, $(HOCH_2)_3CNH_2$) and 45 mM hydrochloric acid at 37 ℃. The composition of the body fluid prepared for this study is presented in Table 1.

Table 1. The composition of the body fluid prepared (Source: Polat et al., 2020).

Reagents	NaCl	$NaHCO_3$	KCl	K_2HPO_4 .$3H_20$	$MgCl_2$.$6H_2O$	HCl*	$CaCl_2$	Na_2SO_4	Tris
Amount (g)	7.996	0.350	0.224	0.228	0.305	40 ml	0.278	0.071	6.57

** from 1 Molar solution*

3.1.1. Pluronic P123

P123, also known as Pluronic® P123, is a triblock copolymer and nonionic surfactant with the PEG-PPG-PEG structure. Its structure contains polyethylene oxide (PEO) and polypropylene oxide (PPO) blocks in the PEO-PPO-PEO sequence. These copolymers with the PEO-PPO-PEO structure can form structures such as micelles and vesicles in water-based solutions. P123 has found many uses in drug delivery systems thanks to these properties. It is primarily used to increase the bioavailability of therapeutic agents that have low solubility and are rapidly degraded at physiological pH. P123 encapsulates hydrophobic drugs in the hydrophobic PPO core, while the PEO outer layer interacts with water to ensure the stability of the drug delivery micelles (Zhao et al., 2017).

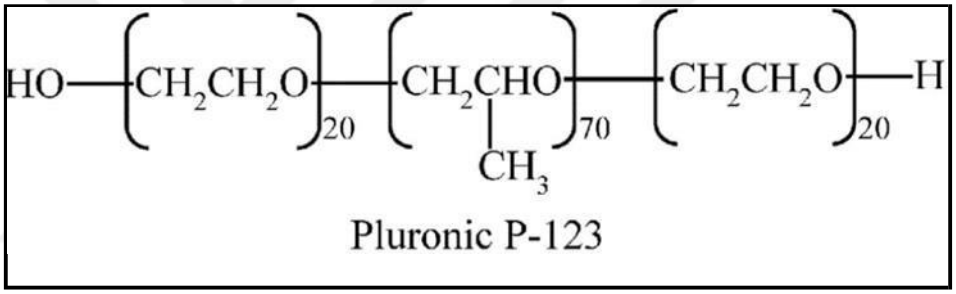

Figure 3.1. Molecular structure of P-123 (Source: Dash et al., 2022).

3.1.2. Docetaxel

Docetaxel (Figure 3.2) is a taxoid antineoplastic agent used in the treatment of various cancers, such as locally advanced or metastatic breast cancer, metastatic prostate cancer, gastric adenocarcinoma, and head and neck cancer (Lyseng-Williamson et al., 2005). Docetaxel inhibits the cell's microtubule structures. Microtubules are components of the cell's apparatus for division and replication. Cell death occurs when these structures are inhibited. Docetaxel is particularly effective against rapidly dividing cancer cells but can also affect the body's healthy, rapidly dividing cells. The side effects that occur when these healthy cells die are as follows; Muscle pain, Joint pain, Missed menstrual periods,

Temporary hair loss, Nausea, and Vomiting. To reduce these side effects, targeted drug carrier systems should be developed.

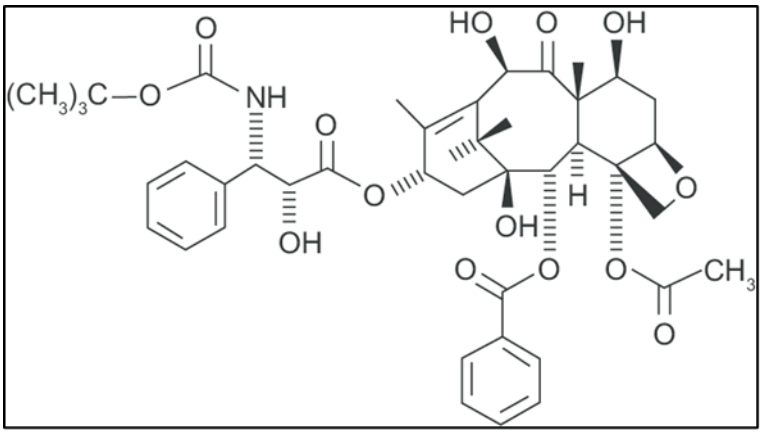

Figure 3.2. Structure of docetaxel (Source: Alken et al., 2013).

3.2. Methods

3.2.1. Synthesis Methods

3.2.1.1 Preparation of Docetaxel-Loaded P-123 Micelles

The triblock copolymer (P123) will first be dissolved in ethanol, and the drug will also be prepared in ethanol. These two solutions will be combined and subjected to evaporation in a vacuum oven to remove the solvent, forming a thin film. Following this, water will be added to the film, promoting the self-assembly of micelles that encapsulate the drug. A schematic representation of this process can be found in Figure 3.3. The stability of the resulting micellar systems will be assessed under various conditions, including simulated body fluid (SBF) and distilled water, with and without the presence of a protein (Bovine Serum Albumin, BSA). Dynamic Light Scattering (DLS) will be employed to measure size distribution and evaluate stability. Furthermore, the morphology of the micelles will be characterized by using Scanning Transmission Electron Microscopy (STEM) and Transmission Electron Microscopy (TEM).

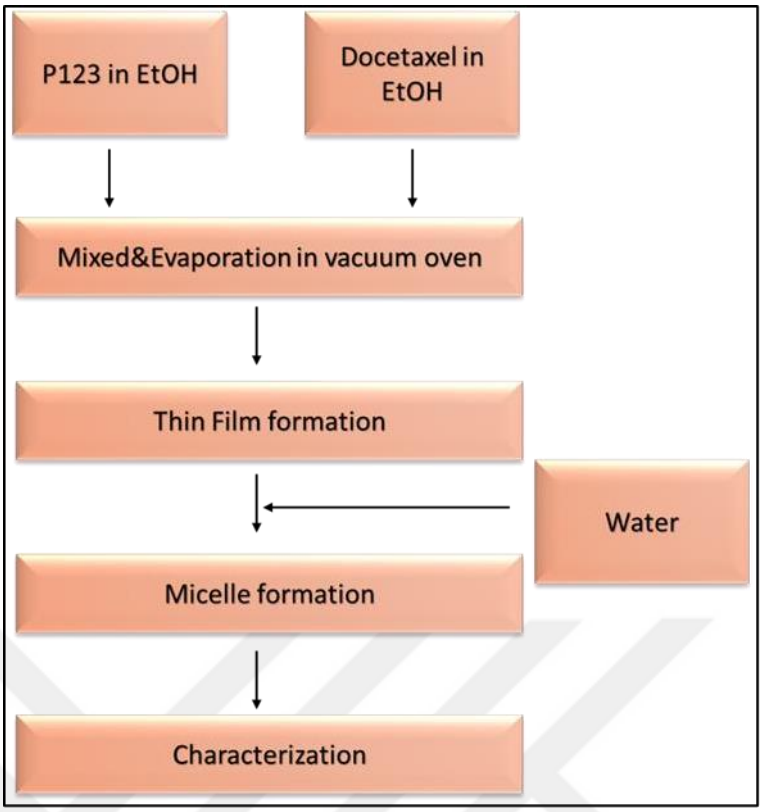

Figure 3.3. Flow sheet of the synthesis method for drug-loaded- P123 micelles.

3.2.1.2 Preparation of Docetaxel-Loaded Modified Chitosan Micelles

Chitosan will be modified with different kinds of anhydride by using the N-acylation method. The modified chitosan will be characterized by FTIR and NMR. Then, both the modified chitosan and the drug will be dissolved in an acetic acid solution and mixed to keep in the vacuum oven until the solvents evaporate. Then the known amount of water will be added to the thin films formed to prepare the micelle solutions. Then, the stability of these systems will be tested by dilution in both simulated body fluid and distilled water in the absence and presence of a protein (BSA will be used in this study) using size distribution measurements (DLS). The morphology of the micelles will be examined by STEM and TEM images. Also, micelles and drug interaction will be examined by FTIR. The general methodology of bio-polymer modification and its relation to micellization is given in Figure 3.4.

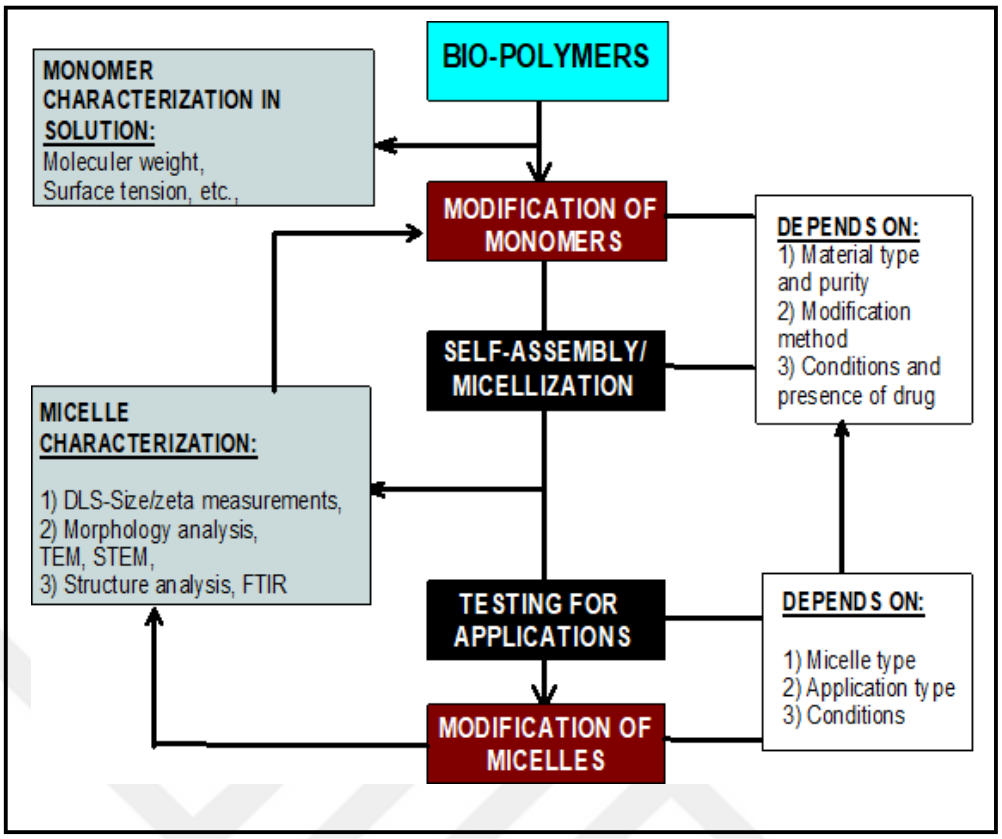

Figure. 3.4. The general methodology of bio-polymer modification and its relation to micellization.

3.2.1.3. Hydrophobic modification of Chitosan: Production of Partially N-Acylated Chitosan

Chitosan derivatives were obtained by partially N-acylation because Chitosan has a highly reactive free amine group that offers great potential for N-acylation (Ramos, et al., 2003). Benzoic anhydride was used for the N-acylation. For this reason, chitosan was acylated with these reagents. To a solution of chitosan (1g) in 100 ml, aqueous acetic acid 1 % (v/v) solution at room temperature, and the solution was stirred overnight to ensure total solubility. Molar equivalent (0.1, 0.5, and 1) of benzoic anhydrides was dissolved in methanol at a ratio of 2% (w/w) (Lee et al., 1995). After that, an acid anhydride-dissolved methanol solution was poured into a chitosan solution and stirred for 1 hour. Then a mixture of methanol aqueous solution of ammonia (7/3, v/v, 100 ml.) was added to the chitosan-acid anhydride solution, and a polymer precipitate was obtained. Then the polymer precipitate was filtered off and washed with methanol and with diethyl ether to

get rid of unreacted acid anhydrides. Finally obtained precipitates were dried at 40 ℃ under vacuum for two days.

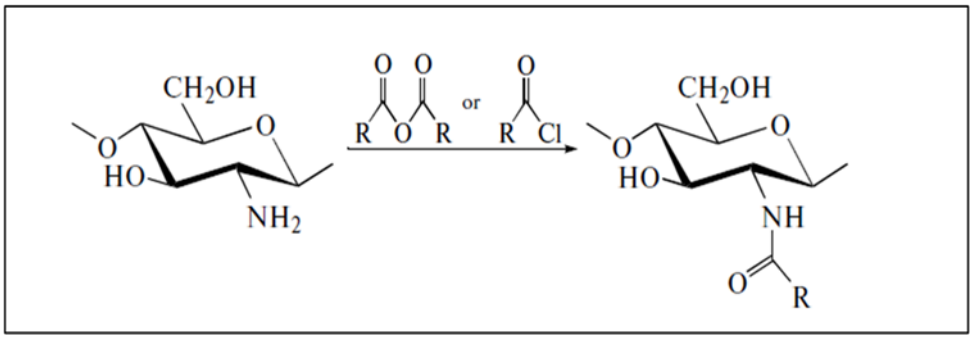

Figure 3.4. N-acylation of chitosan with an acid anhydride.

3.2.1.4. Production of Chitosan-Docetaxel Conjugation

First, Docetaxel (DOC) (100 mg, 0.12 mmol), succinic anhydride (22 mg,1.8 equiv.), and DMAP (0.5 mg, 0.033 equiv.) were dissolved in dry dichloromethane (DCM, 5 mL). After stirring for 24 h at room temperature, DCM in the reaction mixture evaporated under reduced pressure, and ethyl acetate (20 mL) was added. Then the organic phase was collected and washed with HCl (1%, w/v) twice and ultrapure water twice. Magnesium sulfate was added to the organic phase and stayed overnight to remove the remaining water. Next, ethyl acetate was evaporated under reduced pressure to get a concentrated solution of the desired product (2 mL). The final solution was subjected to SiO_2 column chromatography for purification with petroleum ether: ethyl acetate (1:2, v/v) as the mobile phase. The fluid phase for chromatography was removed under reduced pressure and dried under vacuum to get dry powder of succinyl-DTX (Lee et al., 2008).

In the next step, 25 mg of succinyl-Doc (0.027 mmol), 13 mg of EDC·HCl (2.5 equiv.), and 14 mg of sulfo-NHS (2.5 equiv.) were dissolved in 3 mL mixture of THF: H2O (50:50) and reacted for 12 h at room temperature to afford the sulfo-NHS ester form of succinyl-DTX. In the final step, 50 mg of CMCS (0.001 mmol) was dissolved in 20 mL of a mixture of THF: H_2O (50:50) and mixed with the sulfo-NHS succinyl- DTX solution in the previous step. After stirring for 24 h at room temperature, the reaction mixture was dialyzed with a dialysis bag (Sigma–Aldrich, molecular weight cut off: 8000–14000 Da) against PBS (phosphate buffered saline, pH 7.4) for 48 h to remove

organic solvents and unreacted reagents. CMCS–DTX conjugates could self-assemble into nanoparticles as the dialysis process went on. The formed CMCS–DTX nanoparticles were sterile filtrated.

3.2.1.5. Biological Tests

The human Caco-2 colorectal adenocarcinoma epithelial cells were maintained in Minimum Essential Medium (MEM) supplemented with 20% (v/v) fetal bovine serum, 1% penicillin-streptomycin solution, 1% (v/v) non-essential amino acid solution and 1% sodium pyruvate. The cells were cultured under standard conditions of 5% CO_2 and 95% O_2 at 37 °C. A total of 4×10^5 cells per well were seeded into 96-well sterile cell culture plates and allowed to adhere for 12 hours. Subsequently, the cells were treated with 5, 10, or 25 µL of the water solutions for 24 hours. Cell viability was assessed using the WST-8 cytotoxicity assay. Briefly, after treatment, the cells were rinsed with phosphate-buffered saline (PBS), followed by the addition of 100 µL of complete cell culture medium containing 10 µL of WST-8 solution per well. The plates were incubated for 4 hours at 37 °C in a cell culture incubator. Absorbance was measured at 460 nm using a Thermo Scientific Multiskan GO spectrophotometer to quantify cell viability. Then the cell death percentages were calculated using this data.

3.2.2. Characterization of Micellar Structures

A Dynamic Light Scattering device (DLS/ZP, Zetasizer, Nano ZS) was used to measure micellar structure size to study micelles' dilution stability in DW and SBF with protein BSA and without BSA.

The morphology of micelles was examined using scanning transmission electron microscopy (STEM) and transmission electron microscopy (TEM). Samples for STEM and TEM analysis were prepared on a copper-covered carbon grid. Additionally, the particle size distribution of the micelles was analyzed to further investigate their stability and surface charge characteristics, providing more detailed insights into their behavior in different environments and their potential for use in drug delivery applications.

Table 2. Characterization methods used in this study.

Analysis	Method	Device
Micellar Size	DLS	Malvern Zetasizer Nano ZS
Micellar Charge	DLS-LDV	Malvern Zetasizer Nano ZS
Micelle Morphology	STEM	Quanta 250 SEM

3.2.3. Characterization of Partially N-Acylated Chitosan (Hydrophobically Modified Chitosan Molecules)

Determination of Substitution Degree: Two different methods were used to determine the substitution degree of chitosan. These are the ninhydrin assay and FTIR methods. In the ninhydrin assay method, modified chitosan samples were dissolved in acetic acid (3% w/v) and hydrochloric acid (1% w/ v) solutions, and 0,5 ml acetate buffer was added to each modified chitosan solution. 2 ml ninhydrin reagent were added to solutions and tubes were placed in a boiling water bath for 20 min. After cooling, their absorbances were read at 570 nm by using a Horiba-Duetta UV-VIS spectrometer. The degree of substitution was evaluated by FTIR spectra. The ratio of absorbance at 1655 cm^{-1} amide-I band at the hydroxyl band at 3450 cm^{-1} applying the equation proposed by Moore and Roberts:

$$DS\% = [(A_{1655} / A_{3450}) - 0.25] \times 100 \qquad \text{Equation (1)}$$

Where DS % is the degree of substitution and the value of 0.25 represents acetyl groups that exist in commercial chitosan (Tien et al., 2003).

Determination of Molecular Weight: Viscometry was used to the molecular weight of chitosan. The intrinsic viscosity of the polymer is related to its molecular weight according to the Mark-Houwink-Sakurada relation (Equation (2), (Kasaaı, 2007).

$$[\eta] = K[M_\upsilon]^\alpha \qquad \text{Equation (2)}$$

whereas [η] is the intrinsic viscosity, M_υ is the average molecular weight of the polymer, and K and α are related to the percentage of deacetylation degree (DD %) and obtained from the literature. The equations are given below Equation (3) and Equation (4).

$$K = 1.64 \times 10^{-30} \times DD^{14.0} \qquad \text{Equation (3)}$$

$$\alpha = -1.02 \times 10^{-2} \times DD + 1.82 \qquad \text{Equation (4)}$$

In addition, the solvent system and the temperature also depended on the DD % of chitosan. Therefore, the corresponding solvent system was acetic acid/sodium acetate (0.2 M HAc/0.1 M NaAc) at 30 ℃ for DD %75. The stock solution of chitosan was prepared in a way that 0.25 g chitosan was dissolved in 200 mL of 0.2M HAc / 0.1M NaAc solvent system and lower concentrations (0.0000, 0.0100, 0.0125, 0.0250, 0.0375, 0.0625, 0.0875, 0.1250 w/v) were prepared from this stock solution and diluted with the same solvent. Kinematic viscosity measurements of chitosan solutions were carried out by using PETROTEST kinematic viscosity apparatus; an Ubbelohde U-Tube capillary viscometer with 0.004720 CST/s2 viscosimeter constant (C). The capillary viscosimeter was filled with the sample then the sample was passed through the capillary, and the running time was measured. Each measurement was repeated three times. The sample or solvent viscosity was calculated. For the calculation of intrinsic viscosity, (Tsaih and Chen, 1999) were used which is the intercept of the equation derived from a plot of reduced viscosity versus concentration of chitosan solution (g/mL). The molecular weight of chitosan was calculated according to Equation (2).

FT-IR Analysis: The structure of modified chitosan was investigated using FTIR-ATR spectra recorded using a Perkin Elmer Spectrum-FTIR spectrometer in a frequency range of 4000–400 cm^{-1}.

X-Ray Diffraction: XRD analysis was performed using a Philips X'Pert Pro instrument. X-ray diffraction data were collected by using a Cu anode with 0.154056 nm wavelength (λ) in 5-50 θ. The sample's crystallographic properties and the changes in crystallinity of chitosan caused by partial N-acylation were obtained. By using XRD data, the crystal size of samples (t) was also calculated with the application of the Debye Scherrer equation:

$$t = \frac{0.9\lambda}{\beta cos\theta}$$

where 0.9 is the shape factor, λ is the X-ray wavelength, typically 1.542 Å, β is the line broadening at half the maximum intensity in radians, and θ is the Bragg angle, which is the angle of the incident beam and lattice plane, which comes from the theoretical basis of X-ray diffraction.

Surface Tension Measurement: KRÜSS Digital-Tensiometer K10ST measured the surface tension. Thin films were formed from modified chitosans, and thin films were dissolved in distilled water. The surface tensions of the solutions were measured using the Du Nouy Ring method.

Contact Angle Measurement: In this study, the KRÜSS Contact Angle Measurement System G10 instrument was used to measure contact angle values in N-acylated chitosan/air/water systems. The basic parts of this instrument are a light source, sample stage, and microscope as it is a goniometer. Goniometry comprises the observation of liquid droplets on a solid surface and tensiometry that contains measuring the forces of interaction as solid contact with a liquid. Solid disks were prepared from each type of partially N-acylated chitosan for contact angle measurement. Solid disks were prepared before the samples were dried.

Zeta Potential Measurements: The Zeta potential of modified and unmodified chitosan molecules in diluted AcA solutions was determined using the Malvern Zetasizer ZS Nano. The Zeta potential of modified and unmodified chitosan molecules in dilute AcA solutions was determined using the Malvern Zetasizer ZS Nano.

CHAPTER 4

P-123 MICELLES AND THEIR STABILITY

4.1. Size and zeta potential of BSA in DW and SBF Solutions

The bovine serum albumin is a globular protein with dimensions 4x4x14 nm (corresponding to an equivalent volume diameter of 6.1 nm) (McClellan and Franses, 2003). Since BSA is a biological homolog of HSA, it displays similar ligand-binding properties, and is readily available at low cost (Ketrat et al., 2020), it is widely employed as an HSA replacement in many biochemical and pharmacological applications

Figure 4.1. (a) shows the size distributions of protein molecules in distilled water at different concentrations. It was observed that the average size of protein molecules in distilled water was 3 nm, and the size did not change significantly with increasing concentration. Figure 4.1. (b) shows the size distributions of protein molecules in SBF at different concentrations. The average size of BSA molecules is significantly larger in SBF solutions. The average size of 6.5 nm in 0-3 M BSA becomes slightly smaller as BSA concentration increases. These observations agree with the values reported in the literature. The observed increase in the hydrodynamic diameter of protein molecules in SBF solutions is most probably due to the aggregation of molecules. The slight size decrease observed with increasing BSA concentration could be due to the hydrodynamic hindrance of these larger molecules at high concentrations.

Figure 4.2. (a) presents the measured zeta potentials of protein molecules in both SBF and deionized water (DW). The zeta potential of protein molecules is quite different whether they are dissolved in DW or SBF solutions. It is shown that the charge of BSA molecules at DW pH is significantly negative with an average zeta potential of about -25 mV. When protein molecules are placed in SBF solution, the negative charges are somewhat neutralized, and the average zeta potential shifts towards zero. This is most likely the reason for the reported decrease in solubility and the aggregation behavior observed in our DLS size measurements.

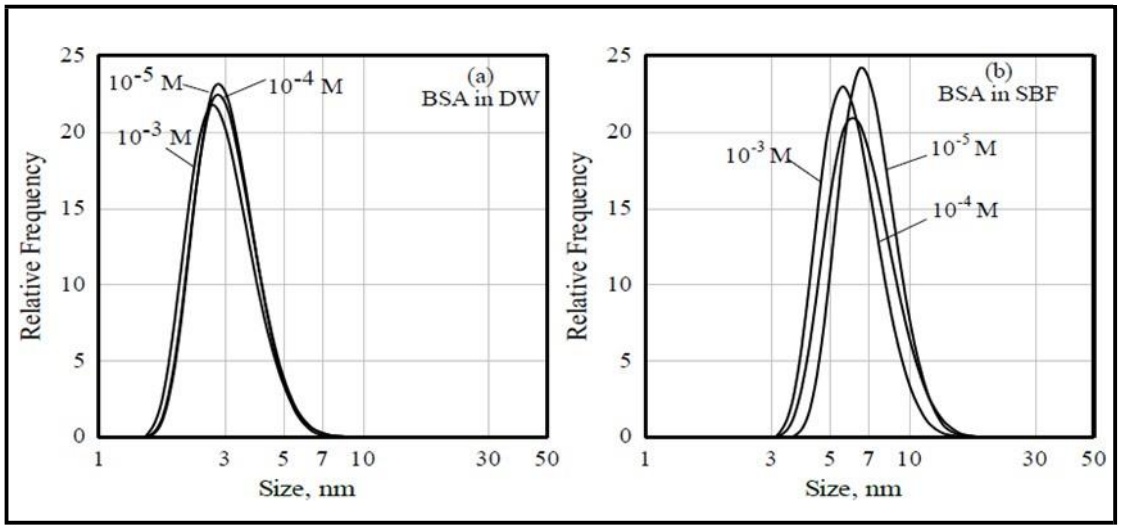

Figure 4.1. Size distributions of the BSA molecules in situ as a function of BSA concentration in a) DW and b) SBF solutions.

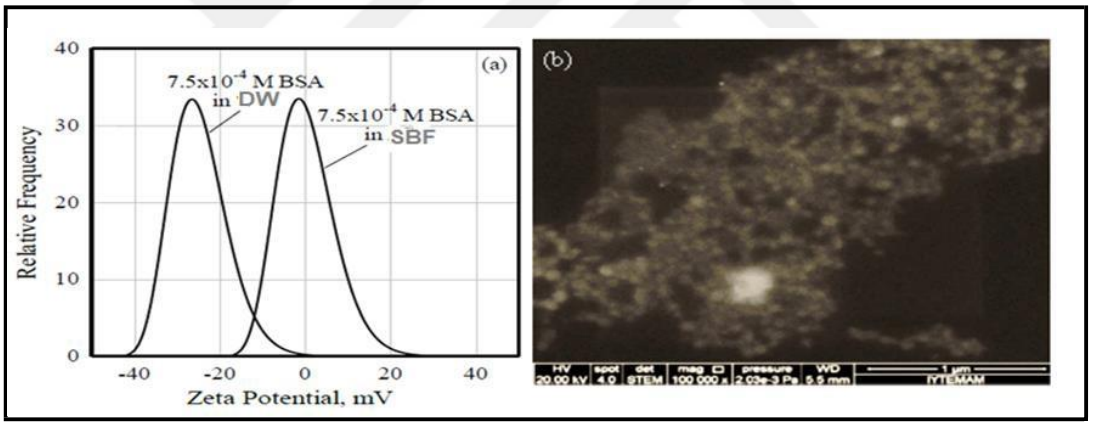

Figure 4.2. a) Zeta potentials of the BSA molecules in situ in DW and SBF solutions; b) STEM picture of the BSA molecules.

4.2. Barren P-123 micelles in DW and SBF solutions

4.2.1. Stability of the barren P-123 micelles in DW and SBF

Polymeric surfactant P-123 of the Pluronic® series was used to form micelles in DW and SBF solutions using the thin film hydration method. The surfactant concentration in the micelle solutions was always 10^{-3} M. The barren P-123 micelles formed were characterized using DLS measurements and STEM imaging. Figure 4.3. (a) shows the size distribution in protein-free DW and SBF solutions after 1 h of formation. The average micelle size in both cases is approximately 16 nm. Despite the well-defined shape and accurately measurable dimensions of P-123 micelles, it should be noted that the size determination of monomers of these surfactants using DLS is unreliable. We are aware of literature claims that monomers of these surfactants are compact, probably with PEO chains forming a relatively tight shell with a hard sphere radius of 1.15 nm around the unhydrated PPO core. However, it is our experience that during size measurements using DLS, the size distribution of P-123 monomers fluctuates greatly and never settles into a well-defined distribution curve; this most likely results in an oscillatory signal in this measurement technique due to the dynamic anisotropic geometry of monomer molecules in water. When BSA molecules were added to the barren micelle medium, the BSA concentration of $7.5x10^{-4}$ M was chosen since the HSA concentration in plasma ranged from $5x10^{-4}$ M to $9x10^{-4}$ M. Figure 4.3 (b) shows the size distribution of micelles 1 hour after they were introduced into the protein solution. The data shown in Figure 4.3 (b) are extremely important: As seen in Figure, when fully formed micelles prepared in DW solutions are brought into contact with BSA molecules, their size decreases from 16 nm to slightly less than 3 nm. Considering that 3 nm is close to the molecular size of BSA molecules in DW, previously intact micelles are broken down in the presence of BSA. DLS measures only the size of protein molecules. The experiment with the SBF solution further strengthens this observation. The 16 nm micelle size observed in SBF solutions of empty micelles decreases to approximately 7 nm when fully formed micelles are brought into contact with protein molecules. Since the average size of protein molecules in SBF solutions is 7 nm Figure 4.3. (b), it can be said that the presence of protein

molecules causes the complete disintegration of micelles into monomer species in SBF solutions as well.

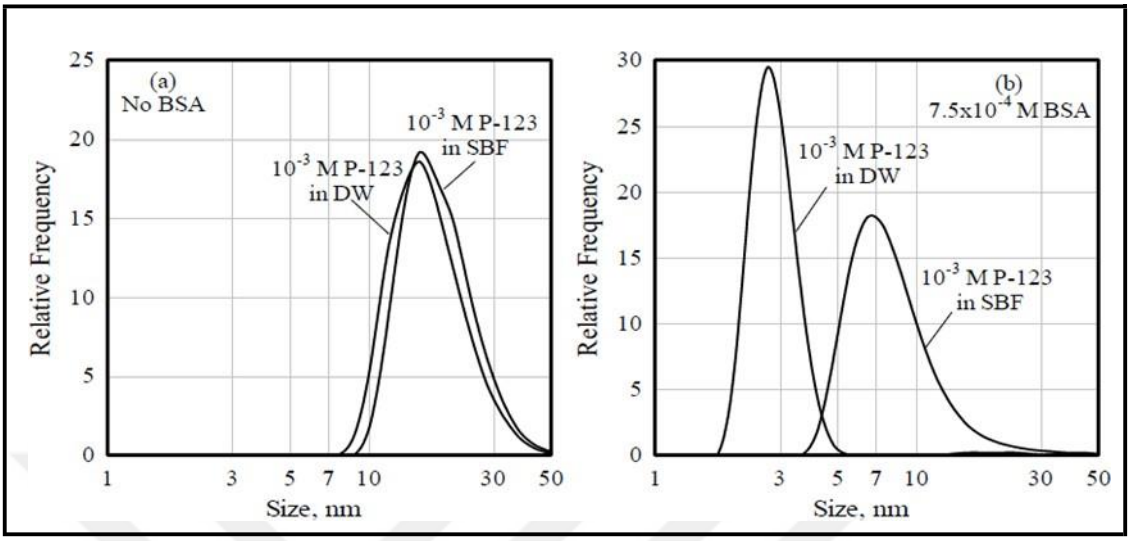

Figure 4.3. Size distributions of the barren micelles (10^{-3} M P-123) in-situ in DW and SBF solutions 1 hour after they have been formed a) in the absence of BSA, and b) in the presence of $5x10^{-4}$ M BSA.

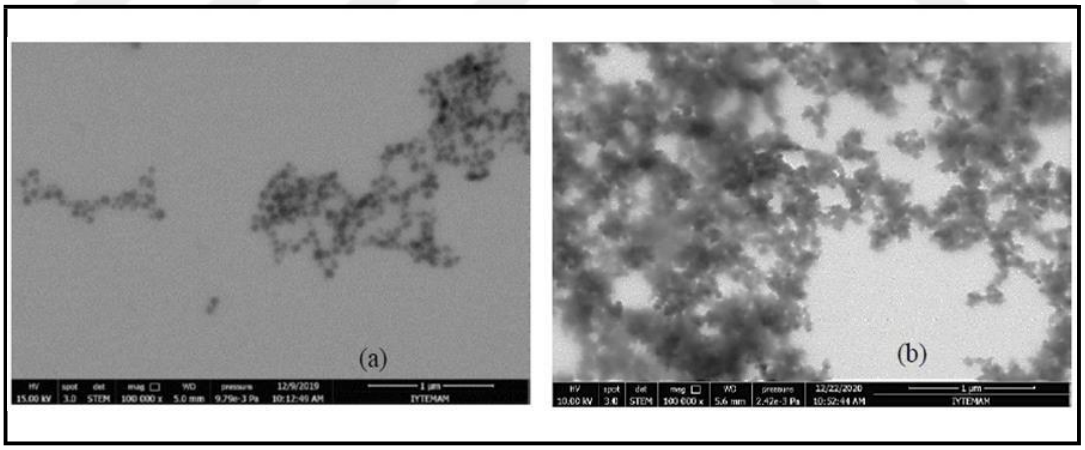

Figure 4.4 STEM images of the barren micelles (10^{-3} M P-123) in a) DW and b) SBF solutions.

The STEM images are presented in Figures 4.4. (a) and 4.4. (b) provide a clear depiction of micelle aggregation. In Figure 4.4. (a), the distinct spherical shapes of the micelles, immobilized from a distilled water (DW) solution, are prominently displayed, showcasing their individual structure. However, upon examining Figure 4.4. (b), it

becomes apparent that these micelles have undergone some degree of aggregation. This clustering likely occurred during the immobilization process on carbon grids, particularly as the micelles were subjected to drying after being extracted from the salt solution, leading to their closer association.

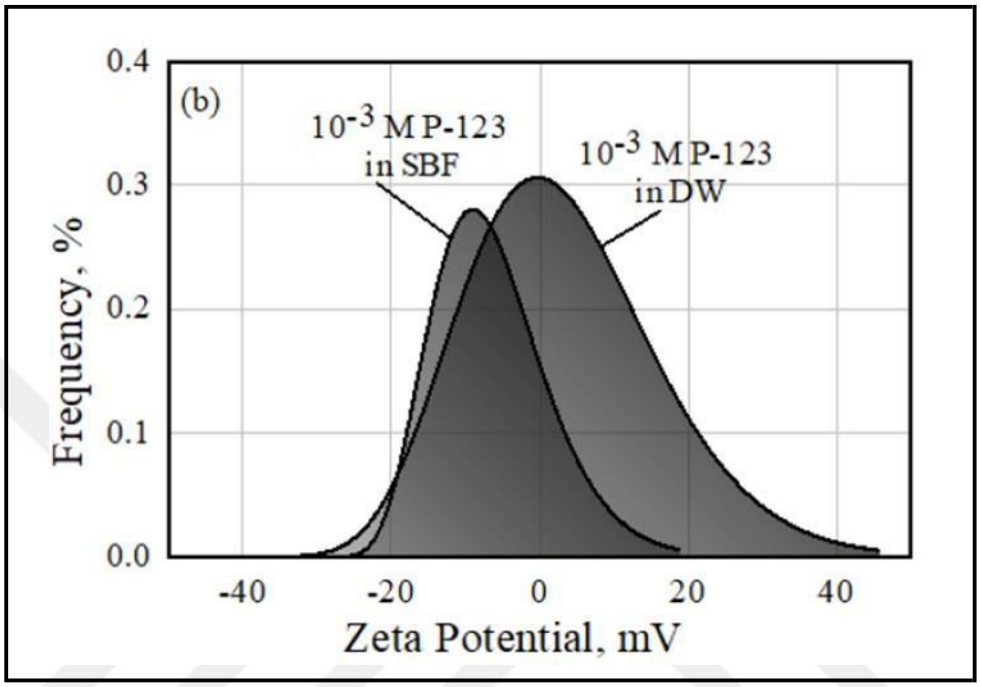

Figure 4.5. Zeta Potentials of P-123 micelles in DW and SBF solutions.

The zeta potential analysis of the 10^{-3} M P-123 micelles conducted in deionized water (DW) and simulated body fluid (SBF) (Figure 4.5) revealed a broader charge distribution for the micelle population in DW, with values ranging from -40 to +40 mV. Despite this variability, the average zeta potential hovers around zero, suggesting a predominantly non-ionic characteristic of the copolymer. In contrast, the charge distribution in the SBF solution is more constrained, falling between -20 and +20 mV. This narrowing is likely attributable to the ionic species in the solution, which may inhibit the presence of highly charged sites on the micelles, resulting in a notable shift of the mean charge towards the negative range.

4.2.2. Stability of the barren P-123 micelles in DW and SBF as a function of the age of the micellar solutions

The stability and size distribution of micelles are crucial factors in their performance for various applications, particularly in drug delivery systems. In this study, we investigate the time-dependent behavior of micelle size in both distilled water (DW) and simulated body fluid (SBF), as well as the impact of protein doping on micellar stability. Figures 4.6. (a) and 4.6. (b) show the DLS size distributions of micelles over time. The label '1 hour' refers to freshly prepared micelles, while '1 day' and '10 days' indicate the age of the micelle solutions stored at room temperature without mixing. Figure 4.6. (a) displays that the mean micelle size remains at 16 nm for up to ten days in distilled water (DW), indicating that micelle formation is a quick process, and the micelles are stable in DW over extended periods under ambient conditions.

In contrast, Figure 4.6. (b) shows that in simulated body fluid (SBF), the mean micelle size increases slightly from 16 nm to 18 nm as the solution ages from 1 hour to 10 days. Figures 4.6. (c) and 4.6. (d) present the effect of aging of protein-doped micellar solutions. Once disintegrated, the surfactant molecules do not self-assemble again with time in the presence of the protein molecules.

The spectra of the P-123 micelles and the BSA are presented in Figure 4.7. It can be seen that clearly, P-123 shows strong major peaks corresponding to the C-H stretching and bending vibrations in the range of 2850-3000 cm^{-1} and 1460 cm^{-1}, respectively. Additionally, the peaks located at 1377 cm^{-1} and 1350 cm^{-1} are assigned to the characteristic stretching modes of the ether (-C-O-C-) functional groups present in the P-123 micelle structure the peak observed at 3299 cm^{-1} corresponding to the stretching vibrations of hydroxyl (-O-H) groups, which are commonly associated with hydrogen bonding and the overall hydration environment of the protein. The absorption bands at 1656 cm^{-1} and 1535 cm^{-1} are characteristic of the amide I and amide II bands, respectively, which primarily arise from the stretching and bending vibrations of the peptide bonds within the protein backbone. When the spectra of the P-123 micelles are obtained in the presence of BSA, both the P-123 and the bovine serum albumin peaks preserve their structure and are visible. This indicates that if there are any interactions between the P-123 micelles and BSA molecules they are physical of origin and do not include any chemical bonding as suggested by (Liu et al., 2005).

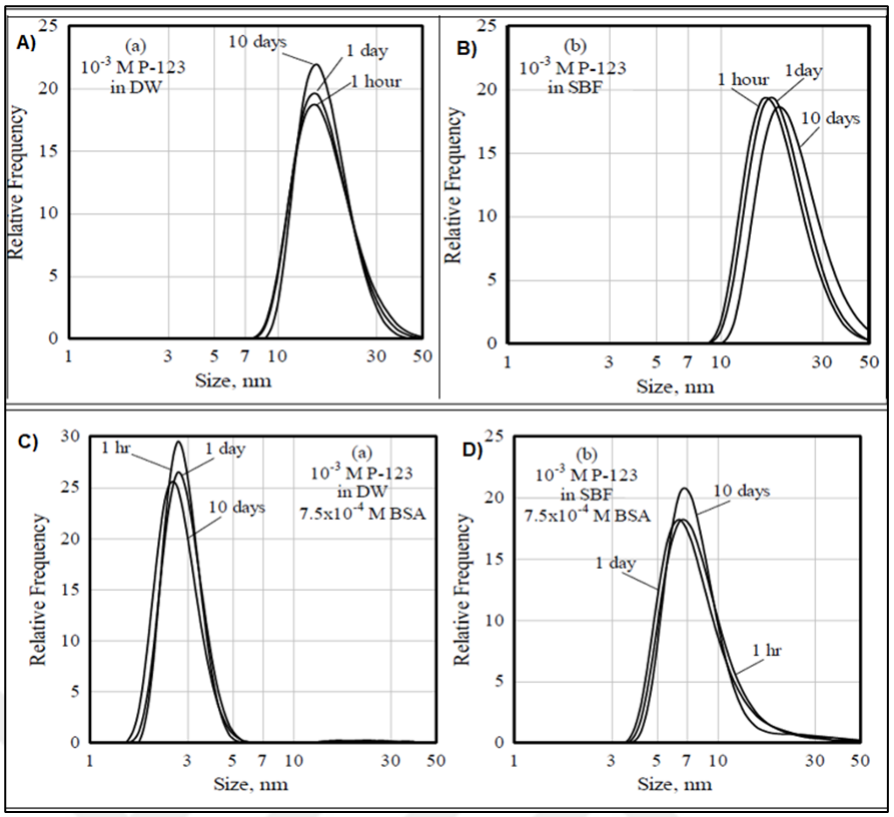

Figure 4.6. Size distributions of the barren micelles (10^{-3} M P-123) in situ in a) DW and b) SBF solutions in the absence of BSA and c) in DW and d) SBF solutions in the presence of $7.5x10^{-4}$ M BSA as a function of the age of the micellar solutions.

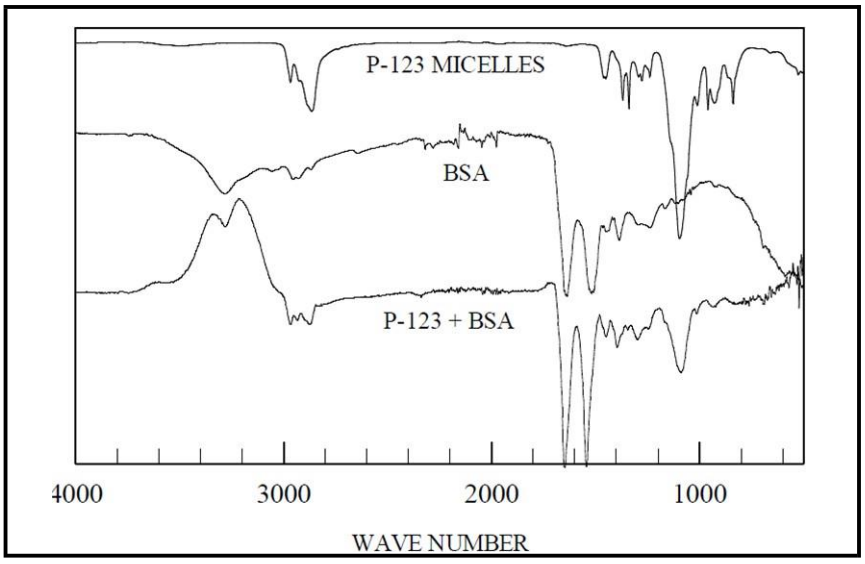

Figure 4.7. FTIR spectra of P-123 micelles and the BSA separately and when they are together in DW solution.

4.3. Docetaxel-loaded P-123 micelles in DW and SBF solutions

The loading of the P-123 micelles with the strongly hydrophobic anticancer drug (Docetaxel) by a modified thin-film hydration method was described in the previous sections. The final concentration of the drug in the micelles was 10^{-4} M, and FTIR, DLS, and STEM characterized the drug-loaded micelles.

4.3.1 Determination of Entrapment Efficiency of Docetaxel-loaded P-123 Micelles

A calibration curve is constructed by plotting the absorbance of solutions with varying concentrations of docetaxel against their corresponding drug concentrations. Figure 4.8 shows the calibration curve of the docetaxel solution at different concentrations, which follows Beer Lambert's law.

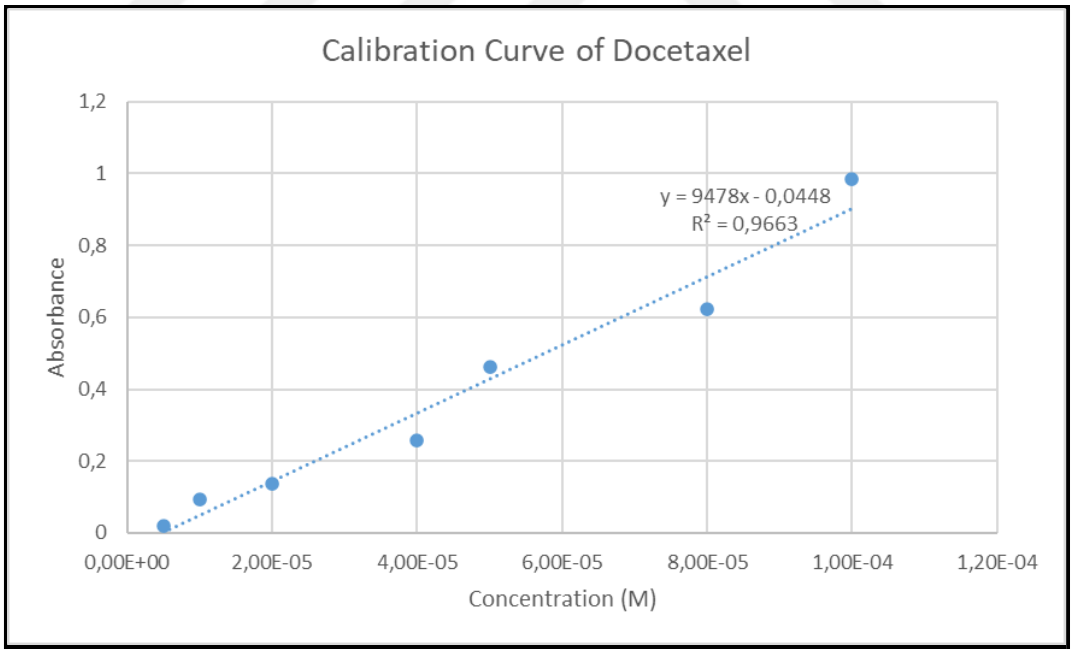

Figure 4.8. Calibration Curve of Docetaxel in Ethanol.

To calculate the entrapment efficiency of docetaxel-loaded P123 micelles, the formed micelles were passed through 25 nm membrane filters. The clear supernatant solution was analyzed with a UV spectrophotometer at λ max value of 237 nm, shown in

Figure 4.9. Using these UV results, the entrapment efficiency of the drug was calculated using the following equation:

$$= \frac{total\ amount\ of\ drug - free\ drug\ in\ the\ supernatant}{total\ amount\ of\ drug} x100$$

Using these UV results, the drug entrapment efficiency was calculated using the equation above. The entrapment efficiency of drug-loaded micelles was found to be 85.19%. The highest entrapment efficiency value of P-123 micelles indicates that the micelle system can effectively retain the drug, and the formulation is generally successful. This suggests that the micelles effectively encapsulate the drug in the hydrophobic cores, and the free drug is low. A high value indicates the system can provide a longer, controlled release.

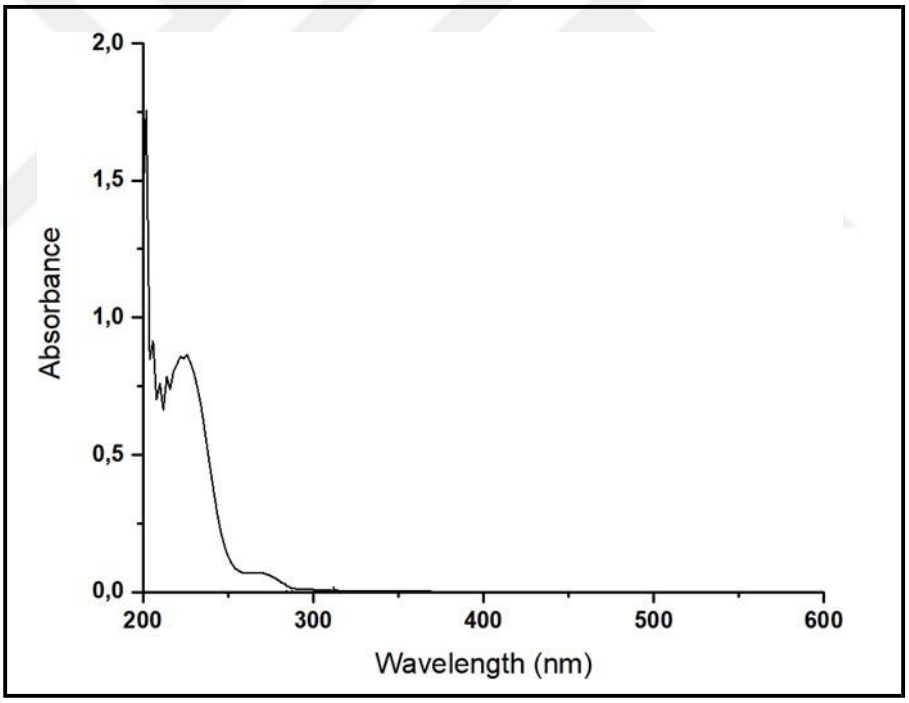

Figure 4.9. Absorbance spectra of supernatant solution of docetaxel-loaded P-123 micelles.

4.3.2 Stability of the drug-loaded P-123 micelles in DW and SBF

Micelle-based drug delivery systems have gained significant attention due to their ability to encapsulate hydrophobic drugs and enhance their solubility. Understanding the stability of these micelles over time is crucial for ensuring their effectiveness as drug carriers. The size distributions of docetaxel-loaded micelles after 1 hour of preparation in DW and SBF solutions in the absence of BSA are presented in Figure 4.10. (a) and 4.10. (b). The behavior of drug-loaded micelles is very similar to that of non-drug-loaded micelles for both DW and SBF solutions. Figure 4.10 also shows the size distributions of drug-loaded micelle solutions after 1 day and 10 days of storage. Based on this graph, it can be said that the micelle size does not change with aging and the micelles maintain their integrity even after 10 days of storage in both DW and SBF solutions.

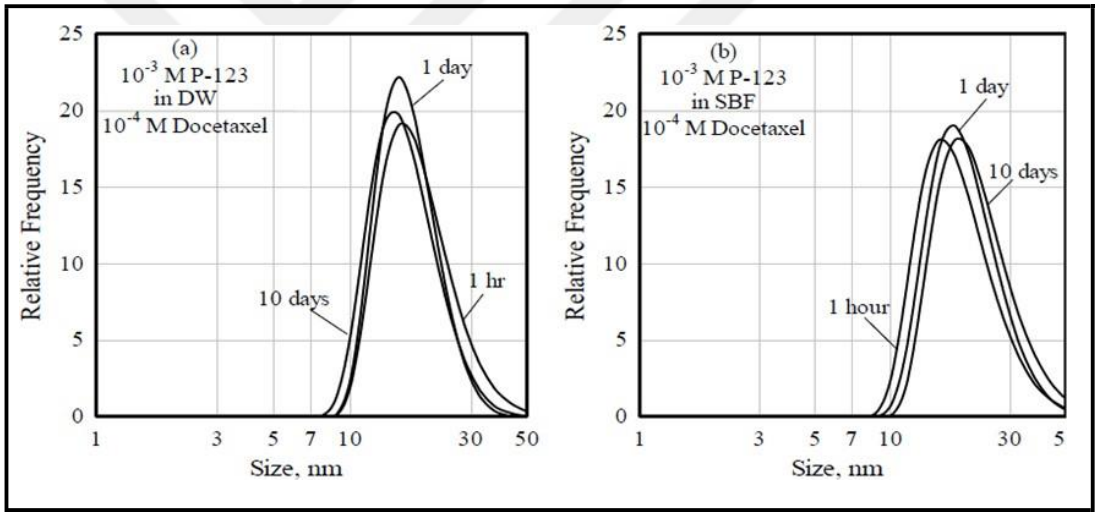

Figure 4.10. Size distributions of the Docetaxel-loaded (10^{-4} M) micelles (10^{-3} M P-123) in situ in the absence of BSA in a) DW and b) SBF solutions as a function of the age of the micellar solutions.

STEM photographs of fresh micelles loaded with Docetaxel in DW solution without BSA are presented in Figure 4.12. (a). As can be seen in the figure, the drug-loaded micelles in the absence of BSA are slightly larger and have well-defined spherical shapes. In addition, STEM photographs of fresh micelles loaded with Docetaxel in DW solution in the presence of BSA are presented in Figure 4.12. (b). The STEM image shows that the drug-loaded micelles in the presence of BSA do not show clearly defined spherical shapes, but instead, they are in the form of aggregated spots, indicating the

disruption of micelle integrity. The spots observed in the figure may be due to the aggregation of broken micelles during drying on carbon grids.

Figure 4.11 presents TEM photographs of P123 micelles loaded with docetaxel in the DW solution. The dense area visible in the image indicates micelle aggregation has occurred. Drug-loaded micelles generally show increased electron density (darker regions) because the electron density of the core increases when the drug is loaded. Based on these images, it can be said that the drug has been successfully loaded.

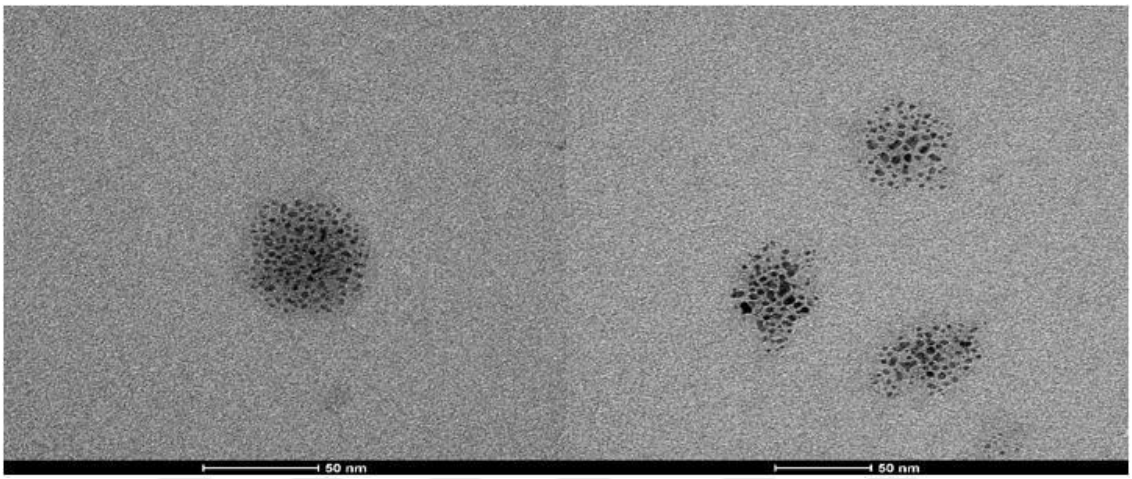

Figure 4.11. TEM images of the Docetaxel-loaded (10-4 M) micelles (10-3 M P-123) in DW.

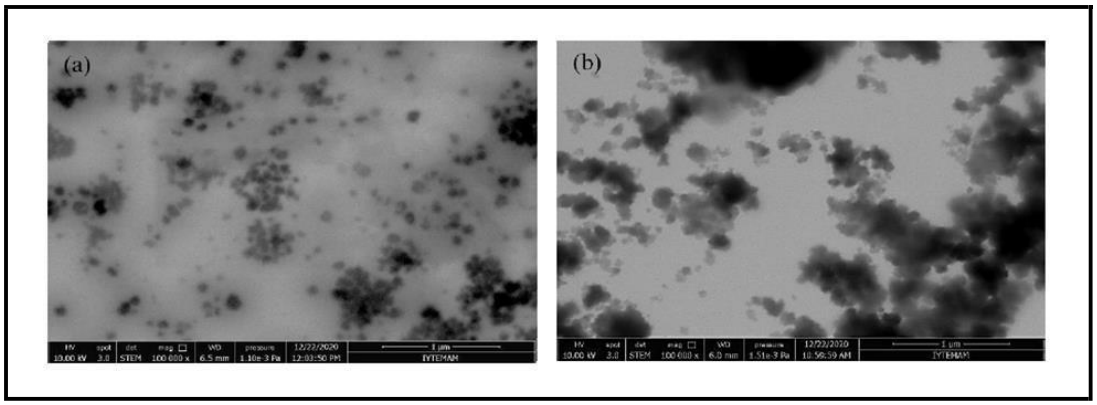

Figure 4.12. STEM images of the Docetaxel-loaded (10^{-4} M) micelles (10^{-3} M P-123) in DW solutions a) in the absence of BSA and b) in the presence of $7.5x10^{-4}$ M BSA (after immobilization on carbon grids of the 1 hr micelle solutions).

Figures 4.13. (a) and 4.13. (b) show the Docetaxel-loaded micelle size distributions as a function of dilution in the absence of bovine serum albumin. In this case, drug-loaded, fully formed micelles were transferred to the appropriate amount of blank distilled water or simulated body fluid solution to obtain the desired dilution concentrations between 10^{-3} M P-123 (undiluted) and 10^{-6} M P-123 (diluted one thousand times). In the distilled water case, the onset of dilution results in an increase in micelle size due to the initial swelling of the micelles followed by a sudden decrease in size below 2 nm, indicating micelle disintegration. However, the effect of dilution on micelle size in simulated body fluid solutions is surprising. The micelle size increases with dilution up to 10^{-6} M. This behavior suggests that micelles swell significantly to form loose aggregates but do not disintegrate completely in the electrolyte solution.

As shown in Figure 4.14. (a) and 4.14. (b), the size distribution of drug-loaded micelles changes with varying concentrations of the protein bovine serum albumin. In the distilled water case, the presence of 10^{-4} M BSA does not cause significant micelle disintegration, while increasing the BSA concentration to 10^{-3} M causes complete disintegration. A protein presence seems to affect micelle integrity when above a specific concentration severely. It is very important to note that this concentration is very close to the upper limit of the plasma concentration of human serum albumin (HSA). For SBF, the drug seems to have a gradual effect, but when the concentration of BSA is 10^{-3} M in the presence of the drug, the micelles dissolve completely, obtaining a value like that achieved by barren micelles at the same concentration. As a result of the presence of the drug, a significant change in the size of the micelles does not appear to be significantly influenced.

Despite the dissolution of micelles under specific conditions, the overall size distribution of the micelles in the presence of the drug does not exhibit a significant change. This indicates that while the drug interacts with the micelles, it does not substantially alter their aggregation behavior or cause major structural rearrangements under normal conditions. These observations provide valuable insights into the behavior of drug-loaded micelles in biological environments, particularly in the presence of serum proteins, which play a crucial role in drug delivery applications.

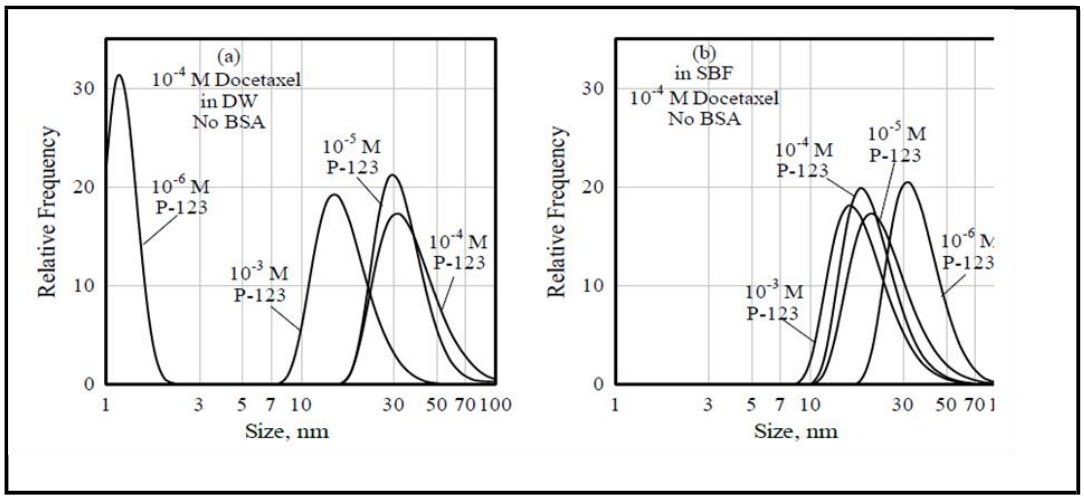

Figure 4.13. Size distributions of the Docetaxel-loaded (10^{-4} M) micelles (10^{-3} M P-123) in situ in a) DW and b) SBF solutions in the absence of BSA as a function of varying degrees of dilution.

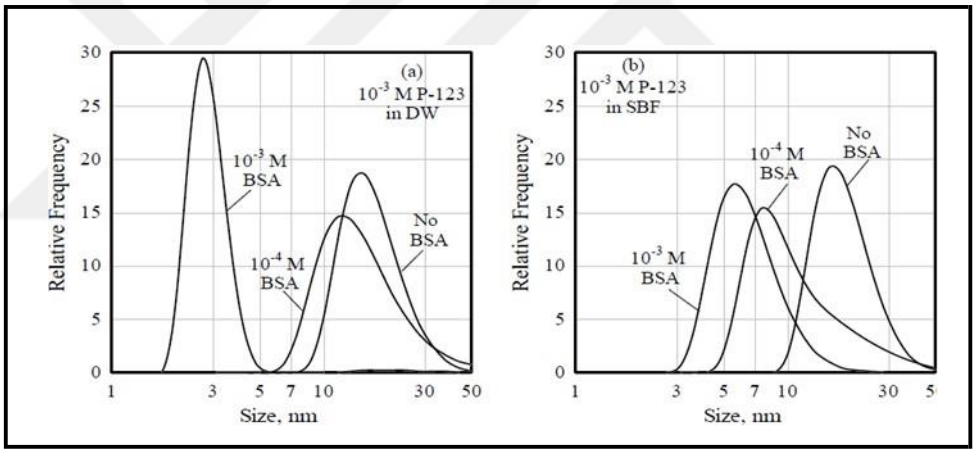

Figure 4.14 Size distributions of the Docetaxel-loaded (10^{-4} M) micelles (10^{-3} M P-123) in situ in a) DW and b) SBF solutions in the presence of varying concentrations of BSA.

The size distributions of drug-loaded micelles (1 h after formation) in DW and SBF solutions are shown in Figure 4.15. (a) and 4.15. (b) under similar conditions, these results are very similar to those obtained with barren micelles. This confirms that high protein concentrations lead to micelle disintegration in DW and SBF solutions. Additionally, aging these micelles for up to 10 days does not cause any change in the DW solution, while a slight increase in micelle sizes is observed in the SBF solution. These findings suggest that BSA can disrupt micelle integrity even when strongly hydrophobic

drug molecules are in the micelle core. The data indicates that micelles disintegrate rapidly and do not re-aggregate over time when BSA is present, regardless of the presence of a hydrophobic drug in the micelle core.

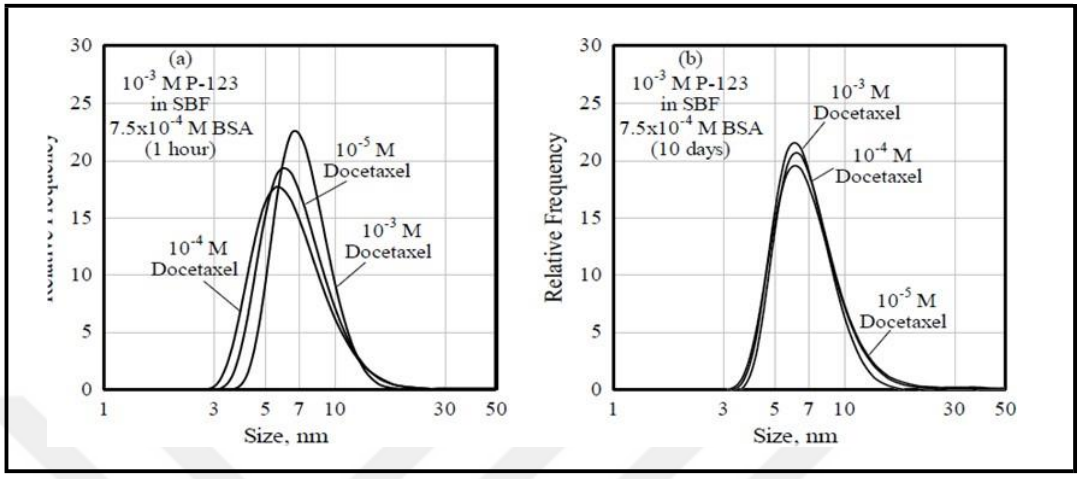

Figure 4.15. Size distributions of the Docetaxel-loaded (10^{-4} M) micelles (10^{-3} M P-123) in situ in SBF solutions in the presence of $7.5x10^{-4}$ M BSA as a function of varying Docetaxel concentrations a) 1 hour after micelle formation and b) 10 days after micelle formation.

4.3.3. FTIR Results of drug-loaded micelles

Determining the effective drug loading and understanding the interactions between the encapsulated medication and the polymeric micelles need the characterization of their molecular structures. Fourier-transform infrared (FTIR) spectroscopy is a useful technique for determining the functional groups in these systems. Fourier-transform infrared (FTIR) spectroscopy can reveal information on the chemical makeup of the system and possible interactions between the drug molecules and micelle.

The characteristic peaks of the P-123 micelles and the Docetaxel powder are presented separately in Figure 4.16. (a) P-123 has major peaks corresponding to the C-H stretching and bending vibrations in the range of 2850-3000 and 1460 cm^{-1}, respectively. Those at 1377 and 1350 cm^{-1} are assigned to the stretching modes of C-O-C on P123. Docetaxel has major peaks that gave a broad band at 3331 cm^{-1} due to N-H bond and O-H bond overlapping and a peak around 2972 cm^{-1} due to C-H stretching. Also, a

characteristic C=C bending vibration at 800 cm^{-1} can be observed. Furthermore, the drug displays another strong C-O stretch peak at around 1050 cm^{-1}.

The infrared spectrum of P-123 micelles suspended in water, which were loaded with Docetaxel concentrations of 10^{-4} M and 10^{-2} M, prominently featured a significant peak attributed to the P-123 polymer within the range of 1000 to 1100 cm^{-1}. This peak indicates the presence of the micelle structure itself. Importantly, when analyzing the spectrum, it was observed that the characteristic C=C bending peak of Docetaxel, which typically appears at 800 cm^{-1}, along with the C-O stretching peak found around 1050 cm^{-1}, were completely absent in the micelle samples in water.

This absence suggests that the drug did not exist in its free form within the micelles. Furthermore, the overall spectrum of the Docetaxel-loaded P-123 micelles lacked any distinctive peaks that would typically correspond to the chemical structure of Docetaxel. This absence of characteristic peaks strongly indicates that the Docetaxel molecules were effectively encapsulated within the micelle structure rather than freely available in the aqueous environment. This encapsulation may influence the drug's stability and release characteristics, highlighting the potential of P-123 micelles as a delivery system for therapeutic agents.

Figure 4.16. (b) presents the spectrum of Docetaxel-loaded P-123 micelles after being immersed in an ethanol solution. This solvent disrupts micelle structures, which should facilitate the release of any encapsulated Docetaxel molecules within the micelles. The spectrum reveals distinct peaks characteristic of Docetaxel, including a C=C bending vibration observed at 800 cm^{-1}, indicating the presence of the drug's molecular structure. Additionally, a C-O stretching peak is identified at 1050 cm^{-1}. These specific peaks appear alongside the characteristic peaks of P-123, the block copolymer used to form the micelles. The detection of these peaks confirms that Docetaxel's encapsulation process within the P-123 micelles was successful, allowing drug release when exposed to ethanol. This analysis underscores the effective loading of the drug in the micellar system and its responsiveness to solvent conditions. Furthermore, the presence of the drug-specific peaks alongside the P-123 peaks suggests that the micelles retain their structural integrity while effectively encapsulating the drug. This confirms the potential of P-123 micelles as efficient carriers for controlled drug delivery systems.

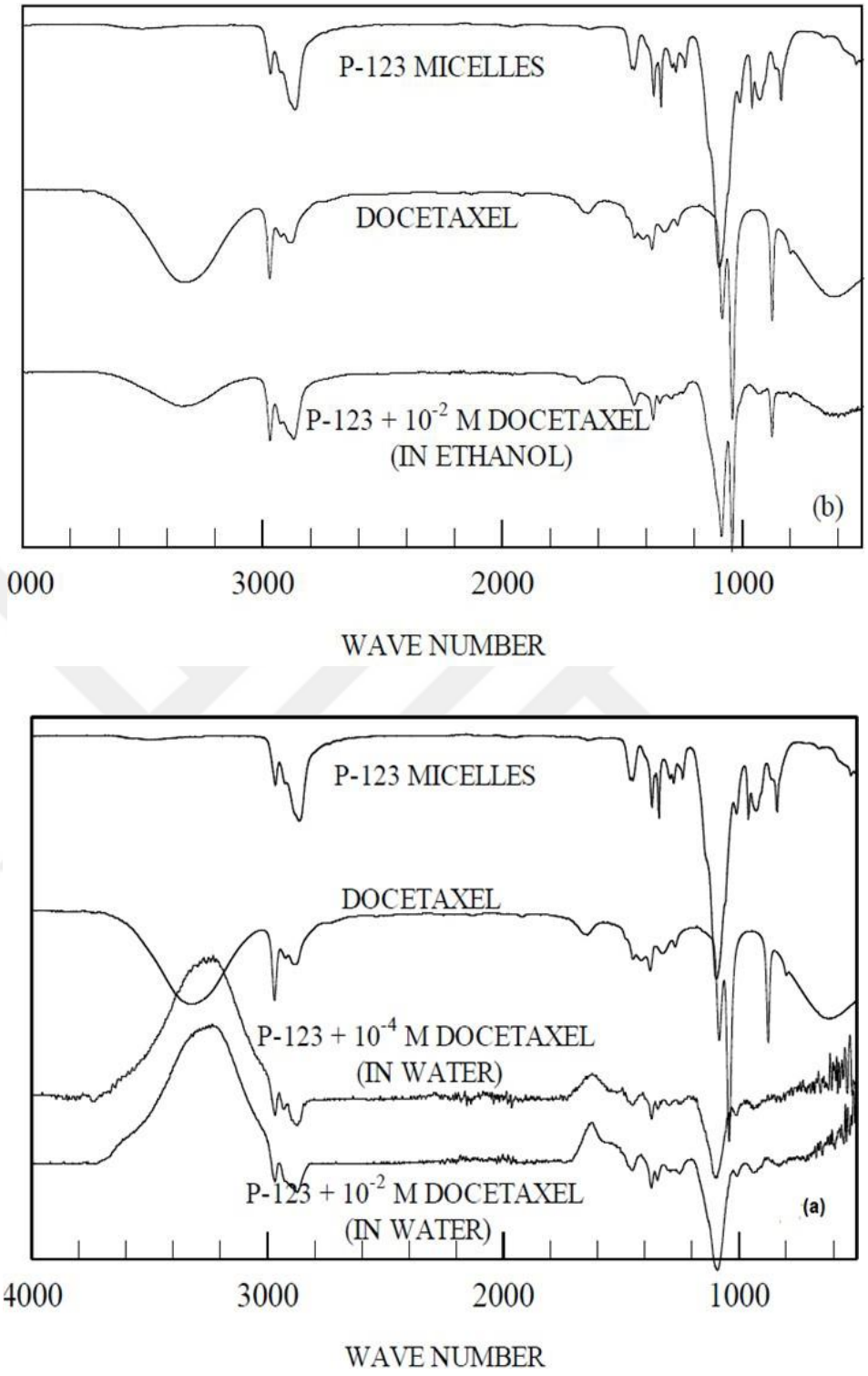

Figure 4.16. FTIR spectra of P-123 micelles and Docetaxel molecules separately and when they are together in solutions of a) DW and b) ethanol solutions.

4.3.4 Stability of drug-loaded P-123 micelles in the presence of FBS

Similar types of dilution studies were repeated in the case of FBS. Fetal bovine serum (FBS) is one of the most widely used additives in cell biology and biotechnology, containing a wide variety of proteins, hormones, growth factors, lipids, and vitamins that have critical functions in cell culture media. FBS is usually composed of serum obtained from the blood of bovine fetuses and contains various biochemical components (Lee et al., 2022). Figure 4.14 presents the in-situ size distribution of the fetal bovine serum (FBS) molecules at approximately 7-8 nm. Then, the size of P-123 micelles in FBS was measured with dilution and reproduced in Figure 4.15. It is seen that the size of the P-123 micelles becomes similar to the size of FBS alone. This shows the disintegration of polymeric P-123 micelles in the physiological environment.

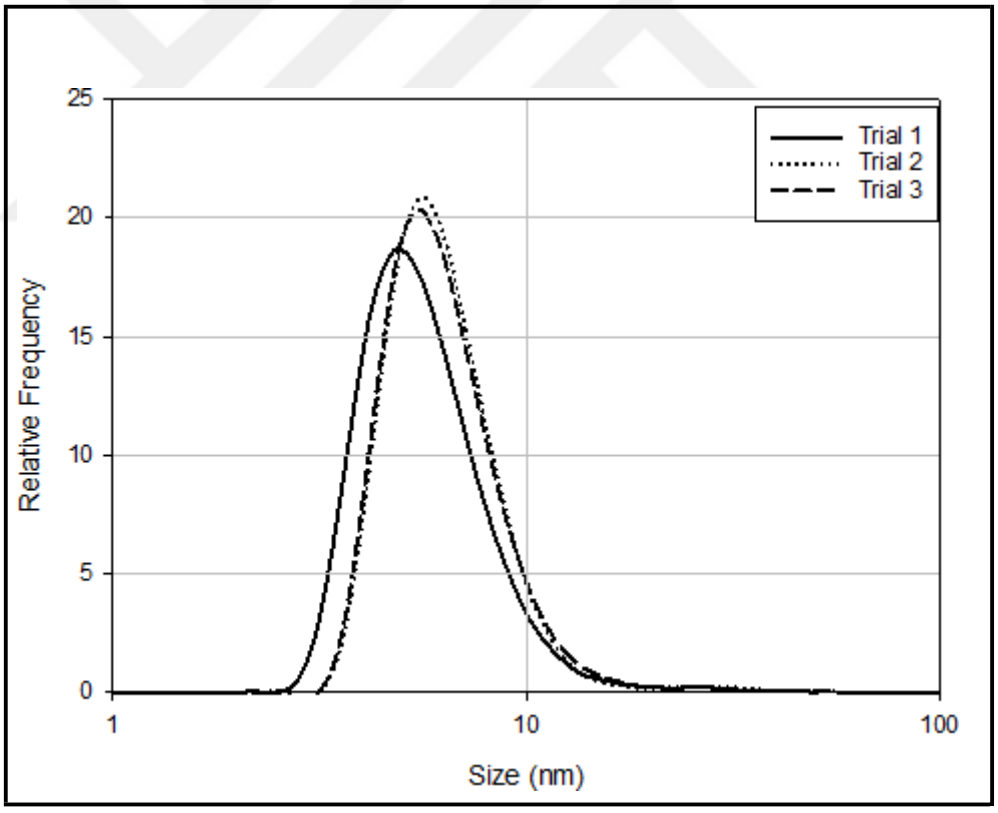

Figure 4.17. Size distributions of the Fetal Bovine Serum (FBS).

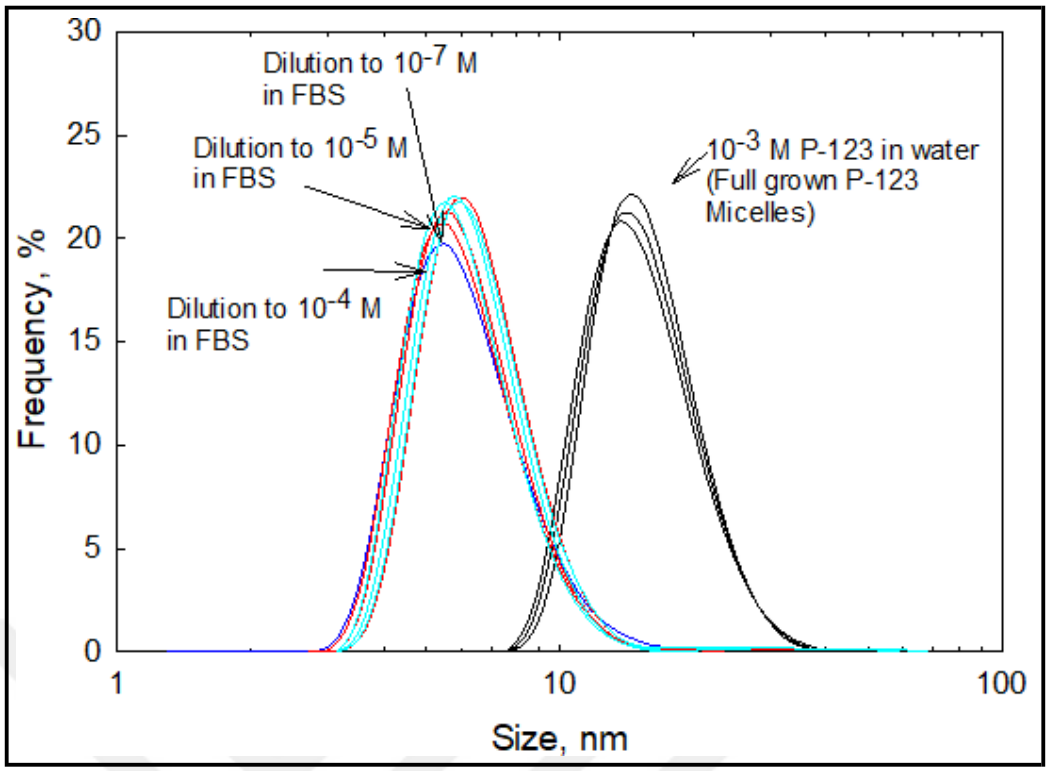

Figure 4.18. Size distributions of P123 barren micelles with increasing concentration of the Fetal Bovine Serum (FBS).

CHAPTER 5

CHITOSAN MICELLES AND THEIR STABILITY

5.1. Characterization of Hydrophobically Modified Chitosan Molecules

5.1.1. Determination of Substitution Degree

At the beginning of the study, the obtained modified chitosan molecules were characterized. Both FTIR and ninhydrin tests were used to measure the degree of binding of the obtained modified chitosan. Firstly, FT-IR spectra were used to evaluate the degree of binding. The degree of binding of chitosan changing at various rates was determined using the equations mentioned above. Then, the ninhydrin test technique was used to calculate the degree of binding. The calculation equation mentioned before for the ninhydrin method was used. When the results obtained from the two approaches are compared, it is seen that the degree of binding is close to each other in all cases. The highest degree of substitution was seen in the highest N-acylated chitosan. When these results are evaluated, it is simple to say that the degree of binding increases directly proportionally with the increase in the N-acylated rate.

Table 3. Estimation of the degree of substitution by FTIR and ninhydrin assay.

SAMPLE	Ninhydrin Assay (%)	FT-IR (%)
CS-B01	66.25	62.58
CS-B05	68.38	63.41
CS-B1	70.36	65.59

5.1.2. Determination of Molecular Weight

The molecular weight of commercial chitosan was determined using the kinematic viscosity measurement and the application of the Mark Houwink equation.

$$[\eta] = K[M_\upsilon]^\alpha$$

K and α values were taken as $2.92x10^{-4}$ (dL/g) and 1.055, respectively. The K and α values for both chitosan and commercial chitosan acylated at different rates were considered the same because the deacetylation degree of commercial chitosan and its derivatives was the same. The molecular weights of chitosan and its derivatives were calculated by substituting the value found in the Mark-Houwink equation. The molecular weight results are shown in the table below.

Table 4. Molecular Weight of Commercial Chitosan and their Derivatives.

SAMPLE	Molecular Weight (g/mol)
Commercial chitosan	102329.29
CS-B01	228674.21
CS-B05	363078.05
CS-B1	512861.38

5.1.3. FTIR Analysis

FTIR spectra were used to identify structures of commercial and benzoic anhydride-modified chitosan. The major peaks of chitosan are listed as follows: Between 3500 and 3000 cm^{-1}, overlapping was observed due to the -OH and -NH peaks occurring in the same region. C-H stretching was observed around 2900 cm^{-1}. The amide I band appeared around 1600 cm^{-1}, and the amide II band was seen around 1560 cm^{-1}.

Additionally, there is a C-H bending peak at 1400 cm^{-1} and a C-O stretching peak at 1050 cm^{-1}. As can be seen, the major peaks of chitosan coincide with those reported in the literature.

Due to primary amid reduction, the overlapping peaks between -OH and -NH disappear between 3500 and 3100 cm^{-1}. The newly observed peaks in the 3000 cm^{-1} band may belong to the C-H bonds of aromatics from benzoic anhydride. Because of the higher number of secondary amides on N-acylated chitosan, the band at 1580 cm^{-1} for acylated chitosan was lower than commercial chitosan. The peak is around 1530 cm^{-1}, which might be ascribed to benzene groups because the aromatic rings are observed around 1540 cm^{-1}, significantly stronger when the ring is further conjugated. When all the results are evaluated, it is seen that chitosan was successfully modified with benzoic anhydride group.

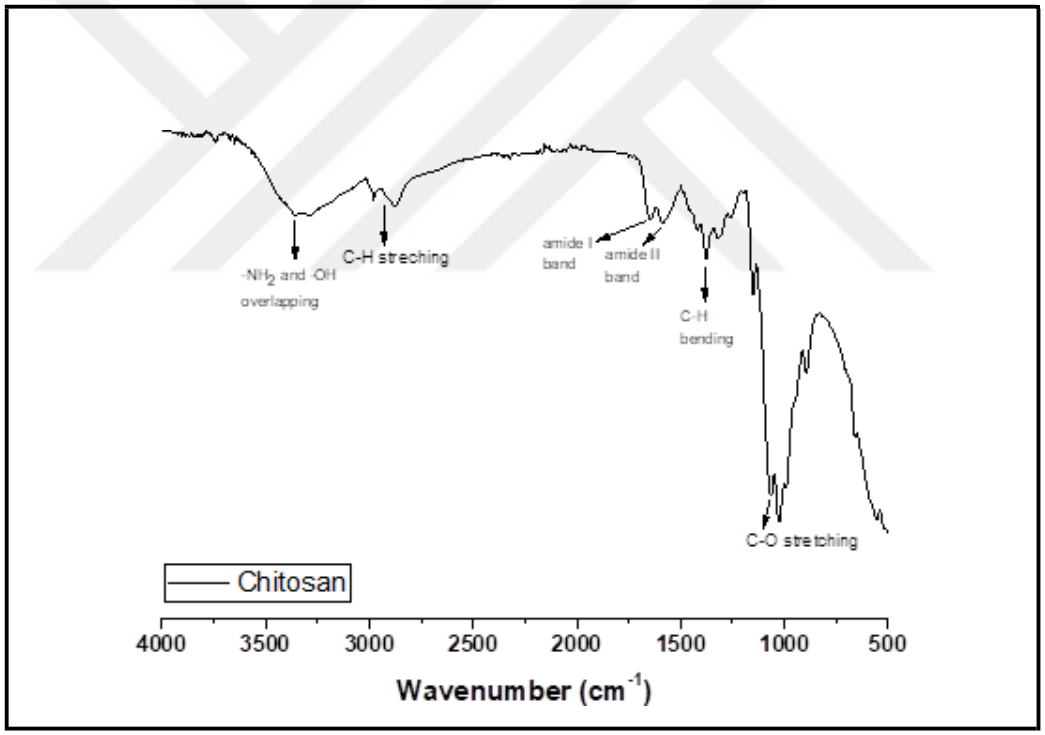

Figure 5.1. FTIR spectra of commercial chitosan.

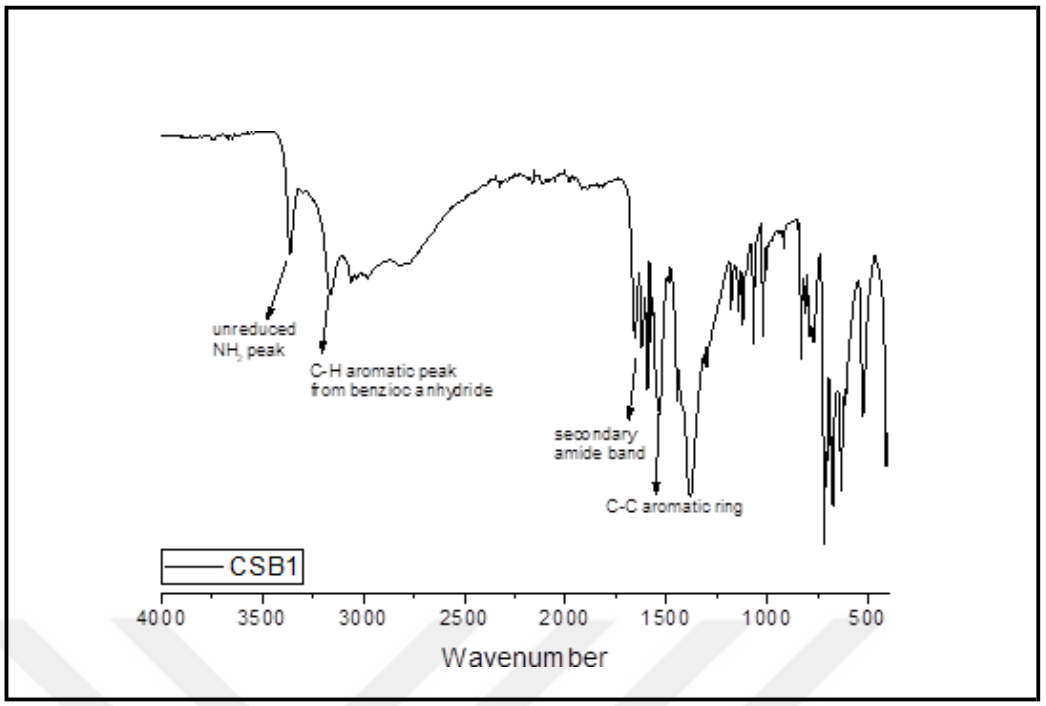

Figure 5.2. FTIR spectra of modified chitosan.

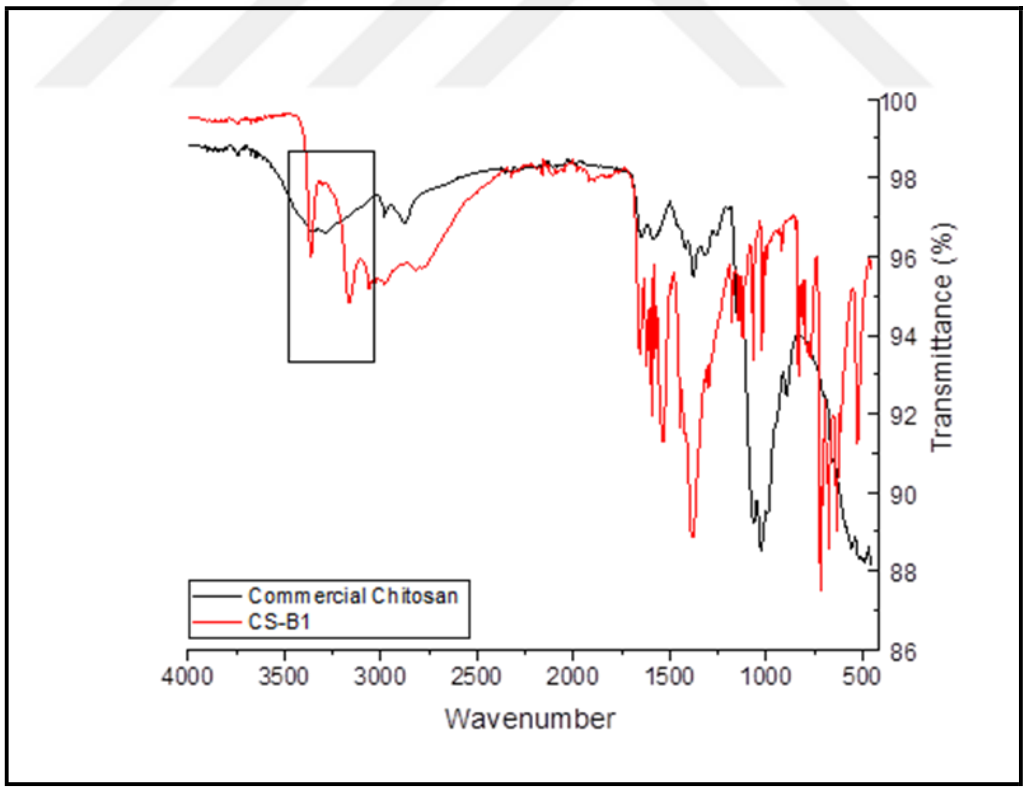

Figure 5.3. FTIR spectra of commercial and modified chitosan with benzoic anhydride between 4000-400 cm^{-1}.

5.1.4. X-ray diffraction (XRD)

The crystalline of chitosan was significantly altered through N-acylation with different mole ratios of benzoic anhydrides, as determined by X-ray diffraction (XRD) analysis. To investigate this structural modification further, the crystal size of the modified chitosan samples was calculated using the Debye-Scherrer equation and applied to the XRD data. The resulting crystal size estimations (denoted as t) are presented in Table 5. These results demonstrate that the crystal size of the modified chitosan derivatives is influenced by the initial mole ratios of benzoic anhydride used during the modification process. Interestingly, the data reveal that the crystal sizes of all modified chitosan derivatives are larger compared to that of unmodified commercial chitosan, indicating that even the lowest initial mole ratio of benzoic anhydride is sufficient to induce noticeable changes in the crystalline structure of chitosan. Moreover, this increase in crystal size highlights the effectiveness of the N-acylation process in modifying the structural properties of chitosan. However, despite this clear impact, a consistent trend correlating higher mole ratios of benzoic anhydride with increased crystal size was not observed. This suggests that while benzoic anhydride plays a crucial role in altering the crystallinity of chitosan, the relationship between the amount used and the resulting crystal size is complex.

Table 5. Estimation of crystal size of commercial chitosan and modified chitosan derivatives.

SAMPLE	Crystal Size (nm)
Commercial chitosan	1.159
CS-B01	2.590
CS-B05	3.087
CS-B1	2.066

5.1.5. Surface Activity, Hydrophobic Property

As explained above, surface tension measurements were conducted using aqueous solutions of CSB1 samples at different percentages (2%, 1%, 0.5%, and 0.2%). As modified chitosan concentrations increase, surface tension decreases from 58 mN/m to 46.3 mN/m. This decrease in surface tension supports a hydrophobic character in modified chitosan molecules.

Contact angle measurements were utilized to determine the hydrophobic characteristics of modified chitosan samples using the method described in the experimental method section. The surfaces produced by unmodified chitosan were hydrophilic; however, the surfaces produced by modified chitosan had displaced angles ranging from 76 to 97, depending on the initial molar ratio. This shows the hydrophobic nature of chitosan derivatives, which increases as the molar ratio increases due to the increase in the number of hydrophobic groups, alkyl, and benzene.

As a result, when all the characterizations were evaluated, it was decided that the most suitable chitosan derivative to form a micelle would be the chitosan with the highest initial mole ratio, given the CSB1 code. This chitosan derivative was chosen because its substitution degree is high, and it has the highest hydrophobicity.

Table 6. Surface tension and contact angle measurements with modified chitosan (CSB1) at different concentrations in water.

Amount of CS-B1 type of modified chitosan (%)	Surface Tension (mN/m)	Mol Ratio	Contact Angle (°)
Unmodified Chitosan		Unmodified Chitosan	0
CS-B1- %0,05	58	CS-B01	76
CS-B1- %0,2	50.7	CS-B05	83
CS-B1-%0,5	46,9	CS-B1	97
CS-B1-%1	46,3		

5.1.6. Surface Charge Distribution: Zeta Potential Measurements

The zeta potential measurement results of unmodified and CS-B1-modified chitosan molecules (at 0.5%) in acetic acid solutions are given in Figure 5.4. The unmodified chitosan molecules have a strong positive charge range between 50 and 80 mV. The modified chitosan molecules, on the other hand, carry less positive charge ranges between 25-50 mV. This shows that the hydrophobic modification of chitosan molecules is not uniform, and there are still unmodified molecules in the system. This has been named as substitution degree (around 70%) above where the characterization of modified molecules has been done. Because of this degree, a mixture of modified and unmodified molecules is in the solution to produce micelles. The positive charge of micelles (with a lower magnitude) might be due to the presence of unmodified molecules in the micelle structure to form a hybrid structure. Therefore, the surface charge of micelles is measured as positive in water. However, if there are ions in water, such as body fluid, the surface charge of micelles is expected to be neutralized and depressing totally. One should take this positive charge issue in the case of modification into consideration since its charge is one of the most desirable properties of chitosan to be used in drug delivery applications.

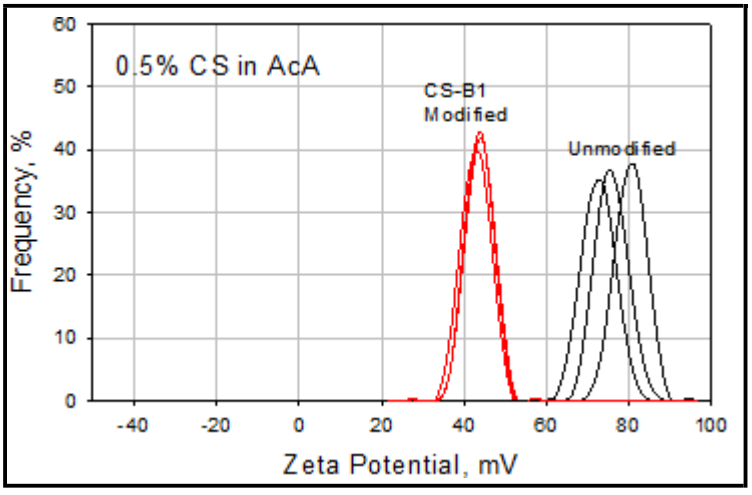

Figure 5.4. Zeta potential distribution of unmodified and modified chitosan molecules in dilute AcA solution of 0.5% (Chitosan 0.5%.).

5.2. Self-Assembly and Characterization of Modified Chitosan Micelles in Water and SBF

Chitosan molecules may self-assemble in water thanks to hydrophobic alteration with a substitution degree of around 73% and a decreased positive charge. As a result of their partly hydrophobic nature, molecules are predicted to assemble and form structures. In this work, these sorts of spherical formations were found to develop in STEM pictures (at a magnification of 200,000x) and displayed in Figure 5.5. for barren CS-Micelles in water solution with a pH of around 5.5. The STEM pictures show that spherical, barren chitosan micelles with diameters ranging from 30 to 50 nm may develop in water. However, considering the high molecular weight of the modified chitosan molecules (~500,000 g/mol) mentioned above and the sizes of chitosan micelles, around 30–50 nm (STEM) observed, these micellar structures could be suggested to be like coil-up forms of the modified molecules among themselves along with the drug, in contrast to the traditional polymeric micelles (such as P-123 micelles around 20 nm in size). Additionally, Micellar structures also form loose aggregates to some extent when they come together. Based on DLS measurements, the distributions obtained appear to be those of micelles aggregates, not single micelles, which are aggregates of molecules (Figure 5.5.).

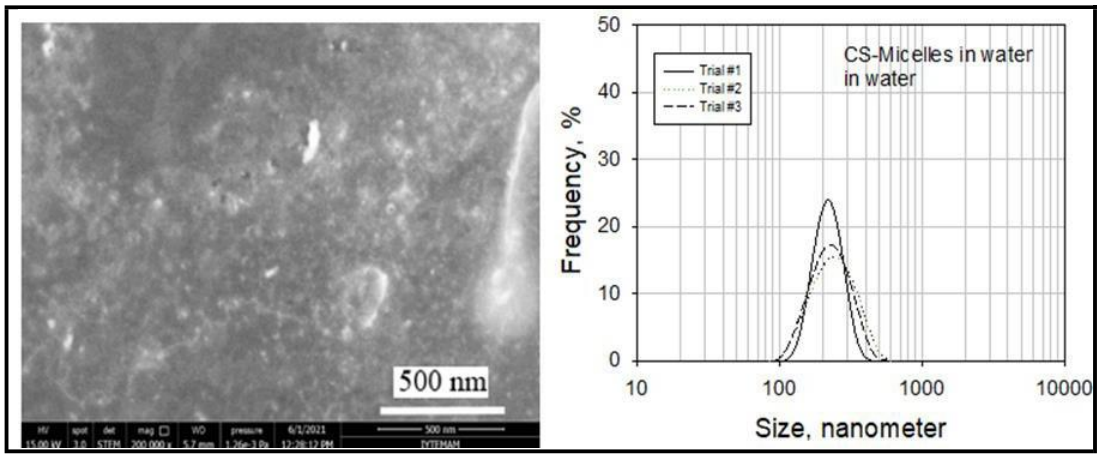

Figure 5.5. STEM images of baren CS-Micelles (left) and DLS size results (right) in water.

As shown in Figure 5.6. (a), unmodified and CS-B1-modified chitosan molecules demonstrate different zeta potentials in water at pH 5.5. Unmodified chitosan molecules

exhibit strong positive charge ranges between +60 and +90 mV. A modified chitosan molecule, which is probably coiled up (called micelles in this study), carries a much lower positive charge range of 30 to 50 mV. There may be unmodified NH_2 groups on chitosan molecules due to the partial modification (73%) and partial modification (73%). If these modified molecules (micelles) are placed in simulated body fluid, the micelles' surface charge will decline further (Figure 5.6. (b)). As shown in the figure, the zeta potentials of chitosan micelles in water and SBF confirm this hypothesis regarding the depression of the positive charge in SBF where ions are present. However, some researchers in the literature determine the charge of micelles as if they were in water, and they do not consider the possible change in both the sign and magnitude of charge in body fluid. The fact that the chitosan micelles will not carry a significant positive charge in body fluid has not been considered in the literature for drug delivery applications.

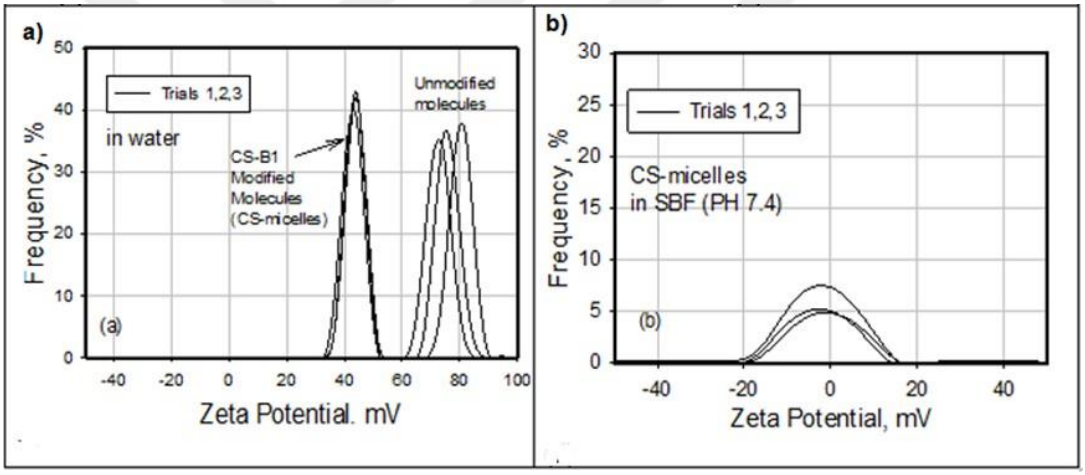

Figure 5.6. a) Zeta potential of unmodified and modified chitosan molecules in water b) Zeta potential of modified molecules (CS-micelles) in SBF (pH= 7.4).

Figure 5.7. shows STEM images of drug-loaded micelles in water and SBF at a magnification of 200,000x. Chitosan micelles are much larger in SBF. The increased degree of aggregation suggests that ions in the system will likely reduce the charge on Chitosan structures, leading to their aggregation.

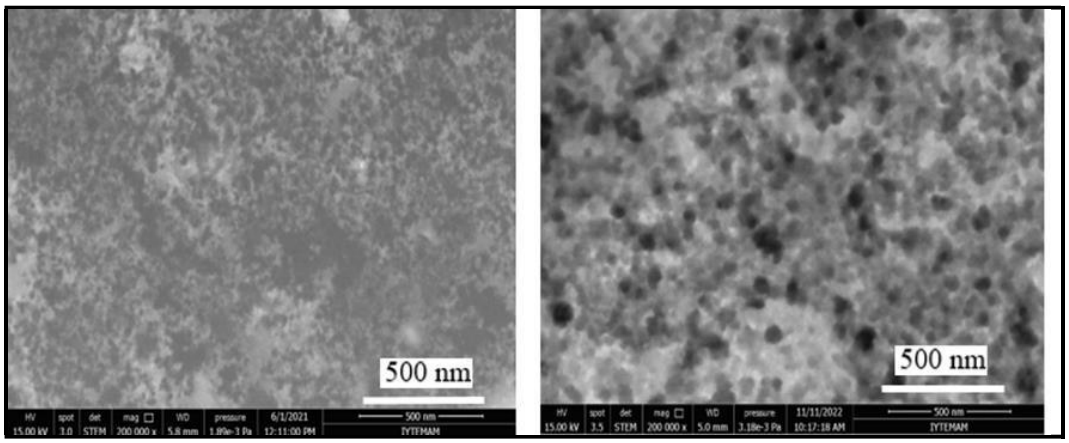

Figure 5.7. STEM images of DOC-CS-Micelles in water (left) and in SBF (Right).

5.3. Determination of Entrapment Efficiency of Docetaxel-loaded Chitosan Micelles

The formed micelles were passed through 25 nm membrane filters to calculate the entrapment efficiency of docetaxel-loaded chitosan micelles. The clear supernatant solution was analyzed by UV spectrophotometer at λ max value of 237 nm, shown in Figure 5.8. Using these UV results, the entrapment efficiency of the drug was calculated using the following equation:

$$= \frac{total\ amount\ of\ drug - free\ drug\ in\ the\ supernatant}{total\ amount\ of\ drug} x100$$

Using these UV results, the drug entrapment efficiency was calculated using the equation below. The entrapment efficiency of drug-loaded micelles was found to be 93%. The entrapment efficiency value of chitosan micelles, being 93 %, indicates that the micelle system can effectively retain the drug, and the formulation is generally successful. This indicates that the micelles effectively encapsulate the drug in the hydrophobic cores, and the amount of free drug is low. A high value indicates the system can provide a longer, controlled release.

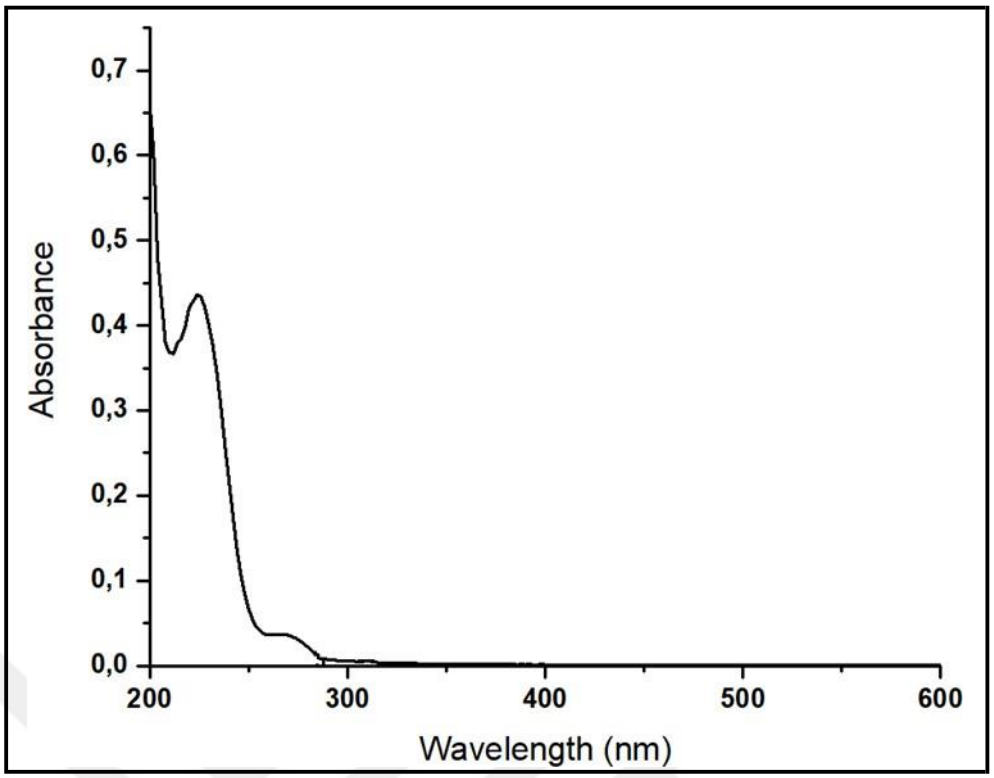

Figure 5.8. Absorbance spectra of supernatant solution of docetaxel-loaded chitosan micelles.

Based on these results, comparing drug-loaded P-123 and chitosan micelles shows that the formulation is more optimized and effective. Efficiency with 85% entrapment efficiency can be considered good but has potential for improvement. The 93% system is more advantageous in therapies that require controlled release and targeting. The 85% system can be preferred in cases where a faster effect is required because the free-drug ratio is higher. Figure 5.9 demonstrates that no chitosan micelles were detected in the supernatant following the 25 nm filtration process, confirming the accuracy and reliability of the entrapment calculations. The absence of micelles in the supernatant suggests that the encapsulation process was efficient, with minimal or no leakage of micelles through the filtration membrane. The observed particle size in the filtrate is attributed to individual chitosan molecules rather than intact micellar structures, indicating that the micelles were successfully retained. When all the experimental findings are considered, it can be concluded that the drug molecules were effectively entrapped within the chitosan micelles. This result not only validates the success of the encapsulation process but also highlights the stability and integrity of the formed micelles under the applied experimental conditions.

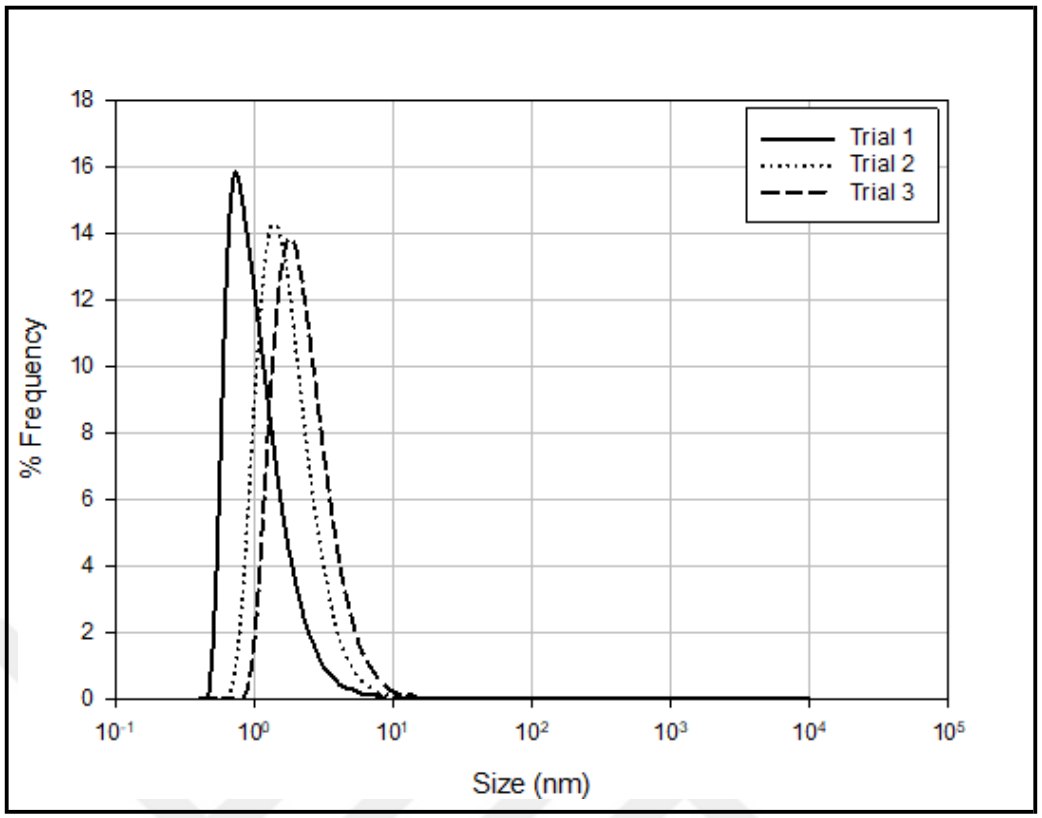

Figure 5.9. Size distribution of docetaxel-loaded chitosan micelles after 25 nm filtration.

5.4. FTIR Analysis of Chitosan Micelles

To better understand the structure of drug-loaded micelles, we performed the following drug-based characterization studies: The micelle solutions were first filtered using cellulose nitrate filter paper (450 nm) to eliminate any water-insoluble substance. Next, using FTIR and UV-Vis, the supernatant expected to contain drug-loaded chitosan micelles was checked for docetaxel to see if any drug molecules were present. However, the UV-Vis analysis revealed that the supernatant, after filtration, was devoid of medicine. On the other hand, FTIR analysis of the same solution reveals certain drug-specific peaks, indicating that the drug may be concealed inside the chitosan micelle structures.

A broad peak around 3500–3000 cm^{-1} indicates the presence of O-H and N-H stretches from both chitosan and docetaxel. Peak around 2900 cm^{-1}, indicating C-H stretches from both compounds. Peak around 1740 cm^{-1}, indicating ester C=O stretch

from docetaxel. Peaks around 1600–1500 cm^{-1} indicate amide I and II bands and aromatic C=C stretches from both compounds. Peak around 1400 cm^{-1}, indicating C-H bending from chitosan. Peaks around 1260–1000 cm^{-1} indicate C-O-C and C-N stretch from both compounds. Any new peaks not in the individual spectra or increasing strength shouldn't be identified to indicate new compounds. So, based on the FTIR analysis, it was concluded that the drug (docetaxel) seems to be physically encapsulated in the structure due to hydrophobic attraction, and no chemical bonding between the drug and chitosan has been observed by FTIR analysis.

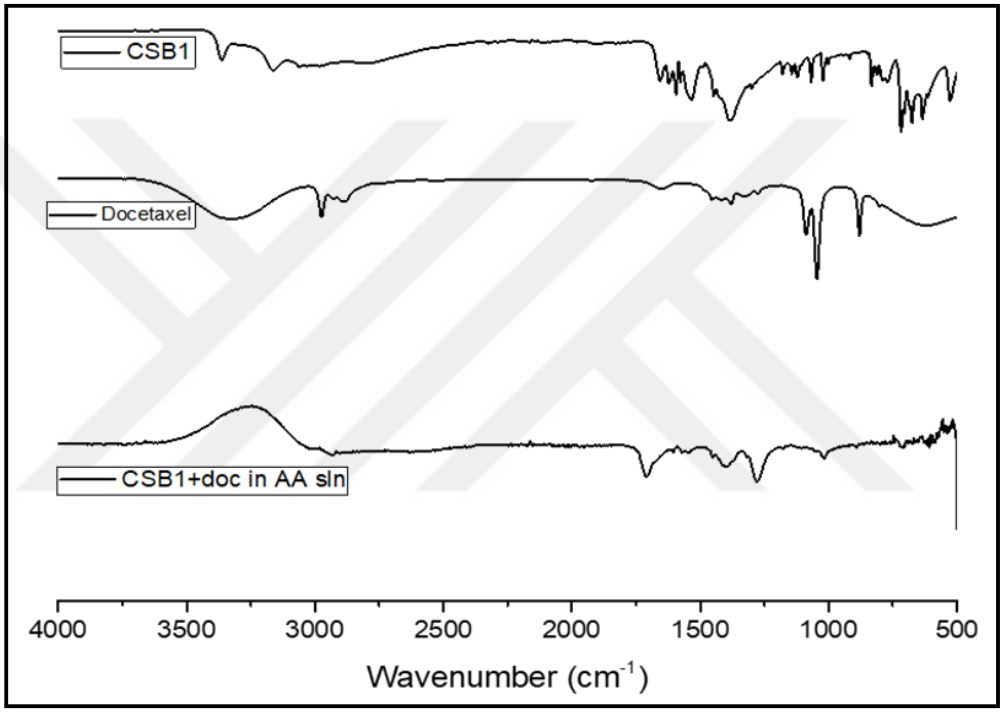

Figure 5.10. FTIR spectra of DOC-CS-Micelles.

5.5. Stability Tests of Drug-Loaded Modified Chitosan Micelles

Micelles' stability in different environments is critical in evaluating their potential for drug delivery applications. Transmission electron microscopy techniques like STEM allow detailed micelle morphology and structural integrity visualization under various conditions. Figure 5.11. shows the STEM images of drug-loaded chitosan micelles in DW and SBF at a magnification of 400,000x. While micelles appear to be more stable and

denser in water, micelles in SBF exhibit a more irregular distribution and structure. This may indicate that the components of SBF may disrupt the micelle structure or create a different dynamic.

The previous chapter, (4), showed that polymeric P-123 micelles disintegrate in both dilution and the presence of protein. Therefore, STEM investigated the stability of chitosan micelles upon dilution, and the images are presented in Figure 5.12. Chitosan structures can still be observed as spherical carriers even after 10000-fold dilution compared to P-123 micelles in the dilution condition.

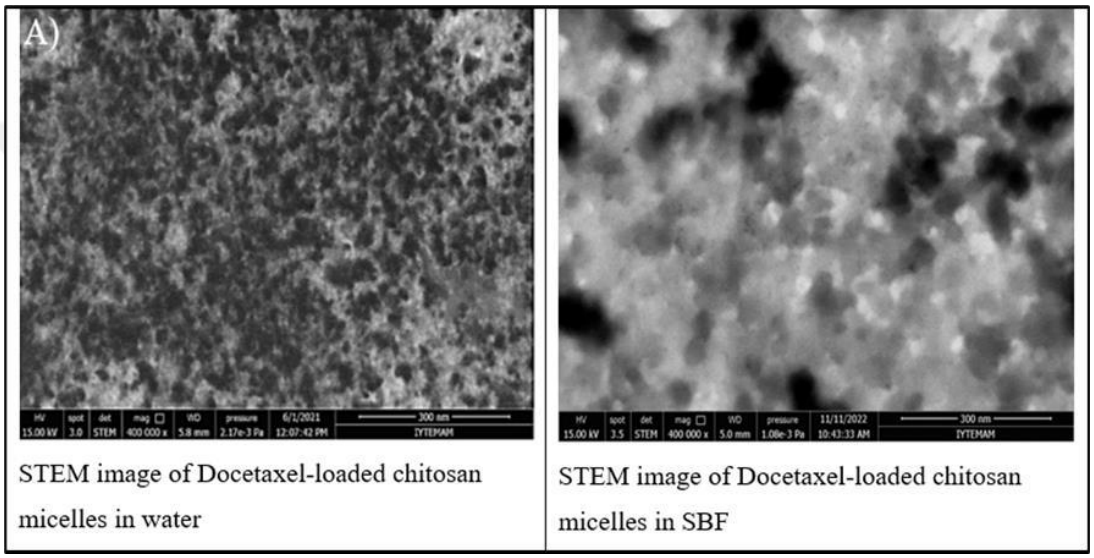

Figure 5.11. STEM images of DOC-CS-Micelles in DW and SBF.

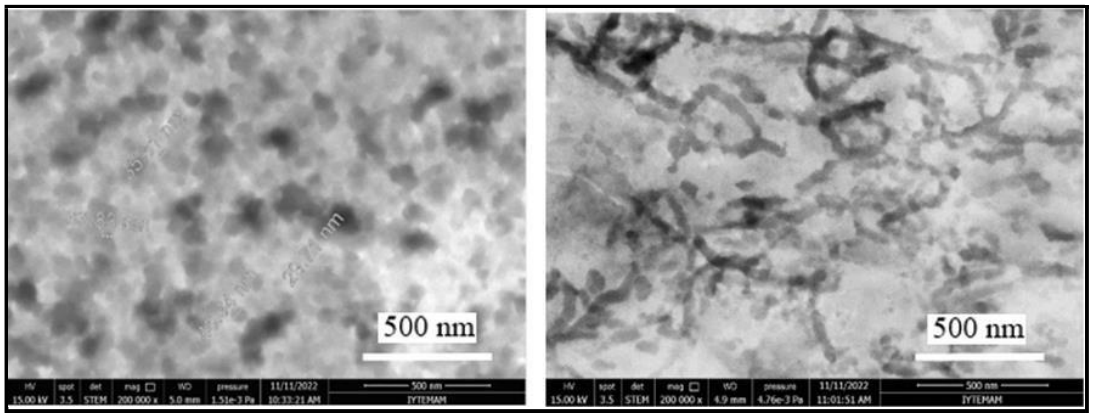

Figure 5.12. STEM images of DOC-CS-Micelles in SBF before dilution (left) and after 10000 times dilution (right).

Considering all the results, the dissolution problem was encountered in the studies. Therefore, acetic acid was added to the medium to observe how the system would react when complete dissolution was achieved. In the acetic acid medium, the size distribution of drug-loaded micelles was between 100-200 nm. Although the dilution process created small changes in the size distribution, it was observed that the overall size average and particle aggregation did not show great differences. In addition, it can be said that the system is still stable even against x10000 dilution (Figure 5.13.). The zeta potential of drug-loaded micelles in an acetic acid medium was measured. It was observed that they had a highly positive zeta potential of approximately 40-60 mV. The dilution process did not significantly affect zeta potential. Each dilution exhibited similar positive zeta potentials.

This indicates that the zeta potential of the samples did not change significantly with dilution. As a result, the drug-loaded micelles examined in terms of particle size distribution and zeta potential have a stable and homogeneous distribution. This shows that the system can last long without precipitation in biological or chemical systems and can be distributed homogeneously.

Figure 5.14. shows a clear photograph of drug-loaded chitosan micelles. The round structures in the image belong to the micelles and exhibit homogeneous distribution. However, agglomeration is observed in some areas. Based on the contrast difference, the inside of the micelles is thought to be drug-loaded.

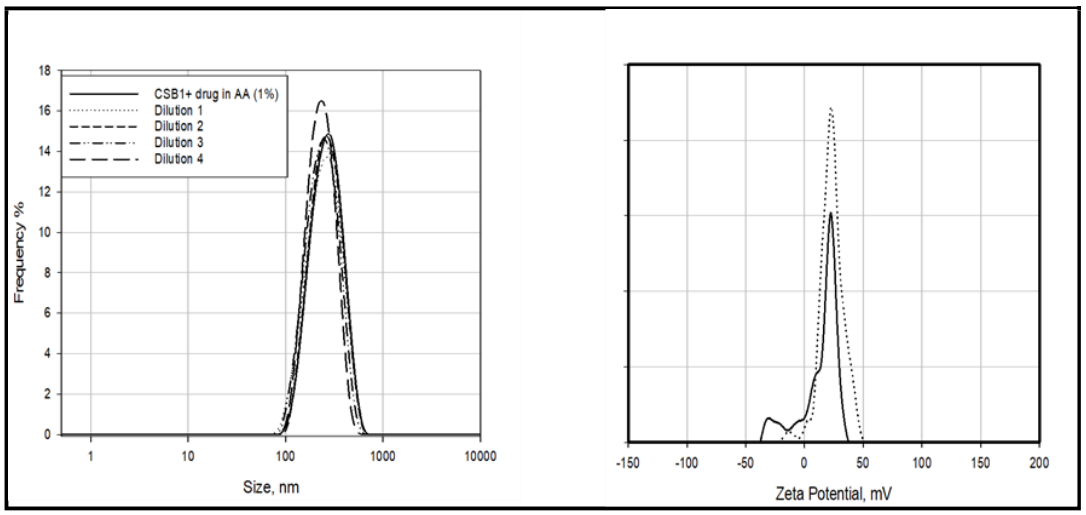

Figure 5.13 DLS size measurement results (right) and DLS-Zeta Potential measurement results of drug-loaded micelles in AA (left).

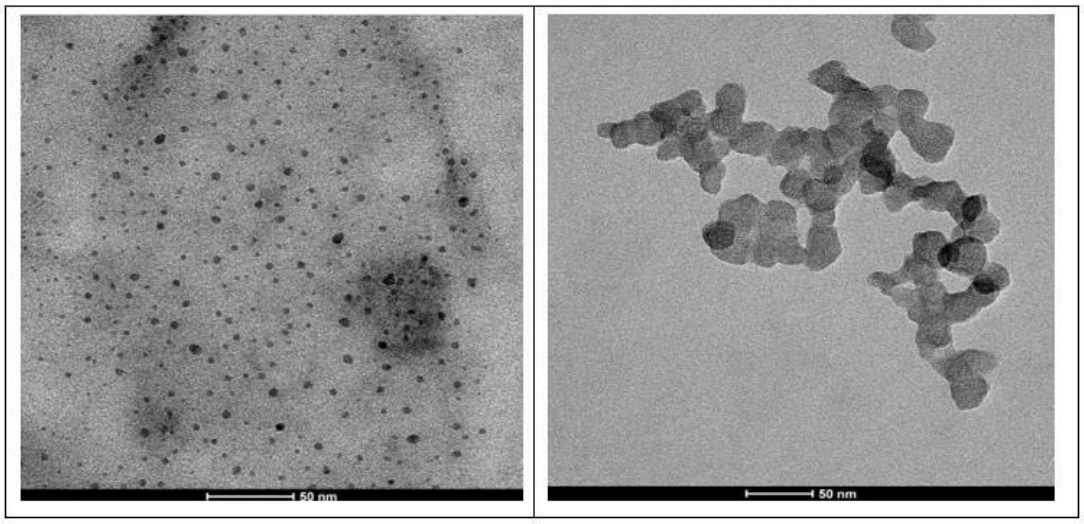

Figure 5.14. STEM images of DOC-CS-Micelles in DW.

5.6. Analysis of Drug-Loaded Chitosan Micelles covered by Fucodian

Then, these systems were further modified by forming a shell around them using fucoidan molecules to prevent protein attraction with similar charges and, therefore, improve stability. Fucoidan, a sulfated polysaccharide found in various species of brown seaweed, is known to have a negative charge at high pH values (with this charge, the molecules are known to present a special attraction for p-selection proteins on cancer tumors). This study will prevent negatively charged bovine serum albumin proteins from reaching the surface of negatively charged micelles. As seen from previous measurements, the systems are known to have a positive charge. In the first stage of the study, the zeta potential of fucoidan-coated micelles in both distilled water and simulated body fluid conditions was measured. As seen in Figure 5.15., the positively charged chitosan micelles became negatively charged after fucoidan coverage in water. In SBF at pH 7.4, however, the magnitude of this negative charge is lower due to the presence of ions to depress this charge.

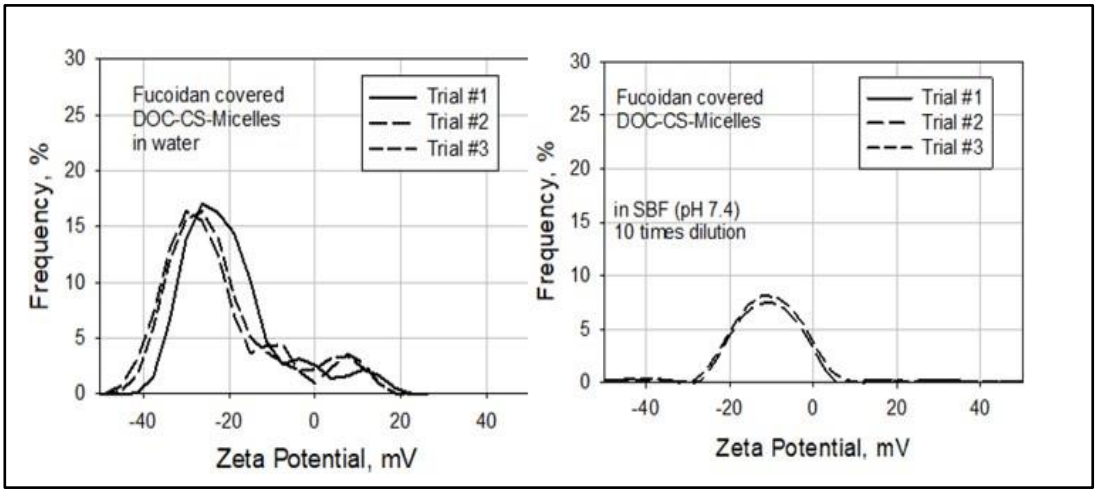

Figure 5.15. DLS-Zeta Potential measurement results of fucoidan-covered DOC-CS-Micelles in water and SBF.

When looking at the STEM images in Figure 5.16, we can say that drug-loaded chitosan micelles are covered by fucoidan. According to the STEM image, it was observed that the size of fucoidan-covered drug-loaded micelles was between 45-60 nm. The zeta potential measurements were repeated in the presence of protein in water and simulated body fluid presented in Figure 5.17. It is seen that the presence of protein does not alter the magnitude of surface charge significantly. This indicates that the protein-micelle attraction is not as significant as mentioned in the case of P-123 micelles, most probably due to the negative charges of micelles that are similar to the charge of the protein.

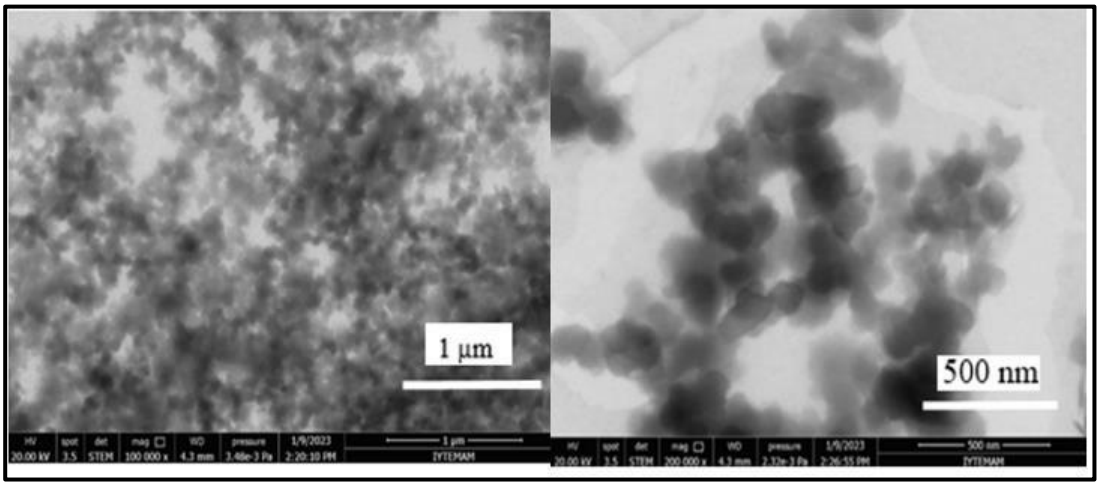

Figure 5.16. STEM images of fucoidan-covered DOC-CS-Micelles in SBF at different magnifications.

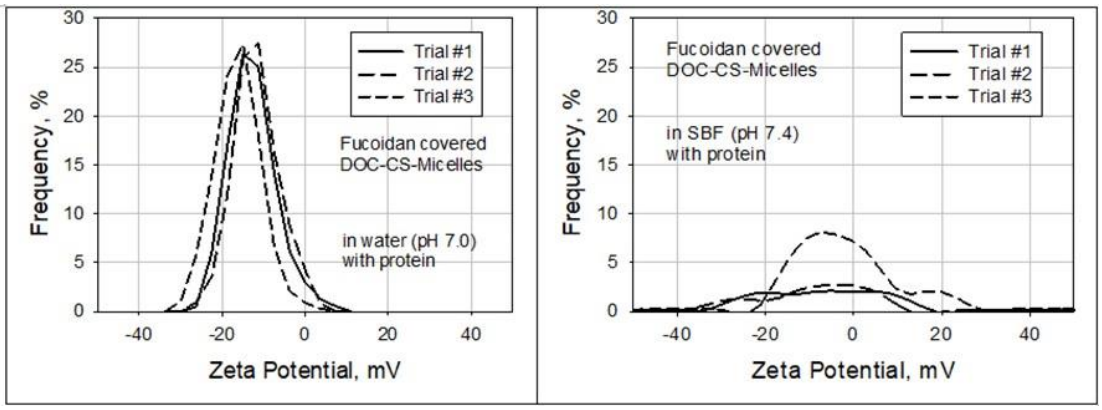

Figure 5.17 DLS- Zeta potential characterization of fucoidan-covered DOC-CS-Micelles in the presence of protein in water and SBF.

Figure 5.18 presents a microscopic image of drug-loaded chitosan micelles encapsulated by a fucoidan layer. As observed in the image, the contrast differences clearly indicate the presence of the drug within the micellar core, while the surrounding area appears to be uniformly coated with fucoidan. This contrast distinction suggests a successful encapsulation process, where the drug is effectively entrapped inside the micelles, and the fucoidan layer forms a protective shell around them. These findings provide strong evidence for the structural integrity of the fucoidan-coated micelles and confirm the effective formation of a core-shell system designed for drug delivery applications.

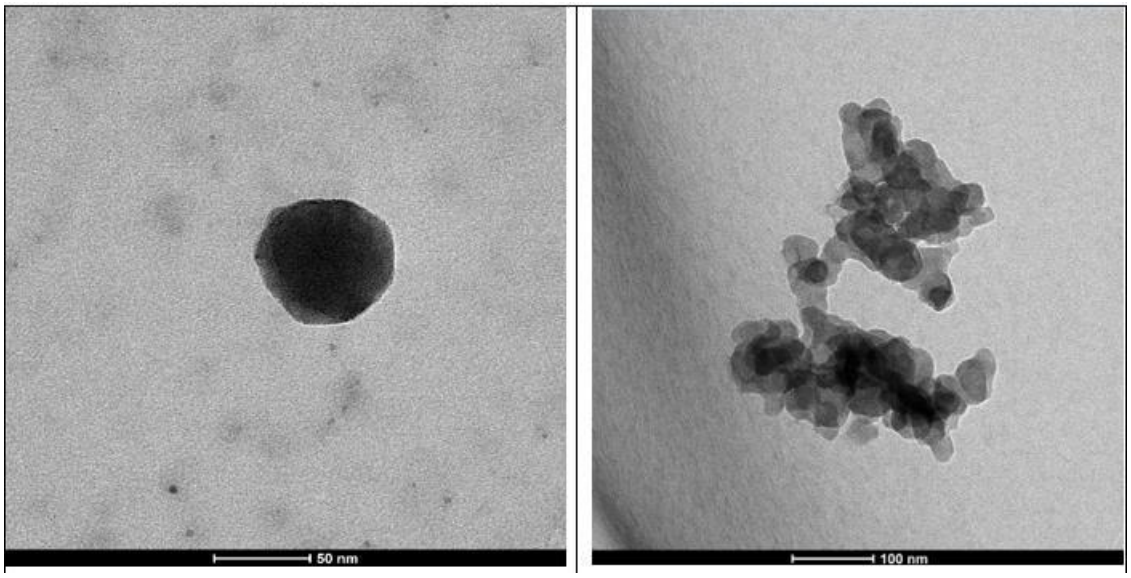

Figure 5.18. TEM images of fucoidan-covered DOC-CS-Micelles in water.

CHAPTER 6

CONJUGATION OF CHITOSAN AND DOCETAXEL

6.1. Synthesis and Characterization of Chitosan-DOC Conjugates

This part of the study includes the formation of chitosan-drug systems where the drug chemically bonds to the structure of chitosan, which is different than the system mentioned earlier. While the integrities of chitosan micelles that encapsulate the drug in its core physically are so important, they are not one of the problems in the case of chemical bonding. The structures are well stable upon dilution and protein interaction-induced disintegration. Therefore, this part of the study develops these micellar structures where the drug provides hydrophobicity.

Docetaxel was covalently attached to low molecular weight chitosan via a succinate linker, as given in Figure 6.1, whose degradability was confirmed under physiological conditions. This synthesis process was carried out in two stages. In the first stage, docetaxel was modified with succinic anhydride (a degradable linker). Then, the resulting molecule was characterized by ^{1}H NMR and observed to be compatible with the literature.

Doc-Suc: ^{1}H NMR (DMSO, 400 MHz, $CDCl_3$) δ=1.09 [s, 3H], 1.18 [s, 3H], 1.67 [s, 3H], 1.88 [s, 3H], 2.0 [m, 3H], 2.2 [m, 3H], 2.3-2.6 [m, 4H], 3.76 [d, 1H], 4.15 [d, 2H], 4.1 [d, 2H], 4.44 [dd, 1H], 4.94 [d, 1H], 5.48 [d, 1H], 5.65 [d, 1H], 5.96 [dd, 1H], 6.20 [t, 1H], 6.25 [s, 1H], 7.07 [d, 1H], 7.23 [s, 5H], 7.38 [m, 5H], 7.48 [m, 5H], 7.71 [d, 5H], 8.08 [d, 5H].

δ= 1.09 [s, 3H], 1.18 [s, 3H], 1.67 [s, 3H], 1.88 [s, 3H]: These shifts correspond to aliphatic methyl groups (CH_3). Being singlets indicates that no other protons are directly attached to the carbon atom to which these protons are bonded. These values are probably related to the tert-butyl groups or methyl side chains of docetaxel.

δ= 2.0 [m, 3H], 2.2 [m, 3H], 2.3-2.6 [m, 4H]: The multiplets in this region correspond to CH_2 and CH groups. These protons can be found in positions close to ester groups or more electronegative groups in aliphatic chains.

Protons bonded with oxygen (δ= 3-5 ppm) δ= 3.76 [d, 1H], 4.15 [d, 2H], 4.1 [d, 2H], 4.44 [dd, 1H], 4.94 [d, 1H]. These shifts are due to CH groups bonded with oxygen (e.g. -CH-OH or -CH_2-OH). 3.76 [d, 1H] and 4.15 [d, 2H]: They are probably protons associated with ester groups or alcohols in the succinate (Suc) unit. 4.44 [dd, 1H]: This proton is affected by two different neighboring protons and may be bonded with oxygen (e.g. -CH-O-).

Aromatic region (δ= 6-8 ppm): δ 5.48 [d, 1H], 5.65 [d, 1H], 5.96 [dd, 1H], 6.20 [t, 1H], 6.25 [s, 1H]: These values probably correspond to protons in the cyclic and aromatic structures of docetaxel. Protons adjacent to double bonds may be involved here. 6.25 [s, 1H]: Singlet, probably belongs to hydrogen or a vinyl group in an aromatic ring. δ= 7.07 [d, 1H], 7.23 [s, 5H], 7.38 [m, 5H], 7.48 [m, 5H], 7.71 [d, 5H], 8.08 [d, 5H]. The signals in this region belong to the protons in the aromatic rings. 7.23 [s, 5H]: The signal of the equivalent 5 protons in the benzene ring. 7.07 [d, 1H] and 8.08 [d, 5H]: These are doublets formed by the spin-spin interaction of the protons in the aromatic rings. Electron-withdrawing groups caused these protons to be more deshielded.

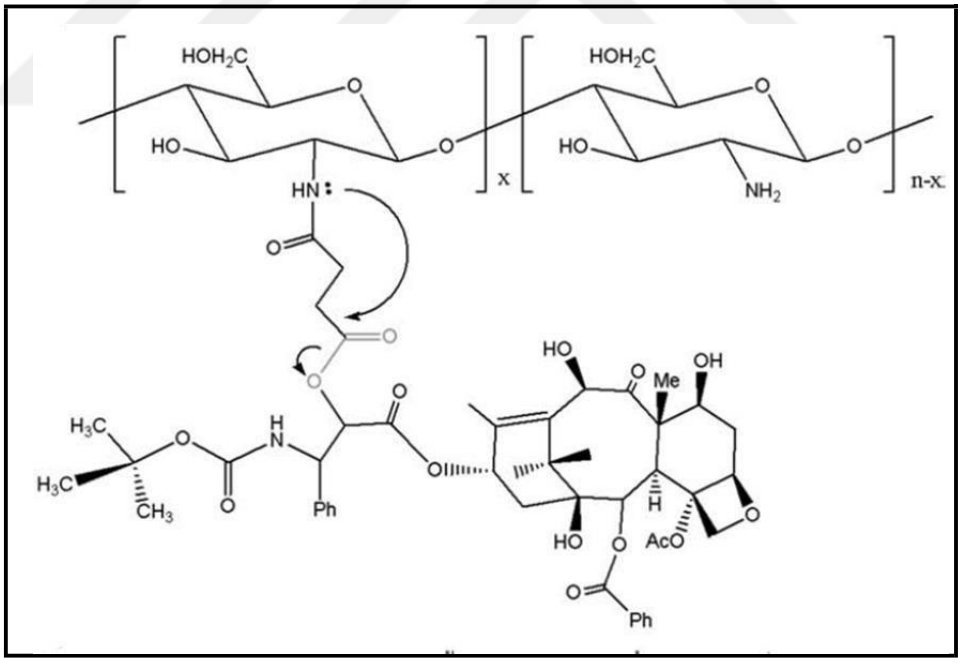

Figure 6.1. Schematic Diagram of Conjugated CS-Doc.

In the second stage of the synthesis, the active ester form of docetaxel modified with succinic anhydride was attached to the amine groups of chitosan. A UV spectrometer was used to characterize the conjugated chitosan and docetaxel structure (Chitosan-DOC

Conjugate) that showed an absorbance at 237 nm similar to docetaxel. This was another indication of the successful conjugated structure.

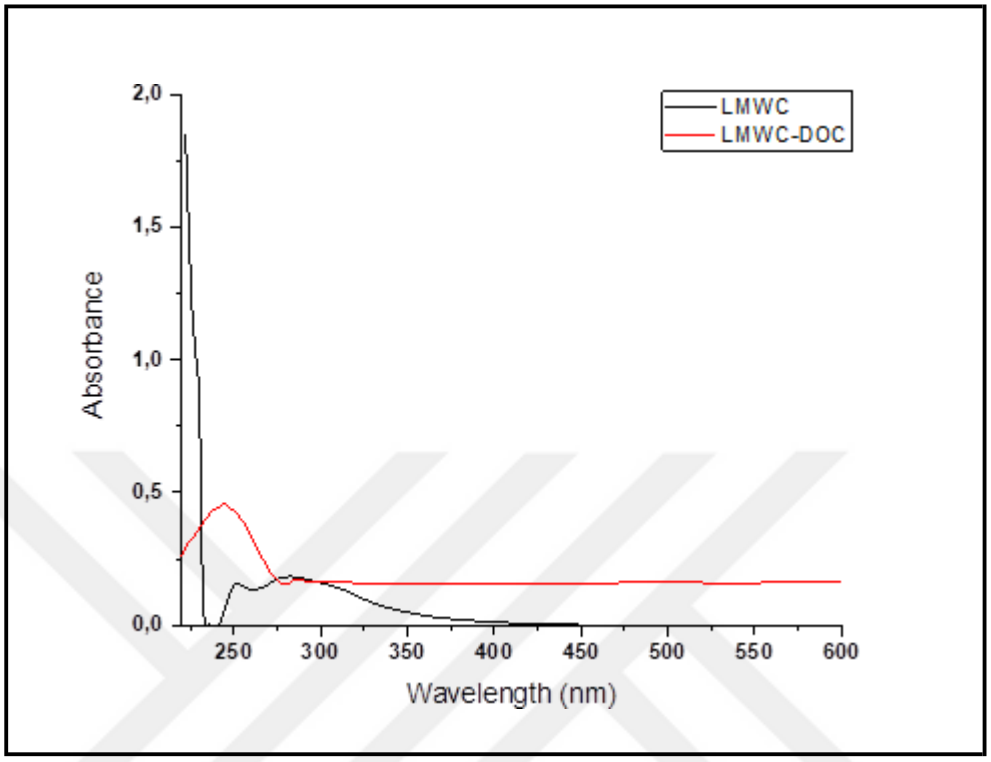

Figure 6.2. UV spectra of chitosan and Chitosan-DOC conjugates.

6.2. Size and zeta potential of Chitosan-DOC Conjugates

Size and zeta potential measurements of Chitosan-DOC conjugates were obtained using a DLS measurement device, and the results are shown in Figures 6.3 and 6.4. It is seen that there is a bimodal size distribution in conjugation. One is from 100 nm to 1000 nm, and the other is from 3000 nm to 5000 nm. The later size distribution might be due to the agglomeration of the more hydrophobic molecules due to conjugation.

As seen from the Figure the zeta potential of chitosan molecules conjugated by DOC showed much less positive charge due to a decrease in the amine groups that are used for conjugation, in their structure. It is known that unmodified chitosan molecules exhibit a strong positive charge (around 90 mV), a characteristic trait of this biopolymer. In the case of conjugation, on the other hand, the conjugated chitosan molecules have

only a slight positive charge. This subtle shift in charge indicates that chemical conjugation significantly impacts chitosan's molecular structure and overall properties. Such modifications can influence its behavior in various applications, emphasizing the importance of understanding how chemical bonding can alter the characteristics of this widely used biopolymer.

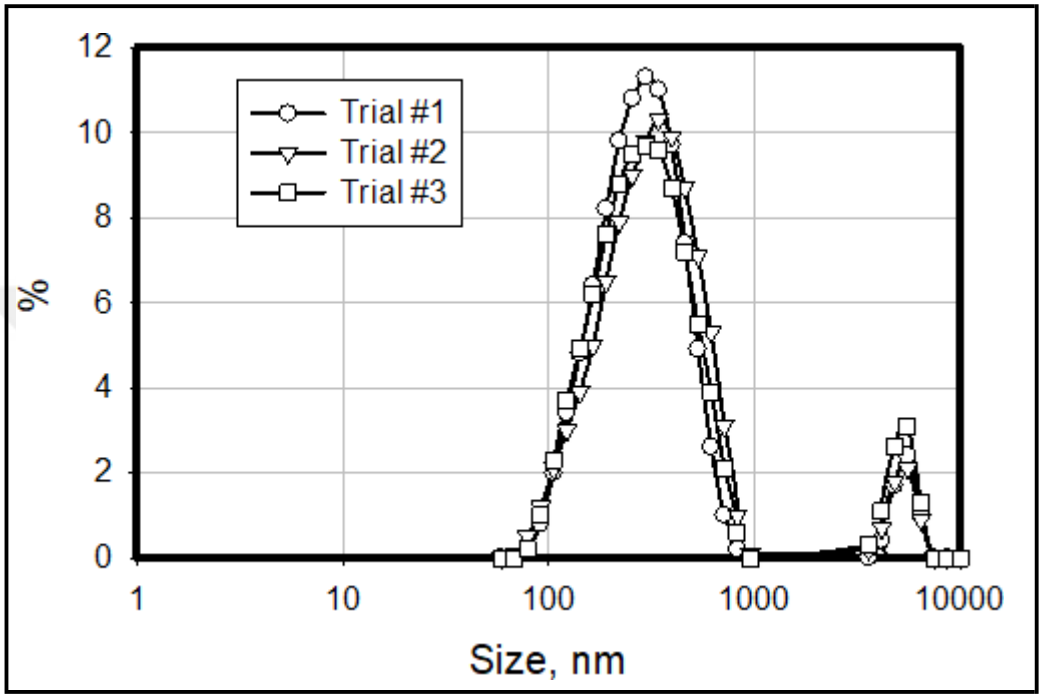

Figure 6.3. Size distribution of Chitosan-DOC.

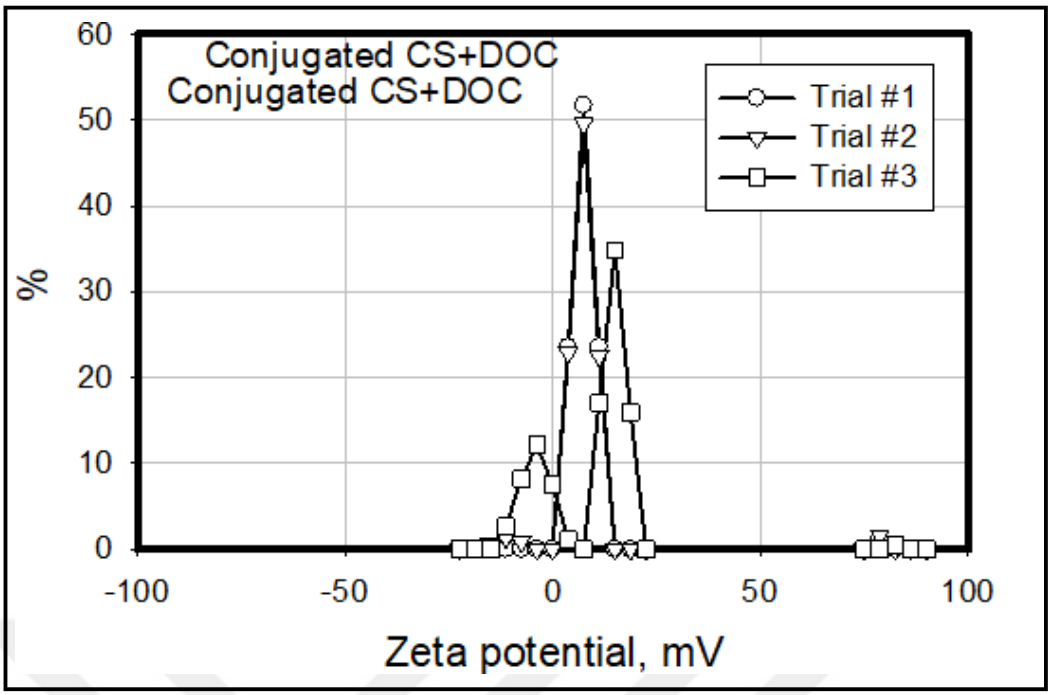

Figure 6.4. Zeta potential of LMWC-DOC.

CHAPTER 7

EFFECT OF CHITOSAN MICELLES ON CANCER CELLS

The development of biomaterial and nanoparticle-based drug delivery systems is gaining increasing attention for optimizing targeted therapies. Biocompatible polymers such as fucoidan and chitosan stand out for their potential to reduce toxicity and regulate drug release. This part of the study is on the micellar systems' efficiency in killing cancer cells. The formation of drug-loaded chitosan micelles was performed in two ways. 1) The physical way: In one of the micellar systems created, the hydrophobic drug was encapsulated in the matrix structure of the micelles by hydrophobic attraction. As discussed in Chapter 5 in detail, chitosan molecules were hydrophobically modified, and micelles were formed due to hydrophobic attraction between molecules. 2) The chemical way: In the other micellar systems created, the hydrophobic drug was bonded to the chitosan micelle structure chemically. The conjugation of the drug and chitosan was discussed in Chapter 6 in detail. The drug-conjugated chitosan molecules then self-assembled and encapsulated the drug inside them. The following paragraphs are on the effect of these encapsulation methods on the efficiency of the drug docetaxel.

7.1. Effect of Physical Drug Encapsulation: Drug-loaded Modified Chitosan micelles with and without fucoidan coverage

The biological tests were conducted using human Caco-2 colorectal adenocarcinoma epithelial cells to determine the percentage of cell death, and the results are given in Figures 7.1 and 7.2. The figure also includes the result of a similar amount of Docetaxel alone. It is seen that the drug (docetaxel), when it is given to the cell medium in the control group, the cell death rate is 100%. So, it is evident that the drug ultimately kills the cells.

When the same amount of drug was loaded in the structure of chitosan micelle structures (at different amounts), the cell death rates were observed to decrease from

100% to the values between 60% and 40% depending on the amount of the chitosan micellar solutions for 24 hours. However, the drug-loaded chitosan micelles (MC+DOC) resulted in a concentration-dependent decrease in cell viability. This decrease indicates that the drug-loaded chitosan micelles increased cell death, and the system worked effectively. This decrease in the killing rate is probably due to the time needed for drug molecules to go out of the structures in the cell to be active. So, the kinetics of drug release in the cell might affect the efficiency of the drug. The release that one talks about here is inside the drug, not the one that happens outside of the cell in the case of large carriers. At the outside of the cell (before entering the cell), the micellar structures have to be stable and protect their integrities in blood. The chitosan micellar structures are known to enter the cells due to their small size and nature. This might be partly because of the positive charge of chitosan. As discussed above, the molecules still have a positive charge after the partial hydrophobic modification.

When another biopolymer covers the chitosan micelles, fucoidan (a natural sulfated polysaccharide with antioxidants and anti-inflammatory and antitumoral properties), to make docetaxel-loaded micelles stable in blood, the cell death rate decreases down to 30%. This might be due to the negative charge of micelles due to fucoidan coverage (as discussed above). It seems too confusing; one can question the use of fucoidan to cover chitosan micelles to make them stable because of its negative charge that also causes a decrease in their entry into cells. This decrease might also be the time required to release the drug in the cell environment. So, a longer time may be necessary. However, it is also very well known that the presence of fucoidan makes micelles target-oriented again due to the presence of sulfate groups that attract them to the p-selecting proteins of cancer cells. So, the sulfate groups make the carrier system suitable for target delivery and increase the time carriers need to enter the cell and release the drug. The system, overall, looks like the combination of all the processes that determine the outcome of the cell uptake mechanism. In conclusion, covering the carriers with fucoidan makes micelles stable in blood. It makes them target-oriented simultaneously, so the damage of toxic drugs will be much lower in the blood than the normal cells.

This data also suggests that fucoidan coating, especially at high concentrations, protects healthy cells and may further reduce the side effects of the toxic anti-cancer drug docetaxel.

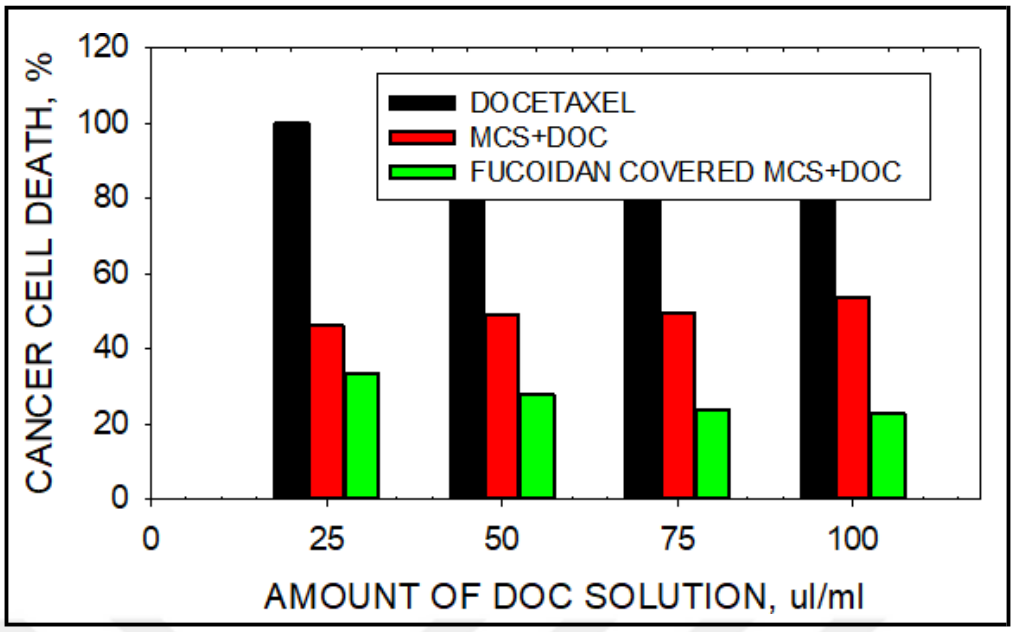

Figure 7.1. The cell death percent in the case of Docetaxel alone, MCS+DOC, and fucoidan covered MCS+DOC.

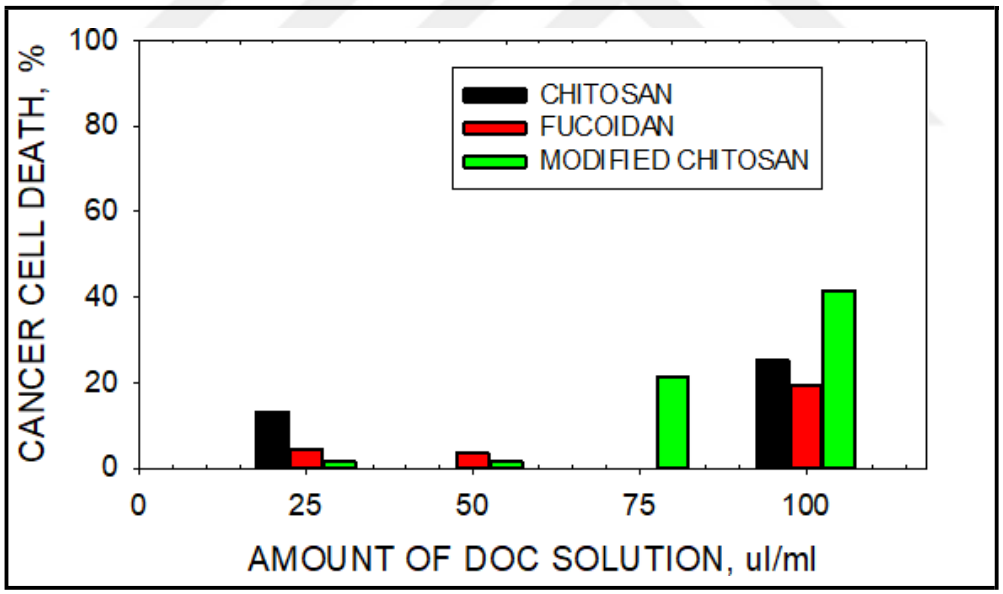

Figure 7.2 The percentage of cell death in the case of chitosan, fucoidan, and modified chitosan molecules.

In another study phase, the effects of the materials used as drug carriers were tested, and the cell death percentages were determined. These results are presented in Figure 7.2. It is seen that the biopolymers, fucoidan, and chitosan dissolved in distilled

water, can not harm cancer cells at any concentrations of them. That is, they do not show any significant cell-killing behavior.

On the other hand, the modified chitosan (MC) may harm the cancer cells depending on their concentration. It may kill cancer cells at high concentrations without any drug. However, this should be further investigated to understand the reason and mechanism of the killing of cells. Because of this reason, drug-loaded chitosan micelles should be covered by other materials (such as fucoidan) before being introduced into the bloodstream to eliminate their potential harm to healthy cells.

7.2. Effect of Chemical Drug Conjugation: Chitosan-DOC

In this part of the study, the chemically conjugated chitosan and drug structures were tested using the cell viability tests discussed above and compared with those with the systems where the drug is physically entrapped. These tests are crucial for understanding drug delivery systems' biocompatibility and therapeutic effects. The results are presented in Figure 7.3 to show the impact of conjugating the drug into the structure of chitosan to make the micellar carriers more stable in blood. Protein will not affect the structure's integrity if there is a chemical bond. However, the question is whether the drug is still efficient enough to kill cancer cells if bonded to the chitosan. It is seen from the result that when the drug molecule is bonded to the chitosan irreversibly, it is still effective in killing cancer cells and shows similar effects to the one system (discussed above) that has physically entrapped the drug inside the micelle. These results indicate that the toxic effect of docetaxel is transferred to cells via chitosan conjugation, leading to cell death, and the presence of chitosan along with the drug molecule is not that significant on the effect of drug efficiency.

In conclusion, the cell uptake mechanism and the efficiency of the drugs depend on several factors that also affect each other. These factors are summarized in Figure 7.4.

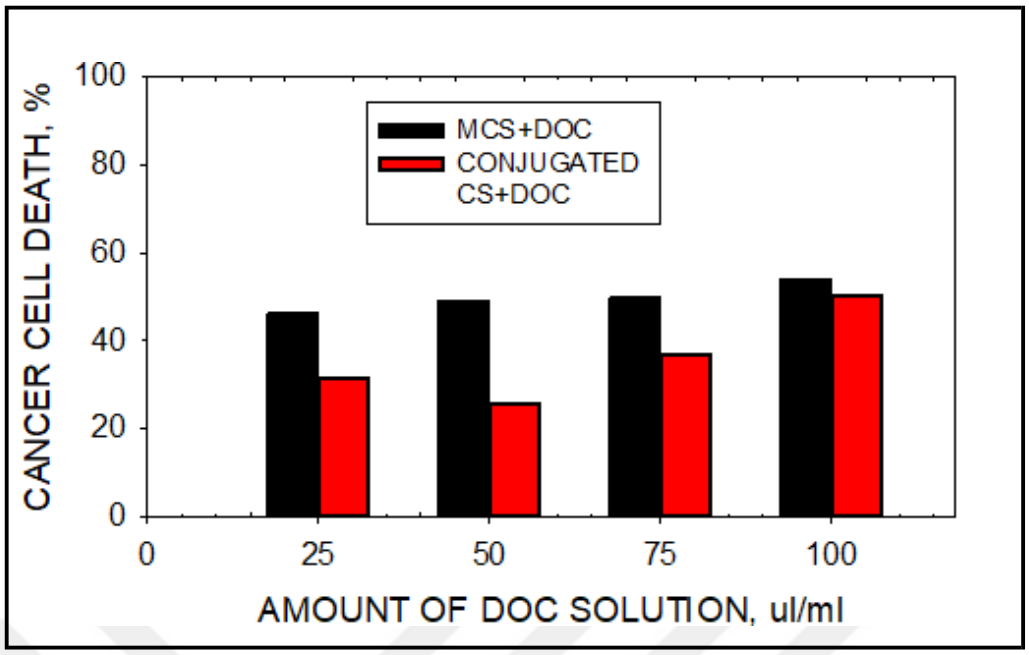

Figure 7.3. The Cell death percent in the case of modified MCS-DOC and conjugated CS-DOC.

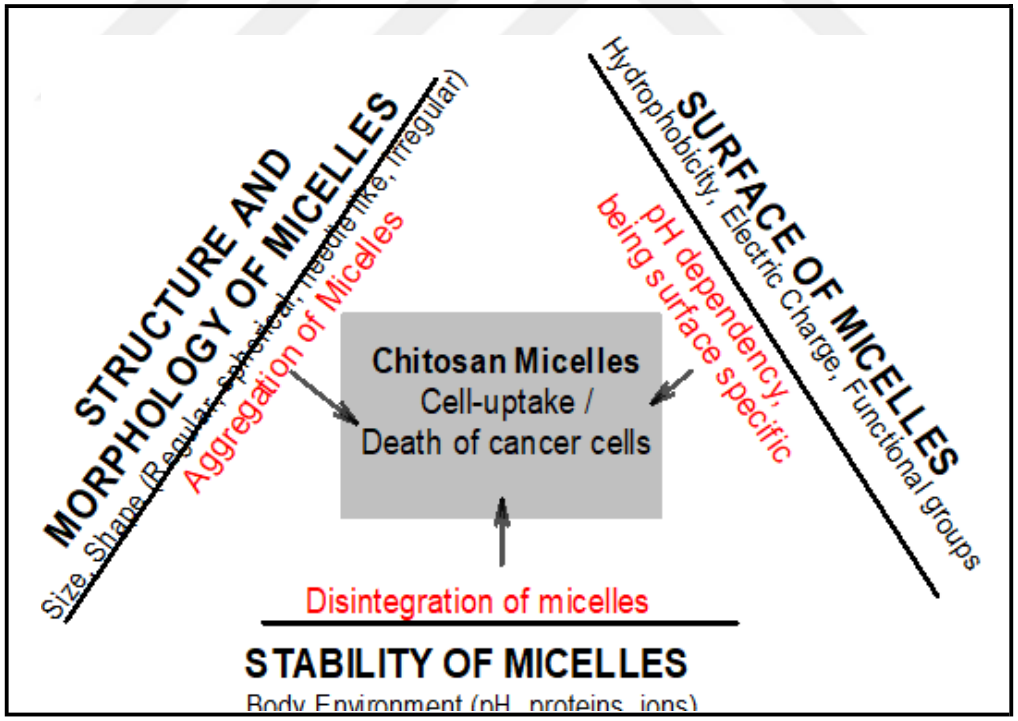

Figure 7.4. Factors and interactions determine the cellular uptake/drug release inside the cell mechanisms of chitosan carriers.

CHAPTER 8

CONCLUSION

This thesis study is on the stability issue of synthetic and natural polymeric micelles in the physiological environment that carries a water-insoluble (hydrophobic) drug concerning drug delivery applications in pharmacy. However, the micellization of natural polymers depends strongly on the degree of modification of their structure. The changes in their superior properties (such as pH sensitivity as in the case of chitosan) depend on the chemical modification type and degree required for self-assembly and micelle formation, on the other hand, is another essential issue that one should consider or be aware of when using bio-polymeric micelles. Based on the literature review conducted on micellar drug delivery vehicles in this study, the following conclusions have been made for the micelles that encapsulate drugs without a chemical bond: Synthetic polymeric micelles are unstable upon dilution in body fluid. Natural polymeric micelles can be stable upon dilution in body fluid, unlike synthetic polymeric micelles. However, upon protein interactions, both artificial and natural polymeric micelles seem to be unstable in body fluids. Therefore, the drug-loaded chitosan micelles were covered by another biopolymer, fucoidan, to stabilize body fluid. However, fucoidan coverage decreases the effectiveness of micelles in killing cancer cells due to their negative charge, which is expected to affect the cell uptake mechanism. When the death percentages of cancer cells were determined in the case of drug-loaded chitosan micelles, it was observed that both the physical and chemical encapsulation of the drug in the micelle structure gave similar results of up to 60% under the conditions of this study, which was lower than the value of docetaxel alone at the same amount, which could be explained by the release kinetics of the drug within the cell.

REFERENCES

Abka-Khajouei, R.; Tounsi, L.; Shahabi, N.; Patel, A. K.; Abdelkafi, S.; Michaud, P. Structures, Properties, and Applications of Alginates. *Mar. Drugs* **2022**, *20* (6), 364. DOI: 10.3390/md20060364.

Adepu, S.; Ramakrishna, S. Controlled Drug Delivery Systems: Current Status and Future Directions. *Molecules* **2021**, *26* (19), 5905. DOI: 10.3390/molecules26195905.

Aderibigbe, B. A.; Buyana, B. Alginate in Wound Dressings. *Pharmaceutics* **2018**, *10* (2), 42. DOI: 10.3390/pharmaceutics10020042.

Agnihotri, J.; Saraf, S.; Khale, A. Targeting: New Potential Carriers for Targeted Drug Delivery System. *Int. J. Pharm. Sci. Rev. Res.* **2011**, *8* (2), Article 020, 120–122. Available online: www.globalresearchonline.net (accessed October 4, 2024).

Akbarzadeh, A.; Rezaei-Sadabady, R.; Davaran, S.; Joo, S. W.; Zarghami, N.; Hanifehpour, Y.; Nejati-Koshki, K. Liposome: Classification, Preparation, and Applications. *Nanoscale Res. Lett.* **2013**, *8*, 102. DOI: 10.1186/1556-276X-8-102.

Al-Dhaheri, A.; Yusof, M. Y.; Ismail, A.; Al-Qasmi, M.; Al-Ali, A. The Role of Antimetabolites in Cancer Treatment: Mechanisms and Applications. *Biomolecules* **2023**, *13* (5), 724. DOI: 10.3390/biom13050724.

Alken, S.; Kelly, C. M. Benefit Risk Assessment and Update on the Use of Docetaxel in the Management of Breast Cancer. *Cancer Manag. Res.* **2013**, *5*, 357–365. DOI: 10.2147/CMAR.S49321.

Alley, S. C.; Okeley, N. M.; Senter, P. D. Antibody-Drug Conjugates: Targeted Drug Delivery for Cancer. *Curr. Opin. Chem. Biol.* **2010**, *14* (4), 529-537. DOI: 10.1016/j.cbpa.2010.06.014.

Alzehr, A.; Hulme, C.; Spencer, A.; Morgan-Trimmer, S. The Economic Impact of Cancer Diagnosis to Individuals and Their Families: A Systematic Review. *Support. Care Cancer* **2022**, *30*(4), 1-16. DOI: 10.1007/s00520-022-07055-0

Anand, U.; Dey, A.; Chandel, A. K. S.; Sanyal, R.; Mishra, A.; Pandey, D. K.; De Falco, V.; Upadhyay, A.; Kandimalla, R.; Chaudhary, A.; Dhanjal, J. K.; Dewanjee, S.; Vallamkondu, J.; Pérez de la Lastra, J. M. Cancer Chemotherapy and Beyond: Current Status, Drug Candidates, Associated Risks and Progress in Targeted Therapeutics. *Genes Dis.* **2022**, *10* (4), 1367–1401. DOI: 10.1016/j.gendis.2022.02.007.

Andersen, T.; Auk-Emblem, P.; Dornish, M. 3D Cell Culture in Alginate Hydrogels. *Microarrays* **2015**, *4* (2), 133–161. DOI: 10.3390/microarrays4020133.

Andrés, C. M. C.; Pérez de la Lastra, J. M.; Munguira, E. B.; Andrés Juan, C.; Pérez-Lebeña, E. Dual-Action Therapeutics: DNA Alkylation and Antimicrobial Peptides for Cancer Therapy. *Cancers* **2024**, *16*, 3123. DOI: 10.3390/cancers16183123.

Ardean, C.; Davidescu, C. M.; Nemeş, N. S.; Negrea, A.; Ciopec, M.; Duteanu, N.; Negrea, P.; Duda-Seiman, D.; Musta, V. Factors Influencing the Antibacterial Activity of Chitosan and Chitosan Modified by Functionalization. *Int. J. Mol. Sci.* **2021**, *22*, 7449. DOI: 10.3390/ijms22147449.

Argüelles-Monal, W. M.; Lizardi-Mendoza, J.; Fernández-Quiroz, D.; Recillas-Mota, M. T.; Montiel-Herrera, M. Chitosan Derivatives: Introducing New Functionalities with a Controlled Molecular Architecture for Innovative Materials. *Polymers* **2018**, *10*, 342. DOI: 10.3390/polym10030342.

Atanase, L. I. Micellar Drug Delivery Systems Based on Natural Biopolymers. *Polymers* **2021**, *13*, 477. DOI: 10.3390/polym13030477.

Attia, Z. I.; Noseworthy, P. A.; Lopez-Jimenez, F.; Asirvatham, S. J.; Deshmukh, A. J.; Gersh, B. J.; Carter, R. E.; Yao, X.; Rubinstein, A. A.; Erickson, B. J.; Kapa, S.; Friedman, P. A. An Artificial Intelligence-Enabled ECG Algorithm for Identifying Patients with Atrial Fibrillation During Sinus Rhythm: A

Retrospective Analysis of Outcome Prediction. *Lancet* **2019**, *394* (10201), 861–867. DOI: 10.1016/S0140-6736(19)31721-0.

Ayre, A.; Kadam, V.; Dand, N.; Patel, P. Polymeric Micelles as a Drug Carrier for Tumor Targeting. *Chronicles Young Sci.* **2013**, *4* (2), 94. DOI: 10.4103/2229-5186.115544.

Baharlouei, P.; Rahman, A. Chitin and Chitosan: Prospective Biomedical Applications in Drug Delivery, Cancer Treatment, and Wound Healing. *Mar. Drugs* **2022**, *20* (7), 460. DOI: 10.3390/md20070460.

Brianna, L.; Lee, S. H. Chemotherapy: How to Reduce Its Adverse Effects While Maintaining the Potency? *Med. Oncol.* **2023**, *40* (3), 88. DOI: 10.1007/s12032-023-01944-3.

Cao, L. M.; Sun, Z. X.; Makale, E. C.; Du, G. K.; Long, W. F.; Huang, H. R. Antitumor Activity of Fucoidan: A Systematic Review and Meta-Analysis. *Translational Cancer Research* **2021**, *10* (12), 5390–5405. DOI: 10.21037/tcr-21-1733.

Chongprakobkit, S.; Maniratanachote, R.; Tachaboonyakiat, W. Oil-in-Water Emulsions Stabilized by Sodium Phosphorylated Chitosan. *Carbohydr. Polym.* **2013**, *96* (1), 82–90. DOI: 10.1016/j.carbpol.2013.03.065.

Cragg, G. M.; Schepartz, S. A.; Stiffness, M.; Grever, M. G. The Taxol Supply Crisis: New NCI Policies for Handling the Large Scale Production of Novel Natural Product Anticancer and Anti-HIV Agents. *J. Nat. Prod.* **1993**, *56* (10), 1657–1668. DOI: 10.1021/np50041a001.

Dash, S.; Rajesh, P.; Joshi, R. G.; Rajeswari, S.; Karunanithi, P. Pre-Irradiation of Surfactants to Enhance Their Capacity to Solubilise Drugs and Dyes. *J. Indian Chem. Soc.* **2022**, *99* (11), 100751. DOI: 10.1016/j.jics.2022.100751.

Dhyani, P.; Quispe, C.; Sharma, E.; Bahukhandi, A.; Sati, P.; Attri, D. C.; Szopa, A.; Sharifi-Rad, J.; Docea, A. O.; Mardare, I.; Calina, D.; Cho, W. C. Anticancer Potential of Alkaloids: A Key Emphasis to Colchicine, Vinblastine, Vincristine,

Vindesine, Vinorelbine, and Vincamine. *Cancer Cell Int.* **2022**, *22* (1), 206. DOI: 10.1186/s12935-022-02624-9.

Elzoghby, A. O.; Samy, W. M.; Elgindy, N. A. Protein-Based Nanocarriers as Promising Drug and Gene Delivery Systems. *J. Controlled Release* **2012**, *161* (1), 38–49. DOI: 10.1016/j.jconrel.2011.11.001.

Fabiano, A.; Beconcini, D.; Migone, C.; Piras, A. M.; Zambito, Y. Quaternary Ammonium Chitosans: The Importance of the Positive Fixed Charge of the Drug Delivery Systems. *Int. J. Mol. Sci.* **2020**, *21* (18), 6617. DOI: 10.3390/ijms21186617.

Gao, Y.; Shang, Q.; Li, W.; Guo, W.; Stojadinovic, A.; Mannion, C.; Man, Y. G.; Chen, T. Antibiotics for Cancer Treatment: A Double-Edged Sword. *J. Cancer* **2020**, *11* (17), 5135–5149. DOI: 10.7150/jca.47470.

Harun-Or-Rashid, M.; Aktar, M. N.; Hossain, M. S.; Sarkar, N.; Islam, M. R.; Arafat, M. E.; Bhowmik, S.; Yusa, S.-i. Recent Advances in Micro- and Nano-Drug Delivery Systems Based on Natural and Synthetic Biomaterials. *Polymers* **2023**, *15*, 4563. DOI: 10.3390/polym15234563.

Hofheinz, R. D.; Gnad-Vogt, S. U.; Beyer, U.; Hochhaus, A. Liposomal Encapsulated Anti-Cancer Drugs. *Anticancer Drugs* **2005**, *16*, 691–707. DOI: 10.1097/01.cad.0000180697.22470.9a.

Hossain, M. S.; Islam, M. T.; Rahman, M. M.; Hossain, S. K.; Nayan, M. N.; Nasrin, R.; Rahman, M. M. A Review on Chitosan-Based Drug Delivery Systems: The Role of Mucoadhesive Polymers. *Prog. Polym. Sci.* **2022**, *130*, 101554. DOI: 10.1016/j.progpolymsci.2022.101554.

Hu, F.-Q.; Meng, P.; Dai, Y.-Q.; Du, Y.-Z.; You, J.; Wei, X.-H.; Yuan, H. PEGylated Chitosan-Based Polymer Micelle as an Intracellular Delivery Carrier for Anti-Tumor Targeting Therapy. *Eur. J. Pharm. Biopharm.* **2008**, *70* (3), 749–757. DOI: 10.1016/j.ejpb.2008.06.015.

Huang, C.; Wu, Y. Recent Advances in Topoisomerase Inhibitors: New Strategies for Cancer Therapy. *Front. Pharmacol.* **2022**, *13*, 867831. DOI: 10.3389/fphar.2022.867831.

Jiménez-Gómez, C. P.; Cecilia, J. A**.** Chitosan: A Natural Biopolymer with a Wide and Varied Range of Applications. *Molecules* **2020**, *25*, 3981. DOI: 10.3390/molecules25173981.

Johnston, M. J.; Semple, S. C.; Klimuk, S. K.; Ansell, S.; Maurer, N.; Cullis, P. R. Characterization of the Drug Retention and Pharmacokinetic Properties of Liposomal Nanoparticles Containing Dihydrosphingomyelin. *Biochim. Biophys. Acta* **2007**, *1768*, 1121–1127. DOI: 10.1016/j.bbamem.2007.01.005.

Kang, J. Y.; Taki, A. Mechanisms of Action and Clinical Applications of Antimetabolites in Cancer Therapy. *Front. Pharmacol.* **2021**, *12*, 653055. DOI: 10.3389/fphar.2021.653055.

Kasaaı, M. R. Calculating Mark-Houwink-Sakurada (MHS) Equation Viscometric Constants for Chitosan in Any Solvent-Temperature System Using Experimental Reported Viscometric Constants Data. *Carbohydr. Polym.* **2007**, *68* (3), 477–488. DOI: 10.1016/j.carbpol.2006.12.011.

Ketrat, S.; Japrung, D.; Pongprayoon, P. Exploring How Structural and Dynamic Properties of Bovine and Canine Serum Albumins Differ from Human Serum Albumin. *J. Mol. Graph. Model.* **2020**, *98*, 107617. DOI: 10.1016/j.jmgm.2019.107617.

Kumar, M. N.; Kumar, N.; Domb, A. J. Pharmaceutical Polymeric Controlled Drug Delivery Systems. *Adv. Polym. Sci.* **2000**, *160*, 45–117. DOI: 10.1007/3-540-48412-4_2.

Kurowiak, J.; Klekiel, T.; Będziński, R. Biodegradable Polymers in Biomedical Applications: A Review—Developments, Perspectives and Future Challenges. *Int. J. Mol. Sci.* **2023**, *24* (23), 16952. DOI: 10.3390/ijms242316952.

Lee, D. Y.; Lee, S. Y.; Yun, S. H.; Jeong, J. W.; Kim, J. H.; Kim, H. W.; Choi, J. S.; Kim, G. D.; Joo, S. T.; Choi, I.; Hur, S. J. Review of the Current Research on Fetal Bovine Serum and the Development of Cultured Meat. *Food Sci. Anim. Resour.* **2022**, *42* (5), 775–799. DOI: 10.5851/kosfa.2022.e46.

Lee, E.; Kim, J.; Lee, K. H.; Kim, S. W.; Lee, H.; Choi, H. J.; Oh, Y. K. In Vivo Antitumor Effects of Chitosan-Conjugated Docetaxel after Oral Administration. *J. Control. Release* **2009**, *140* (1), 79–85. DOI: 10.1016/j.jconrel.2009.06.004.

Lee, K. Y.; Ha, W. S.; Park, W. H. Blood Compatibility and Biodegradability of Partially N-Acylated Chitosan Derivatives. *Biomaterials* **1995**, *16* (15), 1211-1216. DOI: 10.1016/0142-9612(95)93036-U.

Lee, K. Y.; Mooney, D. J. Alginate: Properties and Biomedical Applications. *Prog. Polym. Sci.* **2012**, *37* (1), 106–126. DOI: 10.1016/j.progpolymsci.2011.06.003.

Lee, M.; Nah, J. W.; Kwon, Y.; Koh, J. J.; Ko, K. S.; Kim, S. W. Conjugated Chitosan as a Novel Platform for Oral Delivery of Paclitaxel. *J. Med. Chem.* **2008**, *51* (20), 6442-6449. DOI: 10.1021/jm800647u.

Li, C.; Wang, J.; Wang, Y.; Gao, H.; Wei, G.; Huang, Y.; Yu, H.; Gan, Y.; Wang, Y.; Mei, L.; Chen, H.; Hu, H.; Zhang, Z.; Jin, Y. Recent Progress in Drug Delivery. *Acta Pharm. Sin. B* **2019**, *9* (6), 1145–1162. DOI: 10.1016/j.apsb.2019.08.003.

Lin, J.; Jiao, G.; Kermanshahi-pour, A. Algal Polysaccharides-Based Hydrogels: Extraction, Synthesis, Characterization, and Applications. *Mar. Drugs* **2022**, *20,* 306. DOI: 10.3390/md20050306.

Liu, F.; Zhang, H.; Wang, Y.; Cheng, Y.; Li, S.; Zhao, H. Synthesis, Characterization and Antitumor Evaluation of CMCS–DTX Conjugates as Novel Delivery Platform for Docetaxel. *Int. J. Pharm.* **2013**, *451* (1-2), 41–49. DOI: 10.1016/j.ijpharm.2013.04.032.

Liu, J.; Zeng, F.; Allen, C. Influence of Serum Protein on Polycarbonate-Based Copolymer Micelles as a Delivery System for a Hydrophobic Anti-Cancer

Agent. *J. Control. Release* **2005**, *103* (2), 481–497. DOI: 10.1016/j.jconrel.2005.04.001.

Lou, J.; Duan, H.; Qin, Q.; Teng, Z.; Gan, F.; Zhou, X.; Zhou, X. Advances in Oral Drug Delivery Systems: Challenges and Opportunities. *Pharmaceutics* **2023**, *15* (2), 484. DOI: 10.3390/pharmaceutics15020484.

Lyseng-Williamson, K. A.; Fenton, C. Docetaxel. *Drugs* **2005**, *65* (17), 2513–2531. DOI: 10.2165/00003495-200565170-00007.

Mahmoodi, N. M.; Hayati, B.; Arami, M.; Bahrami, H. Preparation, Characterization, and Dye Adsorption Properties of Biocompatible Composite (Alginate/Titania Nanoparticle). *Desalination* **2011**, *275* (1-3), 93–101. DOI: 10.1016/j.desal.2011.02.034.

McClellan, S. J.; Franses, E. I. Effect of Concentration and Denaturation on Adsorption and Surface Tension of Bovine Serum Albumin. *Colloids Surf., B* **2003**, *28* (1), 63–75. DOI: 10.1016/S0927-7765(02)00263-0.

McFadden, B. A.; Vincenty, C. S.; Chandler, A. J.; Cintineo, H. P.; Lints, B. S.; Mastrofini, G. F.; Arent, S. M. Effects of Fucoidan Supplementation on Inflammatory and Immune Response After High-Intensity Exercise. *J. Int. Soc. Sports Nutr.* **2023**, *20* (1), 2224751. DOI: 10.1080/15502783.2023.2224751.

Min, H.-Y.; Lee, H.-Y. Molecular Targeted Therapy for Anticancer Treatment. *Exp. Mol. Med.* **2022**, *54*, 1670–1694. DOI: 10.1038/s12276-022-00864-3.

Mirzaie, Z. H.; Irani, S.; Mirfakhraie, R.; Atyabi, S. M.; Dinarvand, M.; Dinarvand, R.; Varshochian, R.; Atyabi, F. Docetaxel–Chitosan Nanoparticles for Breast Cancer Treatment: Cell Viability and Gene Expression Study. *Chem. Biol. Drug Des.* **2016**, *88* (6), 850-858. DOI: 10.1111/cbdd.12814.

Mondon, K.; Gurney, R.; Möller, M. Colloidal Drug Delivery Systems—Recent Advances with Polymeric Micelles. *CHIMIA Int. J. Chem.* **2008,** *62*, 832–840.

Newman, D. J.; Cragg, G. M.; Snader, K. M. Natural Products as Sources of New Drugs over the Period 1981–2002. *J. Nat. Prod.* **2003**, *66* (7), 1022–1037. DOI: 10.1021/np030096l.

Oliyaei, N.; Moosavi-Nasab, M.; Mazloomi, S. M. Therapeutic Activity of Fucoidan and Carrageenan as Marine Algal Polysaccharides Against Viruses. *3 Biotech* **2022**, *12*, 154. DOI: 10.1007/s13205-022-03210-6.

Owen, S. C.; Chan, D. P.; Shoichet, M. S. Polymeric Micelle Stability. *Nano Today* **2012,** *7*, 53–65.

Park, J. H.; Choi, Y. J.; Oh, J. M.; Kim, H. S.; Kim, J. H.; Kim, S. Y.; Lee, S. K.; Lee, J. H.; Kwon, I. C. Polymeric Nanomedicine for Cancer Therapy. *Prog. Polym. Sci.* **2008**, *33* (2), 113–137. DOI: 10.1016/j.progpolymsci.2007.11.001.

Parveen, S.; Sahoo, S. K. Polymeric Nanoparticles for Cancer Therapy. *J. Drug Target.* **2008**, *16* (2), 108–123. DOI: 10.1080/10611860701254083.

Peppas, N.; Bures, P.; Leobandung, W.; Ichikawa, H. Hydrogels in Pharmaceutical Formulations. *Eur. J. Pharm. Biopharm.* **2000**, *50*, 27–46. DOI: 10.1016/S0939-6411(00)00121-3.

Polat, H.; Chander, S. Adsorption of PEO/PPO Triblock Copolymers and Wetting of Coal. *Colloids Surf., A* **1999,** *146*, 199–212.

Polat, H.; Kutluay, G.; Polat, M. Analysis of Dilution Induced Disintegration of Micellar Drug Carriers in the Presence of Inter and Intra Micellar Species. *Colloids Surf. A Physicochem. Eng. Asp.* **2020**, *601*, 1-9. DOI: 10.1016/j.colsurfa.2020.125060.

Pringle, S.; Ko, E. M.; Doherty, M.; et al. Addressing Transportation Barriers in Oncology: Existing Programs and New Solutions. *Support Care Cancer* **2024**, *32*, 317. DOI: 10.1007/s00520-024-08514-2.

Purohit, P.; Bhatt, A.; Mittal, R. K.; Abdellattif, M. H.; Farghaly, T. A. Polymer Grafting and Its Chemical Reactions. *Front. Bioeng. Biotechnol.* **2023**, *10*, 1044927. DOI: 10.3389/fbioe.2022.1044927.

Ramos, A.; Sadeghi, S.; Tabatabaeian, H. Battling Chemoresistance in Cancer: Root Causes and Strategies to Uproot Them. *Int. J. Mol. Sci.* **2021**, *22* (17), 9451. DOI: 10.3390/ijms22179451.

Ramos, V. M.; Rodriguez, N. M.; Rodriguez, M. S.; Heras, A.; Agullo, E. Modified Chitosan Carrying Phosphonic and Alkyl Groups. *Carbohydr. Polym.* **2003**, *51* (4), 425-429. DOI: 10.1016/S0144-8617(02)00218-4.

Ravi, P. R.; Vats, R.; Dalal, V.; Gadekar, N.; N, A. Design, Optimization and Evaluation of Poly-ε-Caprolactone (PCL) Based Polymeric Nanoparticles for Oral Delivery of Lopinavir. *Drug Dev. Ind. Pharm.* **2013**, *41* (1), 131–140. DOI: 10.3109/03639045.2013.850710.

Razak, S. A.; Mohd Gazzali, A.; Fisol, F. A.; Abdulbaqi, I. M.; Parumasivam, T.; Mohtar, N.; Wahab, H. A. Advances in Nanocarriers for Effective Delivery of Docetaxel in the Treatment of Lung Cancer: An Overview. *Cancers* **2021**, *13* (3), 400. DOI: 10.3390/cancers13030400.

Rebucci, M.; Michiels, C. Molecular Aspects of Cancer Cell Resistance to Chemotherapy. *Biochem. Pharmacol.* **2013**, *85* (9), 1219–1226. DOI: 10.1016/j.bcp.2013.02.017.

Rezaei, F. S.; Sharifianjazi, F.; Esmaeilkhanian, A.; Salehi, E. Chitosan Films and Scaffolds for Regenerative Medicine Applications: A Review. *Carbohydrate Polymers* **2021**, *273*, 118631. DOI: 10.1016/j.carbpol.2021.118631.

Rizwan, M.; Yahya, R.; Hassan, A.; Yar, M.; Azzahari, A. D.; Selvanathan, V.; Sonsudin, F.; Abouloula, C. N. pH-Sensitive Hydrogels in Drug Delivery: Brief History, Properties, Swelling, and Release Mechanism, Material Selection and Applications. *Polymers* **2017**, *9*, 137. DOI: 10.3390/polym9040137.

Sanjeewa, K. K. A.; Herath, K. H. I. N. M.; Yang, H. W.; Choi, C. S.; Jeon, Y. J. Anti-Inflammatory Mechanisms of Fucoidans to Treat Inflammatory Diseases: A Review. *Mar. Drugs* **2021**, *19* (12), 678. DOI: 10.3390/md19120678.

Satchanska, G.; Davidova, S.; Petrov, P. D. Natural and Synthetic Polymers for Biomedical and Environmental Applications. *Polymers* **2024**, *16* (8), 1159. DOI: 10.3390/polym16081159.

Schirrmacher, V. From Chemotherapy to Biological Therapy: A Review of Novel Concepts to Reduce the Side Effects of Systemic Cancer Treatment (Review). *Int. J. Oncol.* **2019**, *54* (2), 407–419. DOI: 10.3892/ijo.2018.4661.

Senapati, S.; Mahanta, A. K.; Kumar, S.; Maiti, P. Controlled Drug Delivery Vehicles for Cancer Treatment and Their Performance. *Signal Transduct. Target. Ther.* **2018**, *3*, 7. DOI: 10.1038/s41392-017-0004-3.

Shakil, M. S.; Mahmud, K. M.; Sayem, M.; Niloy, M. S.; Halder, S. K.; Hossein, M. S.; Uddin, M. F.; Hasan, M. A. Using Chitosan or Chitosan Derivatives in Cancer Therapy. *Polysaccharides* **2021**, *2*, 795–816. DOI: 10.3390/polysaccharides2040048.

Shikuku, R.; Hasnat, M. A.; Mashrur, S. B. A.; Haque, P.; Rahman, M. M.; Khan, M. N. Chitosan-based pH-sensitive Semi-interpenetrating Network Nanoparticles as a Sustained Release Matrix for Anticancer Drug Delivery. *Carbohydrate Polymer Technologies and Applications* **2024**, *7*, 100515. DOI: 10.1016/j.carpta.2024.100515.

Singh, A. P.; Biswas, A.; Shukla, A.; Choudhury, S.; Prakash, S. Targeted Therapy in Chronic Diseases Using Nanomaterial-Based Drug Delivery Vehicles. *Signal Transduct. Target. Ther.* **2019**, *4*, 33. DOI: 10.1038/s41392-019-0068-3.

Siretli, Ç. Synthesis of Silica Nanoparticles with Custom-Made Morphology for Controlled Drug Delivery. M.Sc. Thesis, İzmir Institute of Technology (IYTE), 2012.

Slavkova, M.; Tzankov, B.; Popova, T.; Voycheva, C. Gel Formulations for Topical Treatment of Skin Cancer: A Review. *Gels* **2023**, *9*, 352. DOI: 10.3390/gels9050352.

Tien, C. L.; Lacroix, M.; Ispas-Szabo, P.; Mateescu, M. A. N-Acylated Chitosan: Hydrophobic Matrices for Controlled Drug Release. *J. Control. Release* **2003**, *93* (1), 1–13. DOI: 10.1016/j.jconrel.2003.07.008.

Tiwari, G.; Tiwari, R.; Bannerjee, S.; Bhati, L.; Pandey, S.; Pandey, P.; Bannerjee, S. K. Drug Delivery Systems: An Updated Review. *Int. J. Pharm. Investig.* **2012**, *2*(1), 2-11. DOI: 10.4103/2230-973X.96920

Tsaih, L. M.; Chen, R. H. Molecular Weight Determination of 83% Degree of Deacetylation Chitosan with Non-Gaussian and Wide Range Distribution by High-Performance Size Exclusion Chromatography. *Carbohydr. Polym.* **1999**, *40* (1), 109–117. DOI: 10.1016/S0144-8617(99)00025-2.

Wang, K.; Xu, X.; Wei, Q.; Yang, Q.; Zhao, J.; Wang, Y.; Li, X.; Ji, K.; Song, S. Application of Fucoidan as Treatment for Cardiovascular and Cerebrovascular Diseases. *Therapeutic Advances in Chronic Disease* **2022**, *13*, 20406223221076891. DOI: 10.1177/20406223221076891.

Wang, T.; Zou, H.; Liu, Y.-X.; Zhang, X.-W. Effects of Paclitaxel-conjugated N-Succinyl-Hydroxyethyl Chitosan Film for Proliferative Cholangitis in Rabbit Biliary Stricture Model. *Chinese Med. J.* **2018**, *131* (6), 696-703. DOI: 10.4103/0366-6999.226904.

Wang, W.; Meng, Q.; Li, Q.; Liu, J.; Zhou, M.; Jin, Z.; Zhao, K**.** Chitosan Derivatives and Their Application in Biomedicine. *Int. J. Mol. Sci.* **2020**, *21*, 487. DOI: 10.3390/ijms21020487.

Wang, W.; Meng, Q.; Li, Q.; Liu, J.; Zhou, M.; Jin, Z.; Zhao, K. Chitosan Derivatives and Their Application in Biomedicine. *Int. J. Mol. Sci.* **2020**, *21* (2), 487. DOI: 10.3390/ijms21020487.

Wang, W.; Xue, C.; Mao, X. Chitosan: Structural Modification, Biological Activity and Application. *Int. J. Biol. Macromol.* **2020**, *164*, 4532–4546. DOI: 10.1016/j.ijbiomac.2020.09.042.

Wang, Y.; Xing, M.; Cao, Q.; Ji, A.; Liang, H.; Song, S. Biological Activities of Fucoidan and the Factors Mediating Its Therapeutic Effects: A Review of Recent Studies. *Mar. Drugs* **2019**, *17*, 183. DOI: 10.3390/md17030183.

Ways, T. M.; Lau, W. M.; Khutoryanskiy, V. V. Chitosan and Its Derivatives for Application in Mucoadhesive Drug Delivery Systems. *Polymers* **2018**, *10*, 267. DOI: 10.3390/polym10030267.

Wu, D.; Xu, Y.; Yu, L.; Yang, Z.; Zheng, Q.; Li, Y.; Zuo, W.; Feng, X. Nanoparticle-Based Drug Delivery Systems Targeting Cancer Cell Surfaces: Mechanisms and Applications. *RSC Adv.* **2023**, *13*, 34099–34111. DOI: 10.1039/D3RA02969G.

Xu, T.; Xu, Q.; Wang, D.; Fan, X.; Yang, L. Synthesis and Characterization of N-Sulfated Chitosan Derivatives with Different Substituent Position and Their Potential Applications. *Carbohydr. Polym.* **2017**, *165*, 209–216. DOI: 10.1016/j.carbpol.2017.02.037.

Xu, Z. P.; Zeng, Q. H.; Lu, G. Q.; Yu, A. B. Inorganic Nanoparticles as Carriers for Efficient Cellular Delivery. *Chem. Eng. Sci.* **2006**, *61* (3), 1027–1040. DOI: 10.1016/j.ces.2005.07.030.

Yang, J.; Xie, Q.; Zhu, J.; Zou, C.; Chen, L.; Du, Y.; Li, D. Preparation and In Vitro Antioxidant Activities of 6-Amino-6-Deoxychitosan and Its Sulfonated Derivatives. *Biopolymers* **2015**, *103* (10), 539–549. DOI: 10.1002/bip.22656.

Zhang, C.; Xu, C.; Gao, X.; Yao, Q. Platinum-Based Drugs for Cancer Therapy and Anti-Tumor Strategies. *Theranostics* **2022**, *12* (5), 2115–2132. DOI: 10.7150/thno.69424.

Zhang, J.; Xia, W.; Liu, P.; Cheng, Q.; Tahirou, T.; Gu, W.; Li, B. Chitosan Modification and Pharmaceutical/Biomedical Applications. *Mar. Drugs* **2010**, *8* (7), 1962–1987. DOI: 10.3390/md8071962.

Zhao, L. Y.; Zhang, W. M. Recent Progress in Drug Delivery of Pluronic P123: Pharmaceutical Perspectives. *J. Drug Targeting* **2017**, *25* (6), 471–484. DOI: 10.1080/1061186X.2017.1289538.

Zhu, Y.; Stark, C. J.; Madira, S.; Ethiraj, S.; Venkatesh, A.; Anilkumar, S.; Jung, J.; Lee, S.; Wu, C. A.; Walsh, S. K.; Stankovich, G. A.; Woo, Y. J. Three-Dimensional Bioprinting with Alginate by Freeform Reversible Embedding of Suspended Hydrogels with Tunable Physical Properties and Cell Proliferation. *Bioengineering* **2022**, *9* (12), 807. DOI: 10.3390/bioengineering9120807.

Zlotnikov, I. D.; Streltsov, D. A.; Ezhov, A. A.; Kudryashova, E. V. Smart pH- and Temperature-Sensitive Micelles Based on Chitosan Grafted with Fatty Acids to Increase the Efficiency and Selectivity of Doxorubicin and Its Adjuvant Regarding the Tumor Cells. *Pharmaceutics* **2023**, *15*, 1135. DOI: 10.3390/pharmaceutics15041135.

CURRICULUM VITAE

Education

2011 – 2016 BS, İzmir Institute of Technology, Chemistry Department

2016 – 2019 MS, İzmir Institute of Technology, Chemistry Department

2019 – 2024 PhD, İzmir Institute of Technology, Chemistry Department

Thesis

Design and synthesis of a fluorescent chemo dosimeter for the analysis of the gold ions (Ref No. 10131399, 2018)

Micellar Carrier Systems for Anticancer Drugs Using Natural Polymers (Ref No. 10698887, 2025)

Projects

MARİN KÖKENLİ DOĞAL POLİMERLERDEN BİYOUYUMLU, KARARLI, HEDEFE YÖNELİK İLAÇ TAŞIYICI MİSELLERİN SENTEZİ (2022IYTE-3-0018)

Publications

Polat, H.; Cevik Eren, M.; Polat, M. The Effect of Protein BSA on the Stability of Lipophilic Drug (Docetaxel)-Loaded Polymeric Micelles. *Colloids Surf., A* **2022**, *635*, 127712. https://doi.org/10.1016/j.colsurfa.2021.127712.

Çevik Eren, M; Eren, A; Dartar, S; Tütüncü, B. B; Emrullahoğlu, M. A Cyclopalladated BODIPY Construct as a Fluorescent Probe for Carbon Monoxide. *Eur. J. Inorg. Chem.* **2022**, *2022* (14), e202200093. DOI: 10.1002/ejic.202200093.

Çevik Eren, M; Eren, A; Dartar, S; Kaya, B. U; Üçüncü, M; Varlikli, C; Karakaya, H. Ç; Emrullahoğlu, M. A Reaction-Based Scenario for Fluorescence Probing of Au(III) Ions in Human Cells and Plants. *Org. Biomol. Chem.* **2023**, *21* (39), 7880–7885. DOI: 10.1039/D3OB01081C.